

AXIAL AND LATERAL RESOLUTION IN OPTICAL  
COHERENCE TOMOGRAPHY AS A FUNCTION OF  
SYSTEM AND TISSUE OPTICAL PROPERTIES

By

Ryan Sipos

---

Copyright © Ryan Sipos 2019

A Thesis Submitted to the Faculty of the  
JAMES C. WYANT COLLEGE OF OPTICAL SCIENCES

In Partial Fulfillment of the Requirements  
For the Degree of

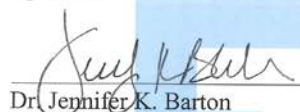
MASTER OF SCIENCE

In the Graduate College  
THE UNIVERSITY OF ARIZONA

2019

THE UNIVERSITY OF ARIZONA  
GRADUATE COLLEGE

As members of the Master's Committee, we certify that we have read the thesis prepared by Ryan Sipos, titled *Axial and Lateral Resolution in Optical Coherence Tomography as a Function of System and Tissue Optical Properties* and recommend that it be accepted as fulfilling the dissertation requirement for the Master's Degree.

  
\_\_\_\_\_

Date: 4/29/19

  
\_\_\_\_\_

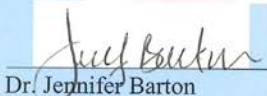
Date: 4/29/19

  
\_\_\_\_\_

Date: 4/29/2019

Final approval and acceptance of this thesis is contingent upon the candidate's submission of the final copies of the thesis to the Graduate College.

I hereby certify that I have read this thesis prepared under my direction and recommend that it be accepted as fulfilling the Master's requirement.

  
\_\_\_\_\_

Date: 4/29/19

Dr. Jennifer Barton  
Master's Thesis Committee Chair  
Biomedical Engineering, Optical Sciences



ARIZONA

## ACKNOWLEDGEMENTS

Thanks to *Dr. Jennifer Barton* for being my advisor on this project. Her contributions truly cannot be overstated, as without her advice and willingness to help me succeed, this study would not have been possible.

Thanks to *Dr. Dongkyun Kang* and *Dr. Tom Milster* for their contributions as part of my Master's Thesis Committee, as well as for their advice and guidance in planning the experimental procedures.

Thanks to *Faith Rice* for being an outstanding source of advice and help throughout the duration of the project, as well as for teaching me the proper laboratory techniques necessary for performing serial dilutions.

Thanks to *Pier Ingram* and the *Center for Gamma-Ray Imaging* for manufacturing the 3D printed components, as well as for providing technical advice during the design phase.

Thanks to *Nick Lyons* and *Hillary Mathis* for supplying test equipment necessary for the completion of this project.

Thanks to *Travis Sawyer* for his significant contribution in writing the lateral resolution data analysis script and for assisting with the subsequent statistical analysis of the results.

Thanks to *Nikola Kapor* for his help in preparing the tissue phantoms and assisting with running the data collection.

Thanks to *Valeria Rascon* for her help in learning how to use ImageJ as well as helping with the axial resolution and multiply scattered photon data analysis procedures.

Thanks to *Nikki Galvez* for her help in preparing graphics for this paper as well as assisting with the data analysis.

Thanks to *Harrison Thurgood* for his assistance in the design of the tissue phantom holder.

Thanks to *Kelli Kiekens* and *Dr. Eric Sipos* for reviewing and editing this manuscript.

And finally, thanks to all the members of the *Tissue Optics Lab*, past and present, for their friendship, advice, and support during my time in the lab.

## TABLE OF CONTENTS

List of Figures .....	6
List of Equations.....	7
List of Tables.....	8
Abstract.....	99
1. Introduction .....	10
1.1 Interference and Low Coherence Interferometry .....	10
1.2 Light-Matter Interactions in Tissue.....	12
1.3 Optical-Coherence Tomography.....	14
1.4 Tissue Phantoms.....	17
1.5 Prior Art .....	19
2. Methods.....	20
2.1 Creation of Tissue Phantoms .....	20
2.2 OCT Alignment and Test Preparation.....	24
2.3 Experimental Procedures and Data Acquisition .....	28
3. Results and Discussion.....	32
3.1 3D Print Design .....	32
3.2 Lens Design.....	33
3.3 Absorption Coefficient Calculation.....	37
3.4 Phantom Dilution Calculation.....	39
3.5 Lateral Resolution.....	40
3.6 Axial Resolution .....	45
3.7 Multiply Scattered Photons .....	48
3.8 Overall Conclusions and Considerations.....	51
4. Future Work.....	53
4.1 Limitations .....	53
4.2 Continued Research.....	54
5. Appendix.....	56
5.1 Determination of Absorption Coefficient for India Ink SOP .....	56
5.2 [Intralipid 20%, Water] Tissue Phantom Dilution SOP .....	60

5.3 [India Ink, Intralipid 20%, Water] Tissue Phantom Dilution SOP.....	64
5.4 Preparation of Tissue Phantom Holder SOP.....	66
5.5 Preparation of Modular Lens System and Alignment SOP.....	68
5.6 Software Manipulation and Troubleshooting SOP.....	72
5.7 [Intralipid 20%, Water] Experimental Procedures SOP.....	76
5.8 [India Ink, Intralipid 20%, Water] Experimental Procedures SOP.....	85
5.9 Engineering Drawings of 3D Printed Components.....	94
5.10 Table of Results for Lateral Resolution.....	97
5.11 Table of Results for Axial Resolution.....	100
5.12 Table of Results for Multiply Scattered Photons.....	103
6. References.....	106

## LIST OF FIGURES

Figure 1.1 – General format for a Michelson Interferometer.....	11
Figure 1.2 – Time-Domain OCT example layout .....	15
Figure 1.3 – Multiply Scattered Photon visualization .....	16
Figure 2.1 – Experimental setup for determining absorption coefficient of India Ink .....	22
Figure 2.2 – Picture of Time-Domain OCT laboratory setup.....	27
Figure 2.3 – Plotted report of the fitting function for the analysis of Lateral Resolution.....	29
Figure 2.4 – ImageJ output for the analysis of the Axial Resolution .....	30
Figure 2.5 – ImageJ output for the analysis of the counts of Multiply Scattered Photons.....	31
Figure 3.1 – 3D Printed Tissue Phantom Holder .....	32
Figure 3.2 – 3D Printed Kinematic Base components.....	33
Figure 3.3 – Lens data, layout, and aberration coefficients for NA=0.0603 system.....	35
Figure 3.4 – Lens data, layout, and aberration coefficients for NA=0.0901 system.....	36
Figure 3.5 – Lens data, layout, and aberration coefficients for NA=0.1186 system.....	36
Figure 3.6 – Modular lens setups .....	37
Figure 3.7 – Results from India Ink absorption coefficient calculation experiment.....	38
Figure 3.8 – Lateral Resolution vs % Intralipid for $\mu_a = 1.35 \text{ cm}^{-1}$ .....	41
Figure 3.9 – Lateral Resolution vs % Intralipid for $\mu_a = 6.075 \text{ cm}^{-1}$ .....	42
Figure 3.10 – Comparison between two OCT images for the 1.525% Intralipid case and the 0.1525% Intralipid case .....	45
Figure 3.11 – Axial Resolution vs % Intralipid, $\mu_a = 1.35 \text{ cm}^{-1}$ .....	46
Figure 3.12 – Axial Resolution vs % Intralipid, $\mu_a = 6.075 \text{ cm}^{-1}$ .....	47
Figure 3.13 – Counts, Multiply Scattered Photons vs % Intralipid, $\mu_a = 1.35 \text{ cm}^{-1}$ .....	49
Figure 3.14 – Counts, Multiply Scattered Photons vs % Intralipid, $\mu_a = 6.075 \text{ cm}^{-1}$ .....	49
Figure 3.15 – Counts, Scaled Multiply Scattered Photons vs % Intralipid, $\mu_a = 1.35 \text{ cm}^{-1}$ .....	50
Figure 3.16 – Counts, Scaled Multiply Scattered Photons vs % Intralipid, $\mu_a = 6.075 \text{ cm}^{-1}$ .....	50
Figure A.1 – Tissue Phantom Holder design drawing.....	94
Figure A.2 – Kinematic Base with Rods design drawing .....	95
Figure A.3 – Kinematic Base with Holes design drawing .....	96

## LIST OF EQUATIONS

Equation 1.1 – Super position of two monochromatic plane waves.....	10
Equation 1.2 – Irradiance of a plane wave in terms of complex amplitude .....	10
Equation 1.3 – Irradiance of a resultant wave in terms of component irradiance values.....	10
Equation 1.4 – Mutual coherence function .....	12
Equation 1.5 – Fringe visibility.....	12
Equation 1.6 – Beer’s Law.....	13
Equation 1.7 – Reduced scattering coefficient in terms of the scattering coefficient and anisotropy.....	14
Equation 1.8 – Doppler frequency induced from Time-Domain OCT.....	14
Equation 1.9 – Detector interference signal.....	14
Equation 1.10 – Theoretical lateral resolution of OCT .....	17
Equation 1.11 – Theoretical axial resolution of OCT.....	17
Equation 2.1 – Variable packing dimension .....	20
Equation 2.2 – Linear polynomial fit function for the anisotropy .....	21
Equation 2.3 – Independent scattering coefficient.....	21
Equation 2.4 – Scattering coefficient for dependent scattering.....	21
Equation 2.5 – Anisotropy for independent scattering.....	21
Equation 2.6 – Anisotropy for dependent scattering.....	21
Equation 2.7 – Reduced scattering coefficient for dependent scattering .....	21
Equation 2.8 – Beer’s Law reorganized to find the absorption coefficient .....	23
Equation 2.9 – Beam waist based on wavelength and image space numerical aperture .....	28
Equation 3.1 – Beam diameter through beam collimating optics.....	34
Equation 3.2 – Dilution Factor 1 .....	40
Equation 3.3 – Simulated reduced scattering coefficient.....	40
Equation 3.4 – Dilution Factor 2 .....	40
Equation 3.5 – Simulated depth .....	40
Equation 3.6 – % Intralipid as a function of Dilution Factor 1 and Dilution Factor 2.....	40

## LIST OF TABLES

Table 3.1 – Summary of lens module designs .....	35
Table 3.2 – Data collected from India Ink absorption coefficient calculation experiment.....	37
Table 3.3 – Tissue Phantom dilution calculations and planning .....	39
Table 3.4 – Linear regression analysis for $\mu_a = 1.35 \text{ cm}^{-1}$ .....	43
Table 3.5 – Results of two-tailed test of means and slopes for $\mu_a = 1.35 \text{ cm}^{-1}$ .....	43
Table 3.6 – Linear regression analysis for $\mu_a = 6.075 \text{ cm}^{-1}$ .....	43
Table 3.7 – Results of two-tailed test of means and slopes for $\mu_a = 6.075 \text{ cm}^{-1}$ .....	43
Table A.1 – Results for Lateral Resolution, NA=0.0603 .....	97
Table A.2 – Results for Lateral Resolution, NA=0.0901 .....	98
Table A.3 – Results for Lateral Resolution, NA=0.1186 .....	99
Table A.4 – Results for Axial Resolution, NA=0.0603 .....	100
Table A.5 – Results for Axial Resolution, NA=0.0901 .....	101
Table A.6 – Results for Axial Resolution, NA=0.1186 .....	102
Table A.7 – Results for Multiply Scattered Photons (Scaled and Unscaled), NA=0.0603 ....	103
Table A.8 – Results for Multiply Scattered Photons (Scaled and Unscaled), NA=0.0901 ....	104
Table A.9 – Results for Multiply Scattered Photons (Scaled and Unscaled), NA=0.1186 ....	105

## ABSTRACT

This thesis presents the results of a study investigating the effects on the axial and lateral resolution of a time-domain optical coherence tomography (OCT) system, as a function of tissue optical properties and system numerical aperture. In theory, the equations governing the axial and lateral resolution of OCT are well characterized and defined. However, empirical evidence from previous studies performed by Dr. Jennifer Barton and her colleagues have seemed to indicate that these equations do not fully describe the trends observed when using OCT in the presence of multiply scattered photons due to imaging through highly scattering media. This study aimed to further investigate these observations by performing OCT on a series of tissue phantoms with varying parameters and with varying system parameters in order to identify what trends may exist between the axial and lateral resolutions of the resulting images, the scattering and absorption characteristics of the tissue phantoms, and the numerical aperture of the OCT system itself. Over the course of this study, it was concluded that the optical properties of the tissue being analyzed by OCT do not seem to impact either the axial resolution or the lateral resolution of the results (at least over the range of parameters covered), with the axial resolution being purely a function of the source and the lateral resolution being a function of the optics present in the system. These findings support the theoretical equations governing OCT and suggest that the empirically observed apparent decrease in resolution in highly scattering media may be an artifact due to errors in operation or alignment of the system, or simply not apparent with our setup of a highly reflective object placed at focus.

# 1 – INTRODUCTION

## 1.1 – INTERFERENCE AND LOW COHERENCE INTERFEROMETRY

At the heart of tissue optics is a concept known as interference. When considering the wave nature of light, interference occurs when two or more waves overlap in space and time, and form a composite wave that happens to have an irradiance different than a simple sum of the irradiance values of the component waves. This resulting wave may have a higher or lower amplitude than the sum of the components depending on the phase information of the component waves. By the principle of the superposition of waves, two spatially overlapped monochromatic plane waves will result in the summation of the complex amplitude of the electric field of the component plane waves, shown in Equation 1.1 below <sup>[1],[6]</sup>. As the irradiance of a plane wave is equal to the square modulus of the complex amplitude, the irradiance of the resulting wave can be found as shown in Equations 1.2 and Equation 1.3 below. The final result is that the irradiance of the resultant wave is equal to a sum of the irradiance of the component waves and an “interference term” made up of the component wave irradiance values and a phase delay term <sup>[6]</sup>. When this phase delay term is an even multiple of  $\pi$ , constructive interference will occur, and the resulting irradiance will be greater than the sum of its parts. Conversely, when the phase delay term is an odd multiple of  $\pi$ , destructive interference will occur, and the resulting irradiance will be less than the sum of its parts. For other phase delays, the resulting irradiance will have a corresponding value between the upper and lower maximum irradiance values <sup>[6]</sup>.

$$U(\vec{r}) = U_1(\vec{r}) + U_2(\vec{r}) \quad (Eq\ 1.1)$$

$$I(\vec{r}) = |U(\vec{r})|^2 = \sqrt{I}e^{i\phi} = \sqrt{I}[\cos(\phi) + i\sin(\phi)] \quad (Eq\ 1.2)$$

$$I(\vec{r}) = I_1 + I_2 + 2\sqrt{I_1 + I_2} \cos(\phi_2 - \phi_1) \quad (Eq\ 1.3)$$

From this interference results a pattern of higher and lower irradiance bands that form what is known as a fringe pattern. This fringe pattern can be manipulated and analyzed through a set of techniques called interferometry that take advantage of interference to show information about the wave or the material the wave is propagating

through [6]. Fittingly, interferometric analysis is performed with instruments called interferometers. While there are many kinds of interferometers that suit a wide range of applications, the system used in this study is specifically a Michelson interferometer. In a Michelson interferometer, light from a singular source will be split into a test arm and a reference arm before recombining and interfering later in the system, as shown in Figure 1.1 below. Deviations in the two beam paths will result in the two returning beams having a phase difference that in turn will yield a pattern of interference fringes. From this fringe pattern, details about the differences between the beam paths can be determined [6].

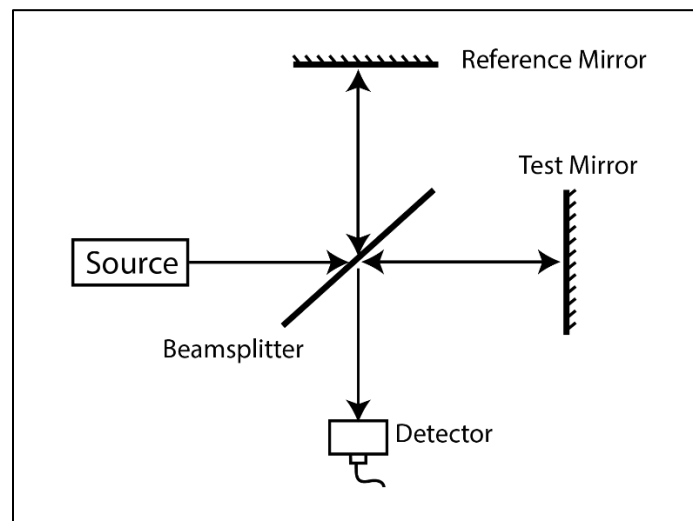


Figure 1.1 – General format for a Michelson Interferometer. Image Credit: Nikki Galvez

Just as there are many types of interferometers, there are also many types of interferometry that offer their own unique advantages and disadvantages. The system used in this study utilizes what is known as low coherence interferometry. Coherence refers to how well two waves are correlated based on the cross-correlation function, which quantifies the ability to predict the phase of one wave based on the phase of another [6]. Perfectly coherent waves will always exhibit the same phase behavior in reference to the other; so long as the phase of one wave is known, the phase of the other is also known. This concept of coherence can be further specified to temporal coherence, or the ability of a wave to interfere with a version of itself that has been delayed in time [6]. Just as coherence is mathematically described using the cross-correlation function, temporal coherence is described using the mutual coherence function, a form of autocorrelation shown below in Equation 1.4 as a function of the electric field  $E$ , position  $r$ , and time  $t$  [6].

$$\Gamma(\vec{r}_1, t_1; \vec{r}_2, t_2) = \langle E^*(\vec{r}_1, t_1)E(\vec{r}_2, t_2) \rangle \quad (\text{Eq 1.4})$$

In the specific application of low coherence interferometry, the light source is broadband and exhibits low temporal coherence [20]. With a low coherence source, interference fringes will only occur so long as the path difference between the test and reference arms is within what is known as the coherence length. The coherence length is the distance over which a temporally coherent wave can interfere with a copy of itself, and is defined based on  $1/e$  or 37% fringe visibility. Fringe visibility, given below in Equation 1.5, quantifies the contrast of an interference pattern based on the maximum and minimum fringe irradiance [6].

$$v = \frac{I_{max} - I_{min}}{I_{max} + I_{min}} \quad (\text{Eq 1.5})$$

## 1.2 – LIGHT-MATTER INTERACTIONS IN TISSUE

When light interacts with matter, there are a number of different phenomena that can occur, such as absorption, reflection, transmission, emission, and scattering. Of particular interest to tissue optics, and this study in particular, are scattering and absorption [34]. Absorption occurs when electromagnetic energy is transferred from light to the matter itself, while scattering occurs when light interacts with a particle, typically in an inhomogeneous medium, and deviates from its original pathway thereby transferring energy from the incident beam into a scattered beam. The degree to which a medium absorbs or scatters light is described by the absorption coefficient  $\mu_a$  and scattering coefficient  $\mu_s$  respectively, which are typically measured in  $\text{cm}^{-1}$  or  $\text{mm}^{-1}$ . The absorption coefficient is defined as the probability that photons will be absorbed after travelling some distance within a material. Similarly, the scattering coefficient is defined as the probability that photons will be scattered after travelling some distance within a material [6]. The total attenuation in a medium is defined with the Beer-Lambert Law (or Beer's Law), in which the amount of light that passes through a medium is shown to exponentially decay with the distance through the medium,  $t$ , and the attenuation coefficient,  $\mu$ , a sum of the absorption and scattering coefficients. Beer's Law is given below in Equation 1.6 [1]. Based on Beer's Law,  $\mu_a$  and  $\mu_s$  can be precisely described as the inverse of the distance light has to travel

through a medium such that 73% or  $\left(1 - \frac{1}{e}\right)$  of the initial irradiance has been absorbed or scattered, respectively.

$$I = I_0 e^{-\mu t} \quad (\text{Eq 1.6})$$

Light-tissue interactions are dominated by scattering effects, as tissues in the body tend to be highly inhomogeneous with many different sizes and shapes of particles with many indices of refraction [1],[2],[28]. With this in mind, scattering behaviors in human tissue are also incredibly challenging to properly characterize. When light scatters off of a particle, the behavior of the scattering can be described by Mie Theory, which uses Maxwell's Equations to determine the direction and magnitude of the scattered fields [6],[23]. While robust, Mie theory can be extremely mathematically intensive to apply to real world situations and becomes further complicated in media with particles of many sizes, shapes, and properties. As a result of this mathematical complication, tissue is nearly impossible model purely with Mie theory. Scattering particles cover a full range of sizes from nanometers to meters, in all manners of irregular shapes. Refractive indices vary substantially from particle to particle, and scattering particles are randomly oriented. While Mie theory could in theory, and with unlimited time and computing power, be used to model the scattering behavior of tissue, it is much more realistic and useful to make approximations of Mie theory instead [6],[12],[23],[28].

The scattering described in Mie theory is highly anisotropic, meaning that much of the scattered light will preferentially follow a specific directionality. Anisotropy,  $g$ , is the expected cosine of the scattering angle and is measured on a scale from -1 to 1, in which an anisotropy of -1 describes purely backscattering while an anisotropy of 1 describes purely forward scattering [1],[12]. The anisotropy of a medium is used in conjunction with the scattering coefficient to calculate the reduced scattering coefficient, given below in Equation 1.7 [30]. The reduced scattering coefficient is of utmost importance in tissue optics, as it describes the light attenuated due to scattering while maintaining information about the directionality of this scattered light. While the reduced scattering coefficient and anisotropy are simplifications of the overall scattering effects of the system, they describe

this behavior extremely well for relatively homogeneous tissue, and as such have become a staple in the field of tissue optics [6],[30].

$$\mu'_s = \mu_s(1 - g) \quad (\text{Eq 1.7})$$

### 1.3 – OPTICAL COHERENCE TOMOGRAPHY

As mentioned previously, optical coherence tomography is a type of low coherence interferometry based on a Michelson Interferometer [20]. The type of OCT used in this study is known as Time-Domain OCT, in which depth scans, also known as A-Scans, are performed by changing the length of the reference arm at a constant speed  $v_{ref}$ , over a distance corresponding to the depth range to be scanned in the sample. The speed of the reference arm introduces a Doppler frequency,  $f_r(t)$ , that results in an amplitude modulated signal. This modulated signal can then be demodulated at the Doppler frequency to generate a high dynamic range depth scan, which is proportional to the backscattering amplitude. The Doppler frequency is given in Equation 1.8, in which  $\lambda$  is the central wavelength of the broadband source. The detector interference signal,  $i_d(t)$ , is given in Equation 1.9, in which  $A(t)$  is the amplitude and  $\phi(t)$  is the phase [26].

$$f_r(t) = \frac{2v_{ref}}{\lambda} \quad (\text{Eq 1.8})$$

$$i_d(t) = A(t) \cos(2\pi f_r t + \phi(t)) \quad (\text{Eq 1.9})$$

As with all low coherence interferometric systems, the interference in Time-Domain OCT will only occur so long as the path lengths differ less than the coherence length of the source [1]. Additionally, by translating the test arm target laterally with respect to the path of the beam, a series of A-scan images can be taken across the surface of the sample, allowing for a cross-sectional scan to be taken. This is what is referred to as a B-Scan. A simplified layout of a fiber based Time-Domain OCT system is shown in Figure 1.2 [16],[20].

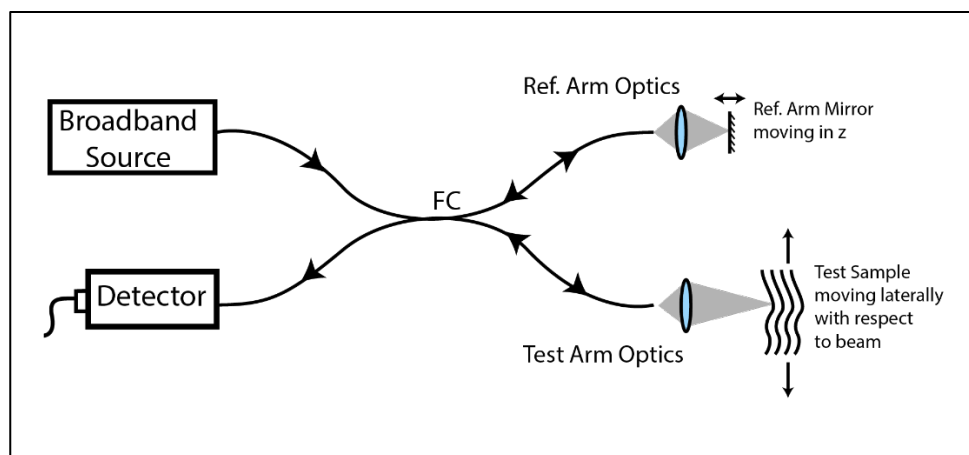


Figure 1.2 – Time-Domain OCT example layout. Image Credit: Nikki Galvez

The system used in this study varies the reference arm path length through the use of a galvanometer that rapidly oscillates a corner cube back and forth. So long as the corner cube remains in the beam path, the light in the reference arm will perfectly retroreflect regardless of the added path length. The broadband light source in this system is a pair of super luminescent diodes (SLDs) with slightly separated peak wavelengths, allowing the system to have a broad bandwidth of 56 nm with a central wavelength of 1300 nm while maintaining relatively similar power over the range of wavelengths.

In OCT, light travels from the source into a sample where it then interacts with the particles in the sample. As the photons are scattered and absorbed throughout the medium, a certain amount of them will backscatter into the system where they will interfere with the light from the reference arm. Based on the total distance the light in the test arm traveled, the OCT will determine that the photon traveled a distance of half that amount into the sample <sup>[1]</sup>. In real world applications however, this analysis poses certain challenges. As the light propagates through the scattering medium, certain photons may repeatedly scatter off of numerous particles, with each scattering event changing the direction of the photons' propagation. As the number of scattering events increase, the distance this photon traveled may become much larger than twice the depth it traveled into the material <sup>[1]</sup>. When these so-called Multiply Scattered Photons return to the detector, the system thinks that, based on the length of their optical paths, they traveled to a much further depth than they might have actually traveled, as illustrated in Figure 1.3. Multiply



A key feature of OCT is that the axial and lateral resolution of the system are decoupled [6]. The lateral resolution is a function of the optics in the system, and more specifically the numerical aperture (NA). This is because, for the purposes of determining the lateral resolution, OCT can be considered a confocal microscope with a very low NA [1],[6]. The equation for defining the lateral resolution in terms of the full width at half maximum (FWHM), the approach taken in this study, is given in Equation 1.10 [6].

$$\delta x, \delta y = \frac{0.37\lambda}{NA} = \frac{0.37\lambda}{n \sin \theta} \quad (Eq 1.10)$$

By contrast, the axial resolution is a function of the coherence length of the source,  $l_c$ , which itself is a function of the central wavelength and the bandwidth of the broadband source. The equation governing the axial resolution is given below, in Equation 1.11.

$$\delta z = \frac{l_c}{2} = \frac{2 \ln 2}{\pi} \frac{\lambda_0^2}{\Delta \lambda} \quad (Eq 1.11)$$

The hypothesis tested in this study is that these resolution equations are idealized and only hold strictly true for non-scattering samples. In practice, perhaps the presence of multiply scattered photons will degrade the image quality and resolution of the system, as photons that never hit the target but have equivalent path length are assumed to have come from the target.

## 1.4 – TISSUE PHANTOMS

In many tissue optics studies, it is not feasible or realistic to use real tissue during experiments. In place of this, it is common to use what is known as a tissue phantom: a mixture of non-biological materials that can be made to simulate the bulk optical properties of a targeted tissue [5]. The primary optical properties targeted for simulation with tissue phantoms are the scattering coefficient, absorption coefficient, and reduced scattering coefficient. By virtue of the inversely proportional relationship between these coefficients, measured in  $\text{cm}^{-1}$ , and distance, it is possible to simulate the properties of a specific depth of an attenuating medium [5]. Beer's Law shows that the total amount of attenuation as light travels a set distance through an attenuating medium is the same as if the light had traveled half as far through a medium with twice the attenuation. This

property is fundamental to the creation of tissue phantoms, as it allows for highly scattering tissue with thicknesses on the order of microns to be simulated in a test environment with any desired tissue phantom depth or thickness [29].

Many different kinds of tissue phantoms exist, some solid, some liquid, that use a wide range of different materials in order to simulate a variety of different tissue types. Liquid tissue phantoms, the kind of tissue phantom used in this study, are typically made of water, an absorbing material, and a scattering material in order to have control over the aforementioned properties [5],[29]. As the anisotropy is a material specific property, in many cases it cannot be properly simulated, which means that only the scattering coefficient or the reduced scattering coefficient can be simulated, but not both.

In this study, the tissue phantoms are composed of water, Intralipid 20%, and India Ink. Intralipid 20%, a 20% concentration of a lipid emulsion typically used as an intravenous source of nutrients, is a commonly used scatterer in liquid tissue phantoms, as the size and shape of the particles are on the proper order as many of the particulates in tissue [27]. Additionally, its optical properties are very consistent between brands and batches, meaning that its properties can be reliably cross-referenced with studies that have been performed previously. The particles also stay in emulsion well, allowing for long periods of use without fear of particles settling or precipitating out of solution. It does tend to have a lower anisotropy value than most bulk tissue, but for many applications, its accessibility combined with its other benefits make it a strong choice in scatterer [27].

India Ink is a strong absorber, but it does pose a few notable challenges that must be addressed when using it in an experimental setting. India Ink is primarily an art supply, not a precision laboratory chemical, so the optical properties from brand to brand and batch to batch tend to vary substantially [25]. Additionally, India Ink is not a molecular absorber, meaning that it can impact both the absorption and scattering effects of a solution. Fortunately, however, both of these challenges can be overcome. Based on the work done in "The use of India ink in tissue-simulating phantoms," it was discovered that while India Ink varies greatly between batches, all of the ink in a single batch has incredibly consistent optical properties [25]. While this means that before use in a laboratory setting, the optical properties of the ink will need to be experimentally determined, it also means that once

defined, one can have confidence that these properties will be true for the full bottle of ink. Additionally, it was found that India Ink can be added to Intralipid without changing its scattering properties, under a certain circumstance that is [25]. India Ink particulates are incredibly small, but tend to coagulate over time and form larger masses of particulates. The small, individual particles do not contribute to Intralipid's scattering properties, but these larger masses will [25]. By immersing an India Ink dilution in an ultrasonic bath, the coagulated particulates will be dispersed before reforming into the larger masses again slowly over time [25]. With these considerations in mind, India Ink and Intralipid can be used to effectively simulate tissue so long as the proper steps are taken to mitigate the inherent challenges associated with these materials [29].

## 1.5 – PRIOR ART

Between the years of 1993 and 1995, Dr. Joseph M. Schmitt and his colleagues released a number of papers detailing the newly discovered ability to use low-coherence interferometry to measure the optical properties of dense biological tissues, with heavy emphasis placed on the limitations of the technology and the effects of multiple scattering on the resulting images [15],[16],[17],[18],[24]. These papers have served as foundation for the continued and widespread use of OCT in tissue optics over the past 25 years. As the technology has grown more sophisticated, it has been used in countless studies as a vital technique to show the optical properties of certain materials or cell structures in specific applications [9],[10],[11],[13],[14],[19],[32],[33],[35].

Conversely, however, there are relatively few studies since the inception of the technology that have discussed OCT as a discipline, and fewer still (if any) that touch on how OCT resolution varies based on the properties of the analyzed media. With this in mind, the questions being investigated by this study and the subsequent findings represent novel information for the field of tissue optics.

## 2 – METHODS

The complete list of materials and instructions for the methods outlined in this section have been included in Appendix 5.1 through Appendix 5.8 for further reference.

### 2.1 – CREATION OF TISSUE PHANTOMS

The first step in the study was to determine the optical properties of Intralipid 20% and India Ink. Much of the documented work done with tissue phantoms is performed in the 300 to 1000nm range and as a result, there is little information available at 1300nm, the desired wavelength for this study. Thus, in order to create the tissue phantoms needed for this experiment, the optical properties of India Ink and Intralipid 20% had to be either calculated or experimentally determined [29]. The other component of the tissue phantom, water, has been well characterized and documented across the UV, visible, and infrared spectra. According to values reported in the papers “The complex refractive index of water,” “Optical properties of water in the near infrared,” and “Refractive indices of water and ice in the 0.65- to 2.5- $\mu\text{m}$  spectral range,” the absorption coefficient of water at 1300 nm is  $1.35 \text{ cm}^{-1}$  [8],[21],[22].

The reduced scattering coefficient of Intralipid 20% used in this study was calculated based on the findings given in “Dependent scattering in Intralipid phantoms in the 600-1850 nm range” [4]. While this paper did not explicitly report a full list of tabulated data for the optical properties within the described wavelength range, it did give fit functions that were matched to their experimental results, as well as plots of  $R^2$  fit values versus wavelength were given to show how well the functions fit the experimental data. These equations, given below, were used to calculate the reduced scattering coefficient for Intralipid 20% at 1300 nm, which was found to be  $49.19 \text{ cm}^{-1}$ . Equation 2.1 describes the variable packing dimension  $p$ , in terms of wavelength. Equation 2.2 describes the wavelength dependent slope,  $k(\lambda)$ , for the linear polynomial fit function for the anisotropy,  $g(\lambda, \phi_p)$ . Equation 2.4, Equation 2.6, and Equation 2.7 are given in terms of volume concentration  $\phi_p$ , and set equal to  $0.227 \text{ mL/mL}$  [4].

$$p(\lambda) = 1.31 + 0.0005481\lambda \quad (\text{Eq 2.1})$$

$$k(\lambda) = -10 + 0.05047\lambda - 9.693 \cdot 10^{-5}\lambda^2 + 8.449 \cdot 10^{-8}\lambda^3 \dots \quad (Eq 2.2)$$

$$\dots - 3.412 \cdot 10^{-11}\lambda^4 + 5.204 \cdot 10^{-15}\lambda^5$$

$$\mu_s^{indep}(\lambda) = 1.868 \cdot 10^{10}\lambda^{-2.59} \quad (Eq 2.3)$$

$$\mu_s(\lambda, \phi_p) = \left( \frac{\mu_s^{indep}(\lambda)}{0.227} \right) \phi_p \left\{ \frac{(1 - \phi_p)^{p(\lambda)+1}}{[1 + \phi_p(p(\lambda) - 1)]^{p(\lambda)-1}} \right\} \quad (Eq 2.4)$$

$$g^{indep}(\lambda) = a \left( \frac{1 - f}{1 + e^{c(\lambda+d)}} + f \right) + b \left( \frac{1 - h}{1 + e^{c(\lambda+d)}} + h \right) \lambda \quad (Eq 2.5)$$

$$\text{given } a = 1.094; b = -5.653 \cdot 10^{-4}; c = 5.3 \cdot 10^{-3};$$

$$d = \frac{a(f - 1)}{b(h - 1)}; f = 0.3516; h = 0.1933$$

$$g(\lambda, \phi_p) = g^{indep}(\lambda) + k(\lambda)\phi_p \quad (Eq 2.6)$$

$$\mu'_s(\lambda, \phi_p) = \mu_s(\lambda, \phi_p)[1 - g(\lambda, \phi_p)] \quad (Eq 2.7)$$

With the scattering coefficient of Intralipid 20% calculated, the absorption coefficient of Intralipid 20% had to be determined. Based on tissue optics standards, as well as findings given in “Supercontinuum laser based optical characterization of Intralipid phantoms in the 500-2250 nm range” and “Optical properties of human skin in the near infrared wavelength range of 1000 to 2200 nm,” the absorption coefficient of Intralipid 20% was assumed to be equivalent to water at 1300 nm [3],[31].

With Intralipid 20% fully characterized, the optical properties of India Ink had to be determined. The paper “The use of India ink in tissue-simulating phantoms” notes that if properly agitated, India Ink particles will not contribute to the scattering properties of an Intralipid 20% and water based tissue phantom [25]. Therefore, the only optical property of India Ink that had to be found was the absorption coefficient. The absorption coefficient had to be experimentally determined due to the inconsistency of India Ink’s inter-batch optical properties [25].

An experiment was designed based on the procedures given in “Determination of Absorption Coefficient of a Solution by a Simple Experimental Setup” [7]. As shown in the following Figure 2.1, 1300 nm laser light from two super luminescent diodes (SLDs) passed

through a single mode fiber (SMF-28) and then passed through a beam collimator. The collimated laser light passed through an ND filter and the test region, and then was detected by a photodiode and processed by a power meter. The ND filter was placed directly after the collimator in order to control the amount of light hitting the photodiode. Additionally, the filter was rotated by a few degrees about the azimuthal axis to help mitigate the impact of any back reflections on the power readings. The test region consisted of a glass cuvette filled with deionized water or a glass cuvette filled with one of three mixtures of India Ink and water. The cuvette was always placed perpendicular to the beam such that the beam always passed through 1 cm of the test material. The cuvette was placed on a test stage such that its position was kinematically constrained between trials. The photodiode was placed such that the beam struck the center of the detector element with normal incidence.

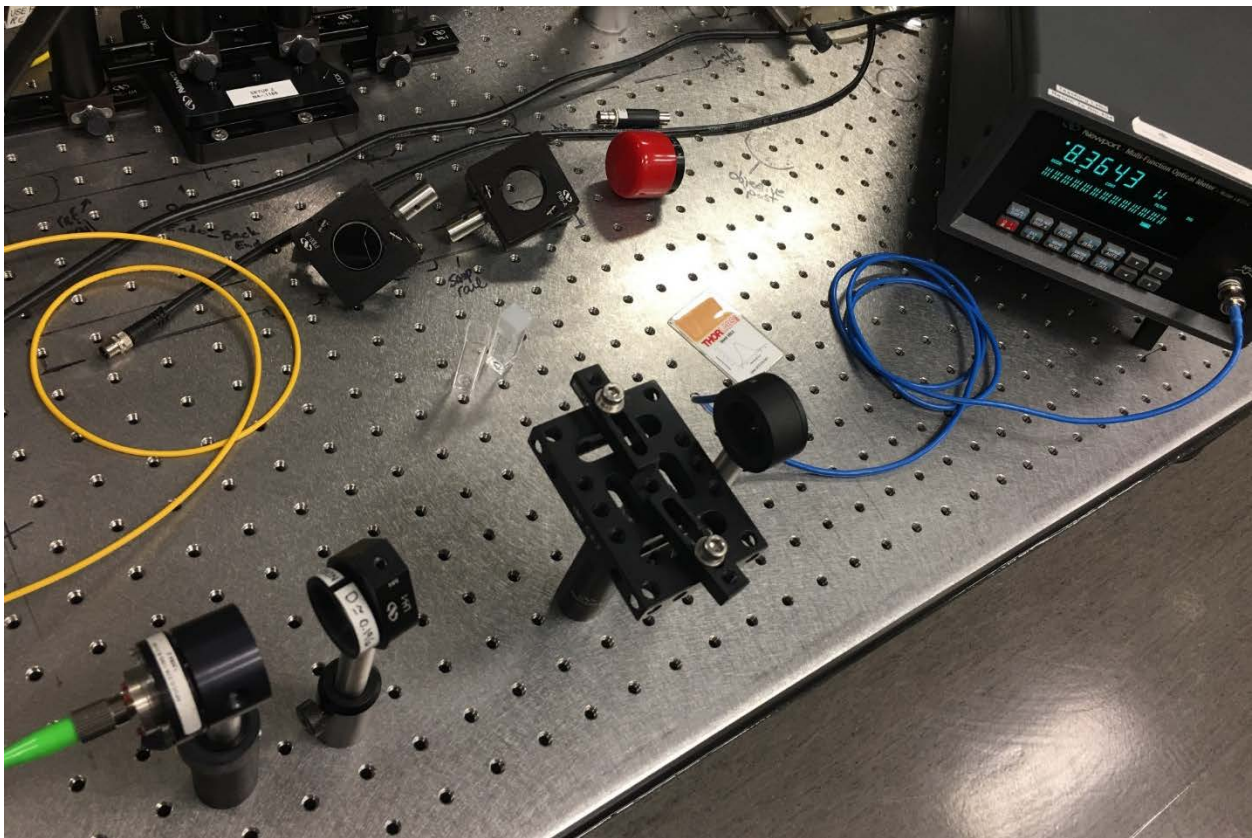


Figure 2.1 – Experimental setup for determining absorption coefficient of India Ink

The India Ink was introduced to an ultrasound bath for 30 minutes at the highest power available before being diluted with water, as well as immediately before testing in

order to prevent the ink particles from clumping and causing unwanted scattering effects as described in “The use of India ink in tissue-simulating phantoms” [25].

Three total trials were performed in which each of the six different test materials were tested once per trial. The test material was introduced into the beam path and then the average value of the power meter was recorded over a 30 second time frame before moving onto the next test material. After three trials, the recorded average power values were again averaged, and then used to calculate the absorption coefficient at 1300 nm for the batch of India Ink used during this study. The equation used, a variant of Beer’s Law, is given below in Equation 2.8. The incident power,  $I_0$ , came from the power measured from the deionized water trial. The distance travelled through the medium,  $t$ , is given in cm and the absorption coefficient,  $\alpha$ , is given in  $\text{cm}^{-1}$ .

$$I = I_0 e^{-\alpha t} \rightarrow \alpha = \frac{-\ln\left(\frac{I}{I_0}\right)}{t} \quad (\text{Eq 2.8})$$

After determining the optical properties of all the tissue phantom components, the tissue phantoms were created. In order to facilitate the dilution process and minimize the amount of Intralipid 20% consumed, the phantoms were made using serial dilutions. Two sets of phantoms were made: one with only Intralipid 20% and water, and one with India Ink, Intralipid 20%, and water.

The serial dilution process began by creating a solution of water and Intralipid 20% that had a high concentration of Intralipid 20%. This solution was diluted three times over, with each dilution reducing the concentration of Intralipid 20% in the solution by half. This process resulted in four “Master Solutions.” A second round of dilutions occurred in which each of the Master Solutions were used to create four “Test Solutions” that would be used when taking OCT measurements. The first dilution was performed to match the desired reduced scattering coefficient, while the second dilution was performed to match the desired effective depth. This amounted to 16 tissue phantoms that simulated 16 combinations of tissue properties in a test environment with a fixed depth. Due to the selected dilution factors, 10 unique concentrations of Intralipid were created, with 6 so-called “redundant dilutions” that were not used during the experimental procedures. The

reasons for this occurring and the implications thereof are explained in Section 1.4 – Tissue Phantoms and in Section 3.4 – Phantom Dilution Calculation.

Creating the tissue phantoms with the India Ink followed nearly an identical process to the trial without the ink present, as the amounts of Intralipid 20% and DI water were not altered. The amount of ink needed to reach the desired absorption coefficient changed the total volume of the solution by an insignificant amount, which meant that the calculation for determining the concentration of Intralipid 20% remained unchanged. The bottle of India Ink was immersed in the ultrasound bath for 30 minutes before dosing the requisite amount of ink into each of the 16 Test Solutions. As in the previous trial, the 10 unique solutions were used for the experiment, while the 6 redundant solutions were set aside.

## 2.2 – OCT ALIGNMENT AND TEST PREPARATION

Upon completion of the phantom creation process, the Time-Domain OCT system had to be set up for proper data collection. In this study, the OCT system was operated at three different numerical apertures that would be regularly exchanged throughout the experiment. Thus, there was a need to create a modular system that could be reliably removed and reintroduced into the system while being confident that the system alignment remained constant. Not only that, the alignment had to be consistent regardless of which numerical aperture was present in the system.

The solution to this was to utilize a set of three kinematic base plates that would each hold a set of two lenses. Each of these two-lens systems formed a beam expander that would change the numerical aperture and could be individually adjusted and aligned without impacting the other trials. Additionally, the kinematic base would serve to reliably position the lenses at the same point each time they were added back into the optical system. The three modular lens systems were designed in Zemax OpticStudio, and then built using mounting fixtures in the lab. The lenses were held in place using threaded retaining rings and fixed lens mounts that were attached to optical posts and then affixed to miniature optical rails. These rails were set onto the tops of the kinematic base plate, and then introduced into the OCT system for alignment.

The alignment process was performed by starting with no beam expanding optics present in the system. The OCT test arm was blocked while an oscilloscope was connected to the detector's DC output. The tip and tilt of the reference arm mirror were adjusted until the signal reached a maximum. The reference arm was then blocked, at which point the tip and tilt of the target mirror were adjusted until the signal again reached a maximum. The reference arm was unblocked, at which point the oscilloscope was used to check for an interference pattern between the two arms, indicative of the reference arm and test arm path lengths being matched. If interference had not been achieved, the reference arm path length was adjusted by slowly moving the linear translation stage attached to the mirror galvanometer, or galvo.

Upon achieving interference, one of the modular lens systems was introduced into the system with only the first lens in the module present. The lens was set to the same height as the beam collimator, and adjusted to ensure the beam path was coincident for both directions of travel: from the fiber to the mirror and from the mirror to the fiber. The second lens was introduced back into the module, and aligned following a similar method to the previous lens. The kinematic base plate and optical rail positions were also adjusted during this process. Once the system had been properly aligned for this lens module, the kinematic base plate was firmly locked in place and not moved for the duration of the testing. This process was repeated for the remaining two lens modules, until the three systems were properly aligned. Proper alignment was achieved when all three modules resulted in the system coming to a focus in the same position, such that the test mirror position did not need to be adjusted when swapping between the modules. It should be noted that even with a properly aligned system, the length of the reference arm had to be adjusted when swapping between the lens modules due to the difference in optical path length caused by the different set of lenses present in each module.

Next, a means of holding the tissue phantom and the test target had to be created. Using SolidWorks, three different components were designed and then 3D printed to accomplish this. The tissue phantom would be held in a box shaped vessel with a sloped edge meant to support a thin piece of cover glass, which would eliminate the meniscus formed by the liquid tissue phantom as well as limit the impact of back reflections. A small

groove was cut into the side to assist with removing the test target. The tissue phantom holder would be supported on a tip-tilt lens mount, but couldn't be directly attached as the phantom holder needed to be easily removed and manipulated during the experiment while maintaining a high degree of positional repeatability. The solution was to create a two-part kinematic mount, one that would be bonded to the tip-tilt stage and one that would be bonded to the phantom holder.

After designing and 3D printing the custom parts, and then bonding them with hot glue and cyanoacrylate glue, the target mirror in the test arm was replaced by the 3D printed assembly. A 1" square mirror was placed in the phantom holder as a temporary test target. The position, tip, and tilt of the assembly was adjusted until proper alignment had been achieved for the new setup. The square mirror was removed and then replaced by the test target, a 1" square Ronchi ruling with 25 line pairs per mm, for which the position of the assembly was once again slightly adjusted in order to reach proper alignment. Figure 2.2 below shows a picture of the test configuration taken upon completion of the alignment procedures, with the individual system components labeled.

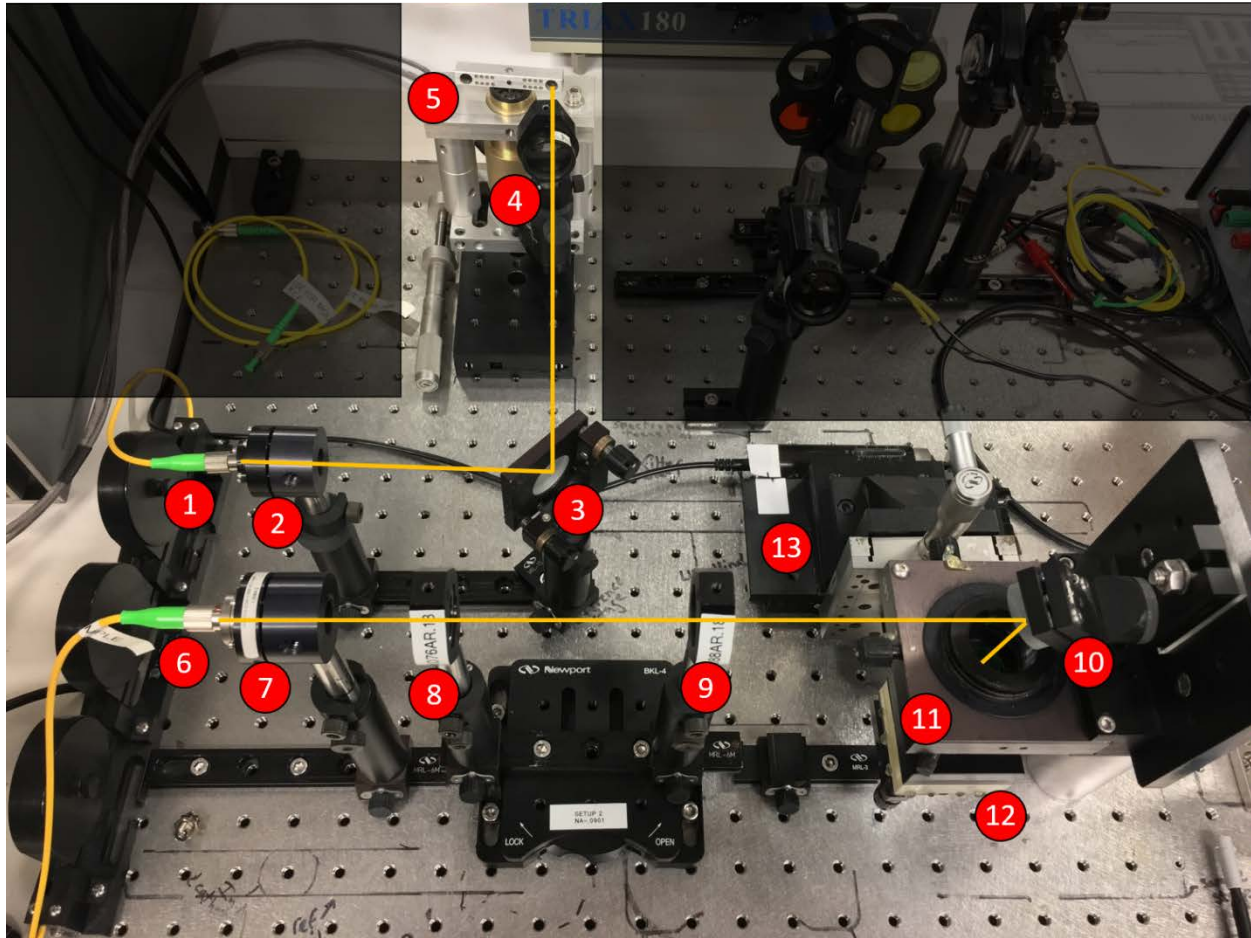


Figure 2.2 – Picture of the Time-Domain OCT laboratory setup. The optical axis for the test arm and reference arm are noted with the yellow lines. The labeled components for the Reference arm are as follows: (1) Fiber output, (2) Beam collimator, (3) Fold mirror, (4) ND Filter for controlling reference arm power, (5) Galvo with a corner cube mounted in the beam path. The labeled components for the Test arm are as follows: (6) Fiber output, (7) Beam collimator, (8) First lens of modular lens setups, (9) Second lens of modular lens setups, (10) Fold mirror, (11) Focusing lens and mounting fixtures, (12) Tissue Phantom Holder mounted to a tip-tilt stage, (13) Motorized linear translation stage for sample.

After the system was aligned and all components had been integrated, the OCT system was used to determine the distance travelled through the phantom. The Ronchi ruling was placed into the bottom of the phantom holder and then the cover glass was moved into position. Using the test arm micrometer, the focus of the OCT system was moved from the top of the Ronchi ruling to the bottom of the coverslip. The micrometer position was noted before and after moving, which was used to calculate the distance.

Prior to beginning the experimental procedures, the settings for the Lock-In Amplifier and LabView code were inputted. Most settings were decided based on previous experiments using this system; however, the lateral range of the B-Scan and the number of A-scans in the B-Scan were determined based on the test target and the NA of the three system setups. The lateral range was set to 2 mm in order to guarantee the scan would cross at least three chrome-glass transitions on the Ronchi ruling, which had a frequency of 25 line pairs per inch (lp/inch). The number of A-Scans was determined based on the size of the beam waist at the focus position for each of the three systems. The size of the beam waist drives the required lateral pixel size to properly resolve the chrome-glass interface, which in turn drives the number of scans. From the calculations performed using Equation 2.9, it was determined that at least 250 scans per mm, or 500 scans over the lateral range of 2 mm, were required to adequately resolve the edge of the line pairs. With these settings, the size of the OCT images were 500 pixels by 512 pixels, or 2mm by 2mm.

$$w_0 = \frac{\lambda}{\pi \sin^{-1}(NA)} \quad (Eq\ 2.9)$$

### 2.3 – EXPERIMENTAL PROCEDURES AND DATA ACQUISITION

The experiment itself followed a set of steps that were repeated for each new tissue phantom that was introduced into the system. After inserting the first lens module, aligning the system, and confirming that the signal had been maximized, the Ronchi ruling was placed into the phantom holder. The first phantom was slowly dispensed on top of the ruling and then covered with the cover glass, at which point the holder could be placed back into the system. Upon verification of the alignment and software settings, image acquisition could begin. Three images were captured with the same system settings in order to test intra-run repeatability. A fourth image was captured in which the signal from the chromed sections of the Ronchi ruling was overloading the detector, while the glass sections were not overloaded. The lenses were swapped for the second module, the images were acquired, and then this was repeated for the final lens module. The phantom holder, Ronchi ruling, and cover glass were removed, drained, cleaned, and dried. This process was then repeated for each of the tissue phantoms for both of the trials. For the tissue phantoms made using India Ink, the only difference in the test procedure was that the

phantoms had to be immersed in the ultrasonic bath for at least 30 minutes prior to use. If the data acquisition process took longer than 30 minutes after being removed from the ultrasonic bath, the phantom was reintroduced into the sonicator and the data collection was restarted for that specific phantom.

The OCT LabView software outputs the acquired images as tab separated text files. These text image files were manipulated with Python code and the ImageJ software to calculate the lateral resolution, axial resolution, and a count of the number of multiply scattered photons. The lateral resolution was analyzed with a Python script put together by Travis Sawyer in support of this study. The pixel values are taken across a glass-chrome transition line, fit to the logistic function to yield a sigmoid curve, numerically differentiated, and then fit to a Gaussian, the FWHM of which defines the resolution. The FWHM was found for each of the three runs for a given numerical aperture and tissue phantom, and then averaged to find a single representative value for that combination. Figure 2.3 below shows the steps performed by the fitting function as a set of raw data from a glass-chrome transition is analyzed and ultimately fit to a Gaussian function.

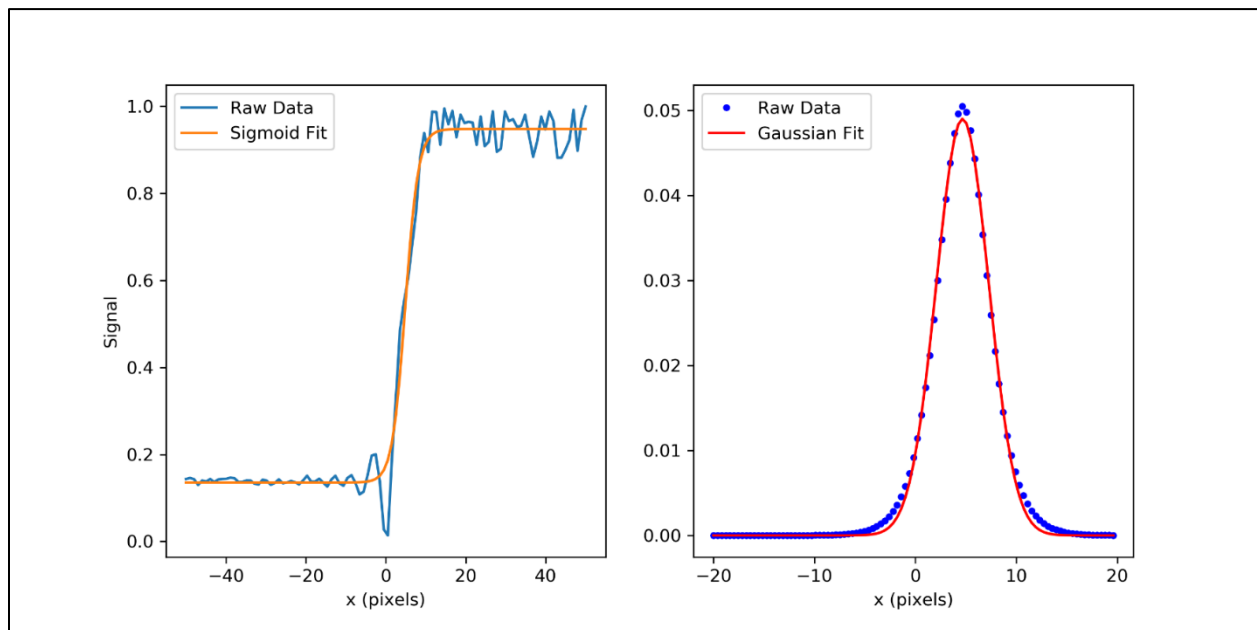


Figure 2.3 – Plotted report of the fitting function for the analysis of Lateral Resolution, showing an example of the Raw Data from a glass-chrome transition being fit to a sigmoid. The raw data is fit to the logistic function to extract the sigmoid curve, shown in the left image. The re-sampled data was

then numerically differentiated to yield the raw data shown in the right figure, and then fit to a Gaussian lineshape to extract the FWHM.

The axial resolution was analyzed using the *Plot Profile* function in ImageJ. When opened in ImageJ, the text image from the OCT was transposed such that the left side of the image was the tissue phantom and the right side of the image was inside the Ronchi ruling. A rectangular box was drawn across one of the chrome sections, and the *Plot Profile* function was used. The function averages each column of pixels values across the box, resulting in a single Gaussian curve representing the light hitting the chrome interface. Through the use of interpolation, the FWHM of this Gaussian was taken for each run and then averaged with the other runs for the combination of system parameters. Figure 2.4 below shows a test image opened in ImageJ with the rectangular box for the *Plot Profile* function drawn in place, along with a plot of the output from this function and the interpolated FWHM value presented in pixels.

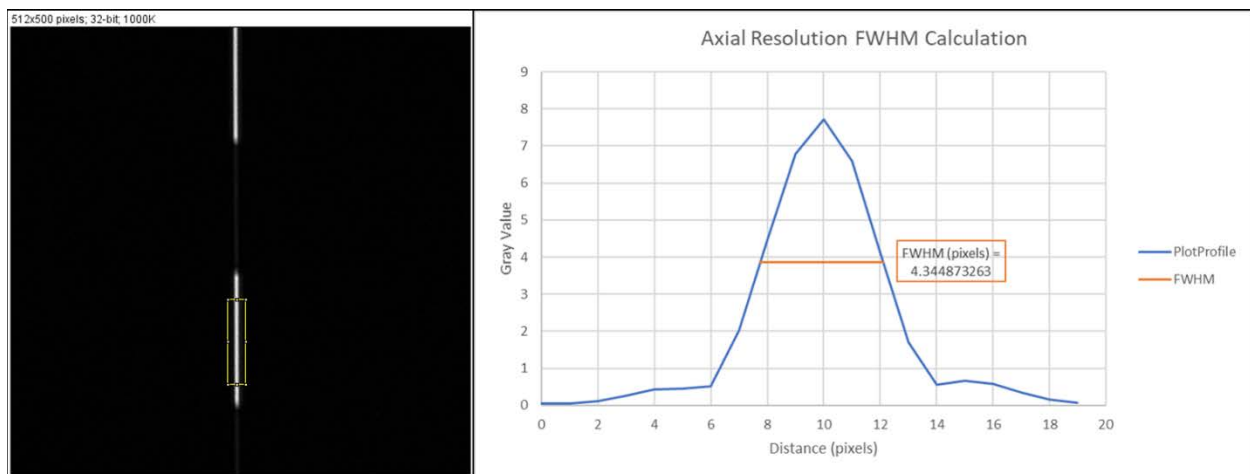


Figure 2.4 – ImageJ output and FWHM interpolation for the analysis of the Axial Resolution.

The count of Multiply Scattered Photons was taken using the *Mean Gray Value* function in ImageJ. When opened in ImageJ, the text image from the OCT was transposed such that the left side of the image was the tissue phantom and the right side of the image was inside the Ronchi ruling. A rectangular box was drawn underneath a glass section of the ruling and the *Mean Gray Value* function was used, which simply reports the average pixel value of the captured section. This rectangular box was kept at the same size from image to image. This value was reported as the count of multiply scattered photons, and

then scaled based on the sensitivity of the Lock-In Amplifier during data acquisition. The count of scaled multiply scattered photons was reported in addendum to the count of multiply scattered photons. Figure 2.5 below shows a test image opened in ImageJ with the rectangular box for the *Mean Gray Value* function drawn in place.

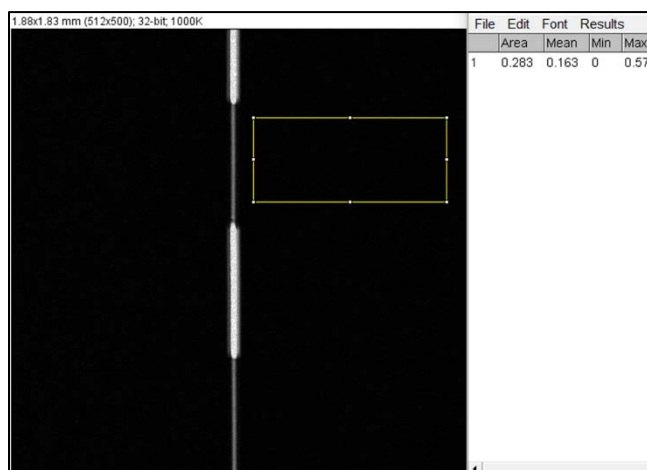


Figure 2.5 – ImageJ output for the analysis of the counts of Multiply Scattered Photons.

## 3 – RESULTS AND DISCUSSION

### 3.1 – 3D PRINT DESIGN

In order to hold the tissue phantoms and integrate them into the optical system, three components were designed and 3D printed. The tissue phantom holder shown in Figure 3.1 below, was designed with a few key considerations in mind. The central cavity was large enough to comfortably fit the 1" square Ronchi ruling test target and allow for the ruling to be easily removed while not allowing for too much slop in the ruling's allowable movement. The sides of the container were to be roughly the same size as the tip-tilt stage, or 50 mm long. A small groove was cut into the central cavity to help facilitate the removal of the Ronchi ruling. A slope was built around the central cavity in order to hold a cover glass. This cover glass served two key roles, the first of which being the removal of the meniscus. As the liquid tissue phantoms were added into the container, a significant meniscus would develop which resulted in the depth of liquid varying across the scan direction. By placing the cover glass over the meniscus, a smooth interface would form and eliminate the variability caused by the meniscus. Additionally, the 8° grade of the sloped surface helped to mitigate back reflections. This design was adapted from a similar design built by Harrison Thurgood in Dr. Barton's Tissue Optics Lab. A full drawing of this part is included in Appendix 5.9.

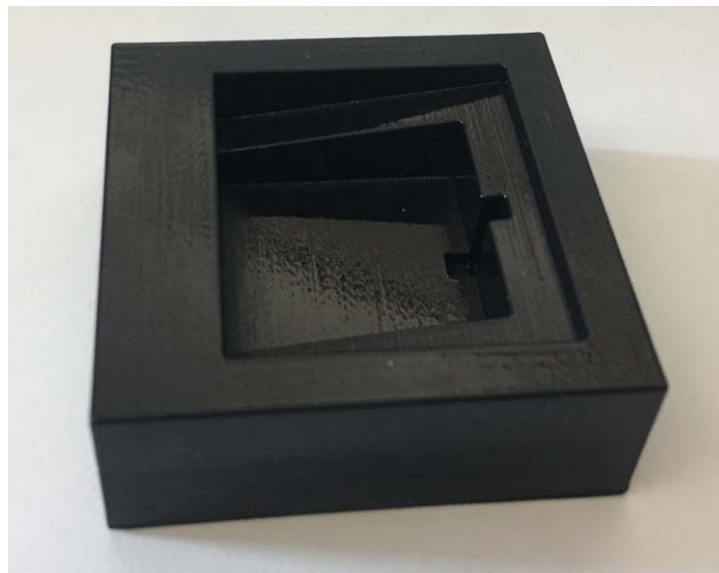


Figure 3.1 – 3D Printed Tissue Phantom Holder

Two pieces were designed to connect the tissue phantom holder to the tip-tilt stage while ensuring that the position of the phantom holder was going to remain consistent from trial to trial. The solution was to create a two-part mount, one that would be bonded to the tip-tilt stage and one that would be bonded to the phantom holder, shown below in Figure 3.2. As with the phantom holder, the sides were built to be the same size as the tip-tilt stage. As it was desirable to be able to remove the phantom holder from the system to make any necessary adjustments or replace the tissue phantom, it was important that the two pieces could be easily separated. As such, one part was built with cylindrical extrusions that would fit into the other part's equivalently sized extruded cuts. The dimensions of these mounting features were dependent on the fidelity of the 3D printed parts, and had to be determined through trial and error. If the fit was too tight, the two parts would be challenging to separate from one another. If the fit was too loose, the parts would not consistently fit in the same way as there would be too much freedom of movement between the parts. Full drawings of these parts are included in Appendix 5.9.

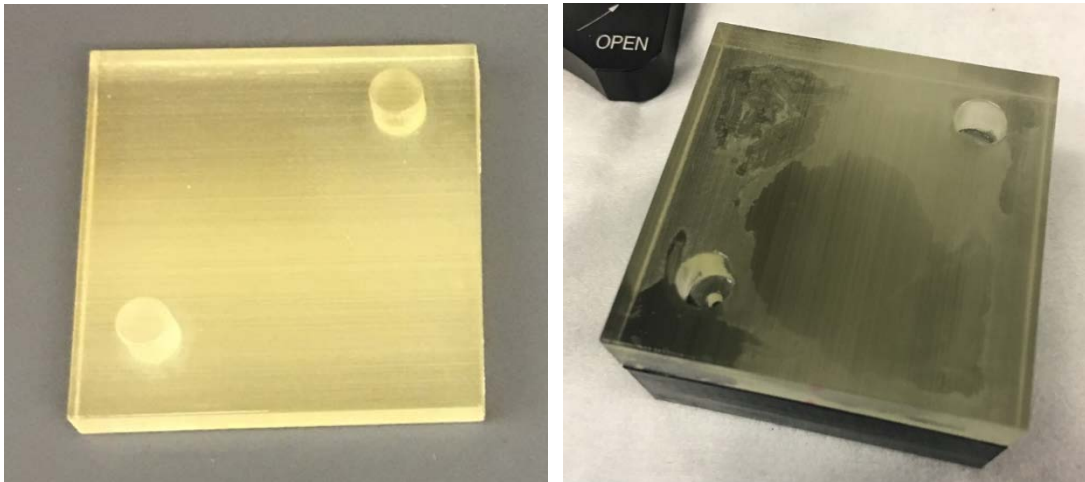


Figure 3.2 – 3D Printed Kinematic Base components

### 3.2 – LENS DESIGN

For this experiment, three different optical prescriptions with different numerical apertures had to be designed and implemented such that they could be easily swapped without sacrificing the system alignment every time the NA was changed. The goal behind the three lens designs for this system was to keep as many components and distances common between them as possible. As such, the beam collimator, the first lens in the

system, and the final focusing lens were kept constant. In order to keep the back focal distance the same between designs, the first and second lenses were used to create beam expanders. As the first lens was kept consistent between each trial, the only variability from design to design was second lens and its position relative to the first lens. The lenses were all oriented with the Plano side towards the focus point in order to minimize spherical aberration, as this would help to keep the back focal distance variation as minimal as possible.

For the purposes of the optical design, the beam coming out of the collimator was simplified as a collimated plane wave. The beam diameter was calculated based on the output of the Corning SMF-28 fiber and the focal length of the aspheric lens present in the OZ Optics HPUCO-23A-1300-S-11AS collimator. The Corning SMF-28 fiber has an NA of 0.14 and a Mode Field Diameter of  $9.2 \mu\text{m} \pm 0.4 \mu\text{m}$ . The aspheric lens in the OZ Optics collimator has a focal length of 11mm. From this, Equation 3.1 was used to find the diameter of the output from the beam collimator, 3.12 mm.

$$D_{beam} = D_{ModeField} + 2 \cdot f_{aspheric} \cdot \tan(\sin^{-1}(NA_{aspheric})) \quad (Eq\ 3.1)$$

The first lens, KPX076AR.18, is a 1 inch diameter plano-convex N-BK7 lens with an effective focal length of 25.4 mm. Each of the three lens designs used a KPX076AR.18 lens as part of the modular beam expander. The final focusing lens, KPX082AR.18, is a 1 inch diameter plano-convex N-BK7 lens with an effective focal length of 50.2 mm. The KPX082AR.18 focusing lens was a common element for all three designs. The lens design outlined in Figure 3.3 uses another KPX082AR.18 as the second lens in the modular beam expander. This design has an image space NA of 0.0603 and a back focal distance of 47.606 mm. The lens design outlined in Figure 3.4 uses a KPX088AR.18, a 1 inch diameter plano-convex N-BK7 lens with an effective focal length of 75.6 mm, as the second lens. This design has an image space NA of 0.0901 and a back focal distance of 47.484 mm. The lens design outlined in Figure 3.5 uses a KPX094AR.18, a 1 inch diameter plano-convex N-BK7 lens with an effective focal length of 100 mm, as the second lens. This design has an image space NA of 0.1186 and a back focal distance of 47.432 mm. All of the lenses being used are from Newport and have a 1000 to 1500 nm anti-reflection coating. Table 3.1 summarizes these design differences below. The results from the beam waist calculations described in Section

2.2 and Equation 2.9 are also included in this table. Figure 3.6 shows what the lens modules look like once properly aligned and mounted onto the kinematic base plates.

		Module 1	Module 2	Module 3
Lens 1	Part Number	KPX076AR.18	KPX076AR.18	KPX076AR.18
	Focal Length (mm)	25.4	25.4	25.4
Lens 2	Part Number	KPX082AR.18	KPX088AR.18	KPX094AR.18
	Focal Length (mm)	50.2	75.6	100
Lens 3	Part Number	KPX082AR.18	KPX082AR.18	KPX082AR.18
	Focal Length (mm)	50.2	50.2	50.2
	Image Space NA	0.0603	0.0901	0.1186
	Distance L1-L2 (mm)	64.537	91.286	116.574
	BFD (mm)	47.606	47.484	47.432
	Beam Waist ( $\mu\text{m}$ )	6.858	4.586	3.481

Table 3.1 – Summary of lens module designs

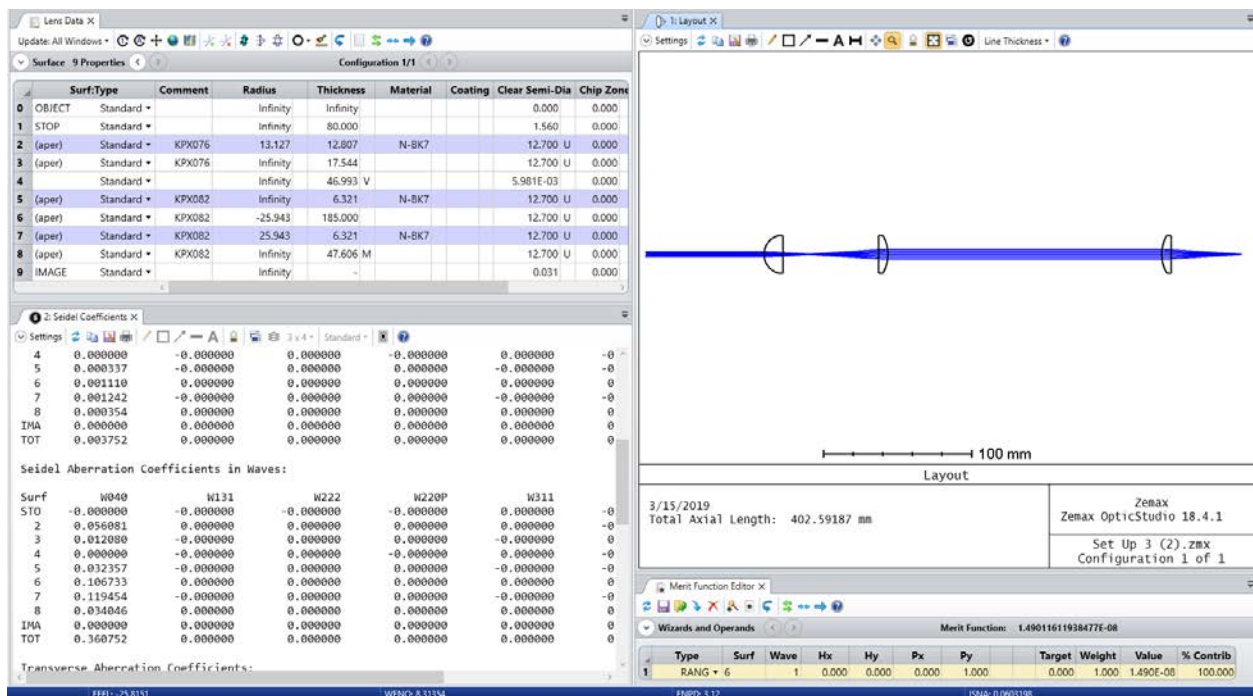


Figure 3.3 – Lens data, lens layout, and Seidel aberration coefficients for NA = 0.0603 system design

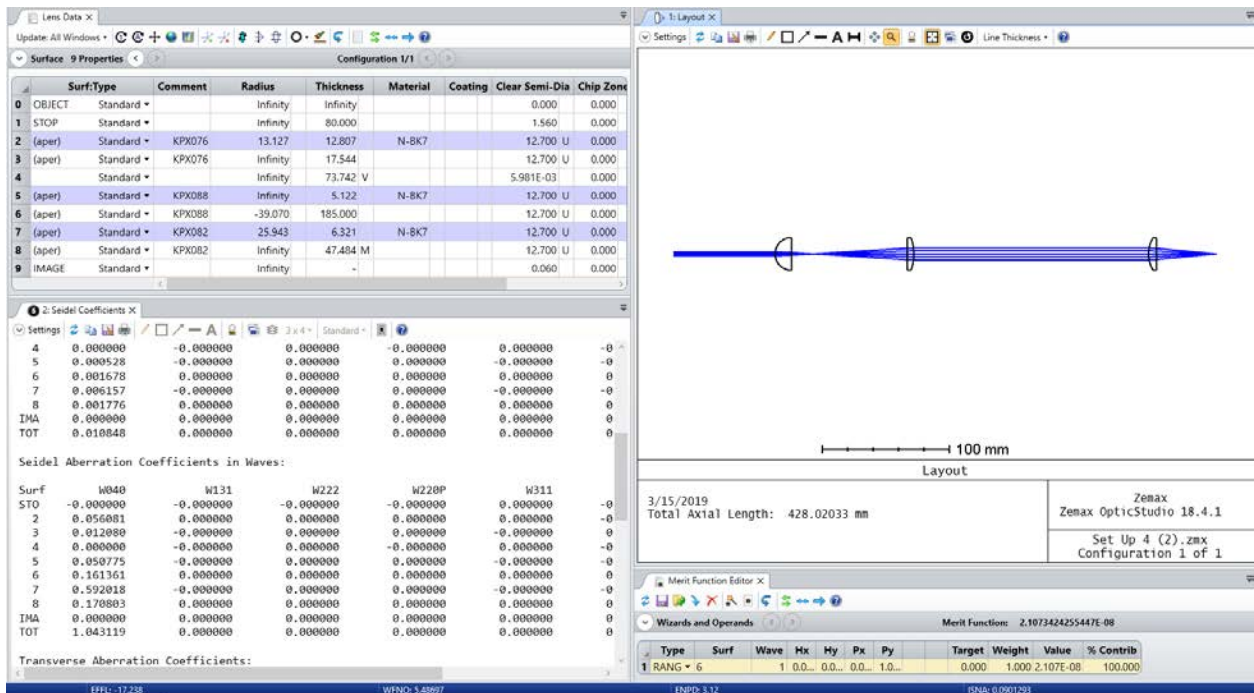


Figure 3.4 – Lens data, lens layout, and Seidel aberration coefficients for NA = 0.0901 system design

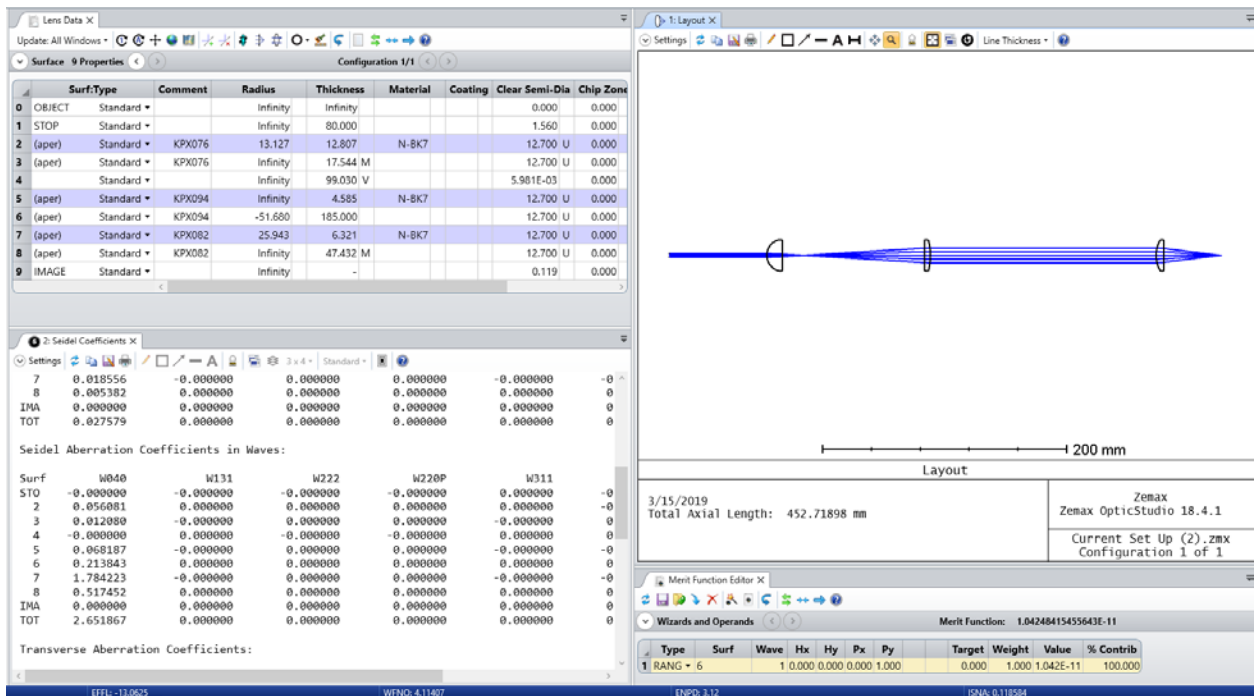


Figure 3.5 – Lens data, lens layout, and Seidel aberration coefficients for NA = 0.1186 system design

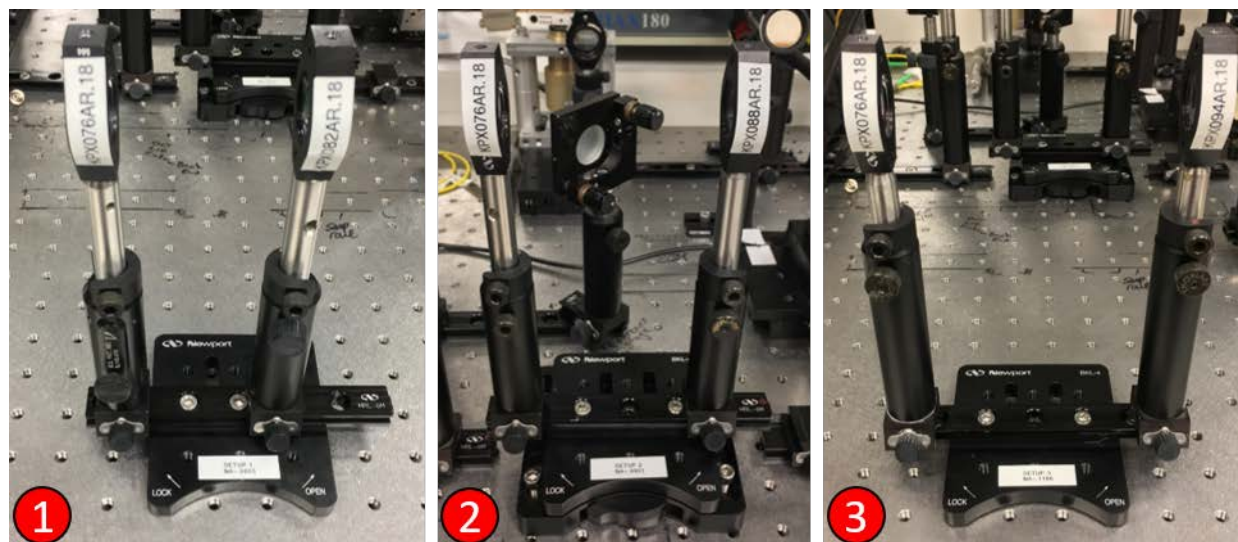


Figure 3.6 – Modular lens setups for (1) NA = 0.0603 system design, (2) NA = 0.0901 system design, and (3) NA = 0.1186 system design. The lenses in (2) have been integrated into the test arm.

### 3.3 – ABSORPTION COEFFICIENT CALCULATION

The following table and plot, Table 3.2 and Figure 3.7 respectively, show the results from the experiment determining the absorption coefficient of the batch of India Ink specifically used during this experiment, as well as a linear equation fit to the experimental data describing the absorption coefficient in  $\text{cm}^{-1}$  as a function of concentration of India Ink in water. It should be noted that since Intralipid 20% and water have the same absorption coefficient at 1300 nm, the amount of ink that must be added to the tissue phantoms to achieve a certain absorption coefficient will only depend on the volume of the Intralipid and water mixture. In all cases, the percent of India Ink required to achieve a target absorption coefficient is so small that the dilution caused by the addition of the ink, and subsequent effects on the scattering coefficient, can be ignored.

	Trial 1 (W)	Trial 2 (W)	Trial 3 (W)	Average (W)	% India Ink
DI Water	1.8214	1.8268	1.8259	1.8247	0
50mL H2O + 50uL Ink	0.029	0.029	0.029	0.029	0.0999001
100mL H2O + 50uL Ink	0.2368	0.2368	0.2368	0.2368	0.049975012
150mL H2O + 50uL Ink	0.4855	0.4864	0.4864	0.4861	0.033322226

Table 3.2 – Data collected from India Ink absorption coefficient calculation experiment

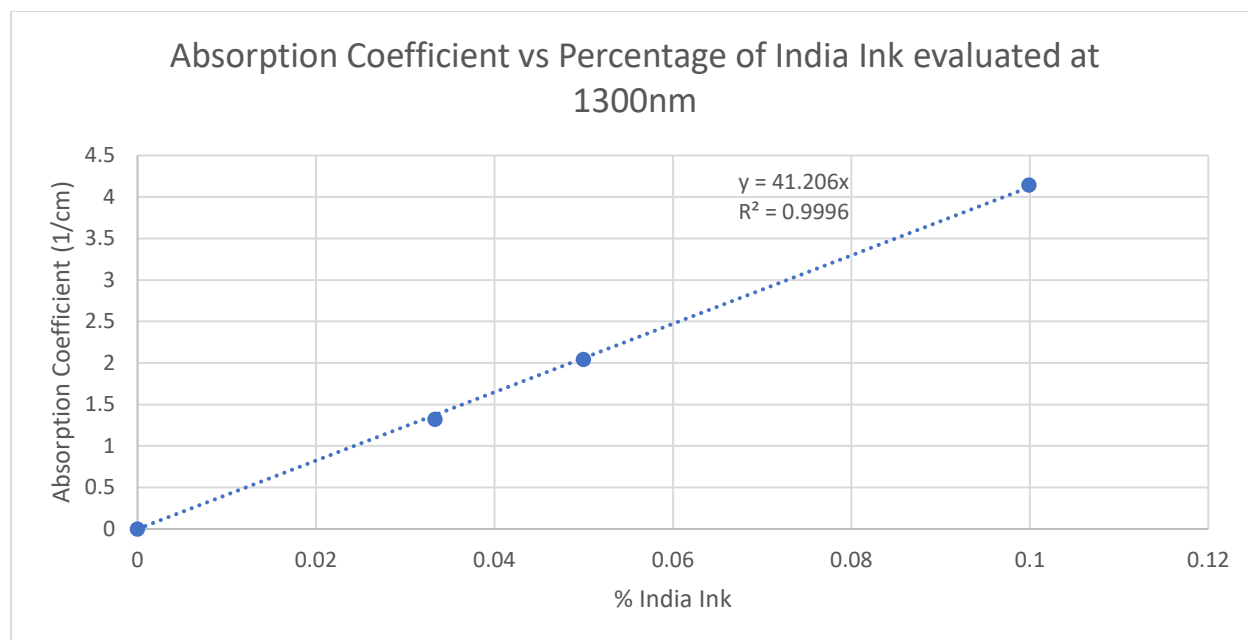


Figure 3.7 – Plotted results from India Ink absorption coefficient calculation experiment with linear trendline and  $R^2$  value.

This test verified the efficacy of using the VWR Model 50D Ultrasonic Bath to limit the scattering effects of India Ink. Power fluctuations did not occur at all during the experimental testing, however after allowing the solutions to stand for roughly 45 minutes, significant power fluctuations were seen. After reintroducing the cuvettes to the ultrasonic bath and then testing again, these power fluctuations stopped occurring, only to begin again after 40 minutes. Observation of this behavior served as validation for the effects discussed in the “The use of India ink in tissue-simulating phantoms” paper [25]. Additionally, this provided valuable information about how long an ink solution would go without noticeable aggregation and scattering effects after spending 30 minutes in the ultrasonic bath. Every sonicator will operate slightly differently and output different amounts of energy, so it was important to determine the amount of time and power required to prevent these effects in the specific sonicator used in this experiment. For the purposes of this experiment, if the data collection was not completed 30 minutes after the phantom had been removed from the bath, that round of data collection was discarded and then restarted after an additional application of the sonicator. This made sure that all data collected would be free of the scattering effects caused by the ink.

### 3.4 – PHANTOM DILUTION CALCULATION

The tissue phantoms needed for this study were created using two separate dilutions: the first to match the reduced scattering coefficient and the second to match the effective propagation distance. A total of four simulated reduced scattering coefficients and four effective depths were decided on prior to performing the calculations, which created the 16 sets of tissue phantom parameters. Once determined, the actual reduced scattering coefficient and actual tissue depth could be used to calculate the two dilution factors used to make the tissue phantoms. The values resulting from this process are given below in Table 3.3, with the corresponding equations, Equation 3.2 through Equation 3.6, noted separately. The color coding on the table helps to provide visual feedback for which Dilution Factor results in the most Intralipid present in the phantom, with Red corresponding to the highest concentration and Green the lowest. Similarly, the bar plot in the “% Intralipid” helps to visualize the relative percentage of Intralipid in each phantom combination.

Phantom #	cm <sup>-1</sup> μ <sub>s</sub> '(desired)	cm <sup>-1</sup> μ <sub>s</sub> '(intralipid)	mm d <sub>real</sub>	mm d <sub>effective</sub>	Dilution Factor 1	Dilution Factor 2	% Intralipid
1	30.0059	49.19	4.57	1.1425	1.639344262	4	3.05
2	30.0059	49.19	4.57	0.57125	1.639344262	8	1.525
3	30.0059	49.19	4.57	0.2285	1.639344262	20	0.61
4	30.0059	49.19	4.57	0.11425	1.639344262	40	0.305
5	15.00295	49.19	4.57	1.1425	3.278688525	4	1.525
6	15.00295	49.19	4.57	0.57125	3.278688525	8	0.7625
7	15.00295	49.19	4.57	0.2285	3.278688525	20	0.305
8	15.00295	49.19	4.57	0.11425	3.278688525	40	0.1525
9	7.501475	49.19	4.57	1.1425	6.557377049	4	0.7625
10	7.501475	49.19	4.57	0.57125	6.557377049	8	0.38125
11	7.501475	49.19	4.57	0.2285	6.557377049	20	0.1525
12	7.501475	49.19	4.57	0.11425	6.557377049	40	0.07625
13	3.7507375	49.19	4.57	1.1425	13.1147541	4	0.38125
14	3.7507375	49.19	4.57	0.57125	13.1147541	8	0.190625
15	3.7507375	49.19	4.57	0.2285	13.1147541	20	0.07625
16	3.7507375	49.19	4.57	0.11425	13.1147541	40	0.038125

Table 3.3 – Tissue Phantom dilution calculations and planning

A set of reduced scattering coefficients and effective depths were created to cover the range of expected tissue optical properties and the usual depth ranges imaged in OCT. The desired reduced scattering coefficients and depth values are not whole numbers for

the sake of simplifying the serial dilutions, and because the real depth was measured after the creation of the phantom holder.

The equations below reflect the calculations performed in Table 3.3. It should be explicitly noted that Dilution Factor 1 describes the reduced scattering coefficient while Dilution Factor 2 describes the effective depth of the phantom. As Dilution Factor 2 was implemented after Dilution Factor 1, the Mixture Volume in the Dilution Factor 2 equation refers to the dilution created from using Dilution Factor 1.

$$\text{Dilution Factor 1} = DF1 = \frac{V_{\text{Intralipid}} + V_{\text{Water}}}{V_{\text{Intralipid}}} \quad (\text{Eq 3.2})$$

$$\mu'_s(\text{simulated}) = \frac{\mu'_s(\text{intralipid})}{\text{Dilution Factor 1}} \quad (\text{Eq 3.3})$$

$$\text{Dilution Factor 2} = DF2 = \frac{V_{\text{Mixture}} + V_{\text{Water}}}{V_{\text{Mixture}}} \quad (\text{Eq 3.4})$$

$$d_{\text{simulated}} = \frac{d_{\text{real}}}{\text{Dilution Factor 2}} \quad (\text{Eq 3.5})$$

$$\% \text{ Intralipid} = 100 \cdot ((DF1 \cdot DF2)^{-1}) \cdot (\% \text{ Intralipid}) \quad (\text{Eq 3.6})$$

From the table, it can be noted that of the 16 total solutions, 6 of these are redundant; that is, they are equivalent in composition to one of the other solutions. The reason this occurred is also the same reason that tissue phantoms can be used to simulate tissue in the first place. In this case, both dilution factors frequently changed by a factor of two, which meant that some redundant solutions were created during the serial dilution process outlined in the Methods.

### 3.5 – LATERAL RESOLUTION

The lateral resolution data are reported in the following two plots, in which the low absorption case is given in Figure 3.8 and the high absorption case is given in Figure 3.9. The y-axes represent the FWHM of the Gaussian in microns, meaning that a larger value on the y-axis corresponds to a worse resolution. For the purposes of this discussion, a “high resolution”, will correspond to a smaller FWHM value, and a “low resolution” will correspond to a larger FWHM. The x-axis is the percentage of Intralipid in the tissue

phantom solution, shown on Table 3.3 and calculated by the formula shown in Equation 3.6, in which the % *Intralipid* is 0.2, for Intralipid 20%. This number can also be reached by dividing the volume of Intralipid in the solution by the total volume of the solution and then multiplying by the 20% concentration of Intralipid. A higher value on the x-axis corresponds to more scattering materials present in the phantom.

The values on these two plots come from the average FWHM of the three runs performed with the same test parameters, with the error bars representing the standard deviation. Linear trendlines were fit to the data, with the equation of the trendline and coefficient of determination,  $R^2$ , given in color next to the appropriate line. Tables with the full sets of values from these plots have been included in Appendix 5.10. A statistical analysis reporting the error of the linear regressions and the results of two-tailed tests comparing the means and slopes of the data sets have been included below in Table 3.4 through Table 3.7.

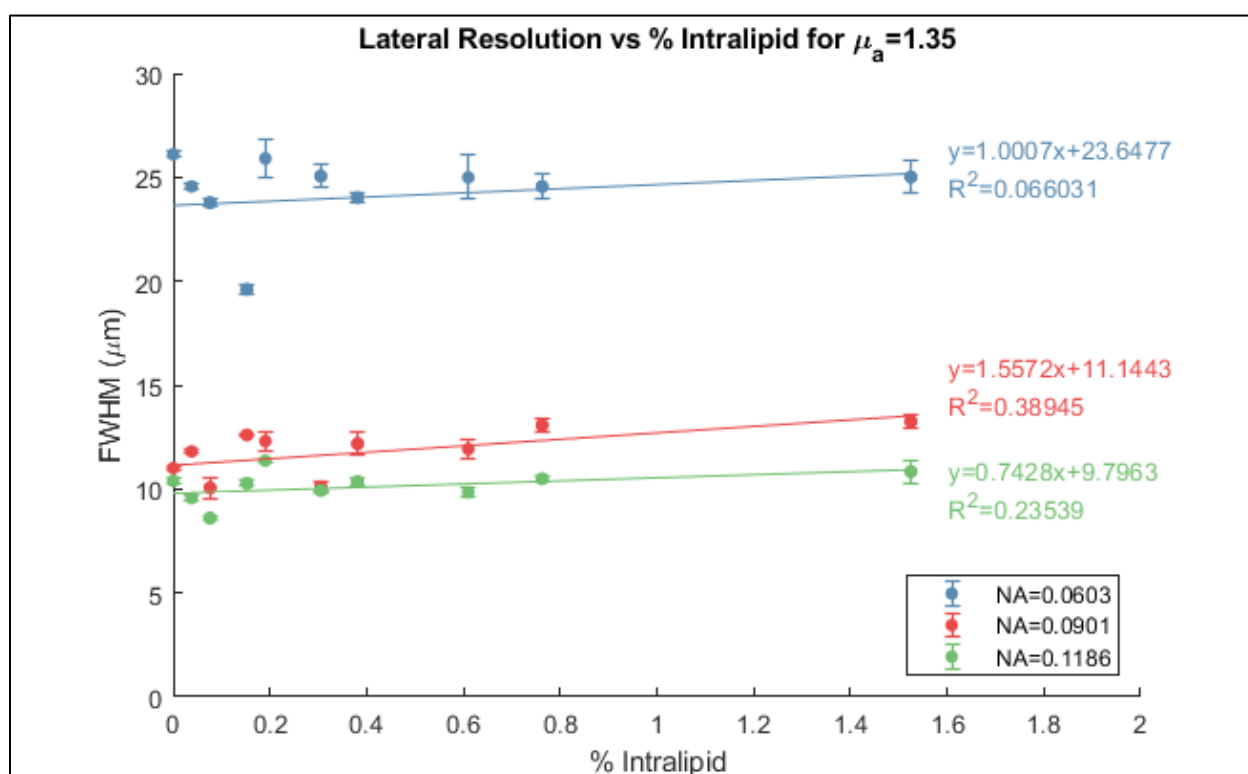


Figure 3.8 – Lateral Resolution measured in FWHM as a function of Intralipid percentage for NA of 0.0603, 0.0901, and 0.1186, and  $\mu_a$  of 1.35  $\text{cm}^{-1}$ , with the equations of the trendlines and  $R^2$  values given next to the associated trendlines.

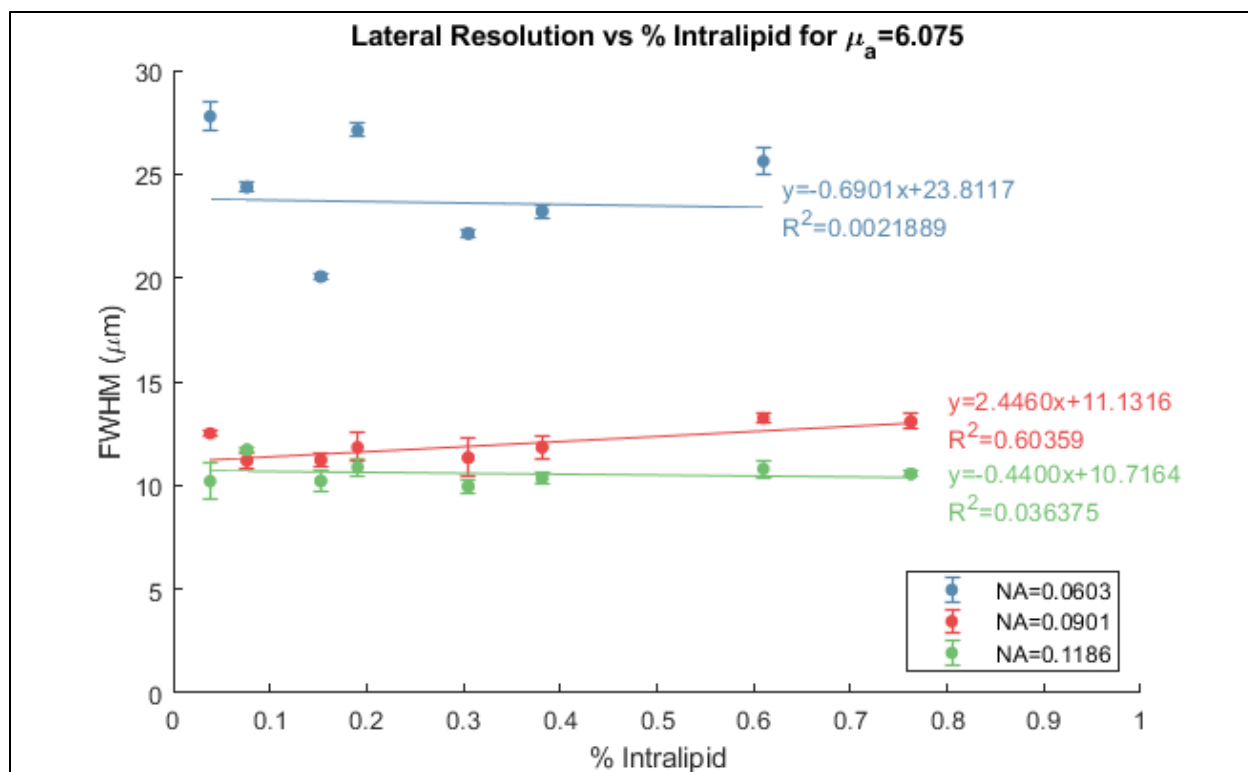


Figure 3.9 – Lateral Resolution measured in FWHM as a function of Intralipid percentage for NA of 0.0603, 0.0901, and 0.1186, and  $\mu_a$  of 6.075  $\text{cm}^{-1}$ , with the equations of the trendlines and  $R^2$  values given next to the associated trendlines.

From these plots, a few details become evident. Firstly, as expected, the lateral resolution depends greatly on the NA of the system, with more than double the resolution when comparing the low NA case of 0.0603 with the high NA case of 0.1186. This remained true for both the low absorption coefficient and high absorption coefficient cases. Additionally, this improvement in resolution was far greater when moving from an NA of 0.0603 to 0.0901 than it was when moving from 0.0901 to 0.1186. This suggests a  $1/x$  relationship between the resolution and the NA, again as expected given the theoretical equation for the lateral resolution, shown in Equation 1.10.

Secondly, the standard deviation for the values of each data point, as shown by the error bars, indicate that there was good repeatability from run to run for each combination of system parameters. Finally, and most notably, there is not a strong trend relating the number of scattering particles and the resolution. While a linear fit did show an increase in the FWHM (decrease in the resolution) over the range of % Intralipid values for the low

absorption case, the slopes of these trendlines were low in magnitude, with slopes of 1.0007, 1.5572, and 0.7428 corresponding to the 0.0603 NA, 0.0901 NA, and 0.1186 NA cases respectively. In addition to this, the trendlines had poor correlation to the data observed or showed little dependency, with  $R^2$  values of 0.066031, 0.38945, and 0.23539. The linear fit trend lines in the high absorption case show conflicting results, with one positively sloped trendline and two negatively sloped trendlines, with magnitudes - 0.06901, 2.4460, and -0.4400. The  $R^2$  values for these plots also differed dramatically, with values of 0.0021889, 0.60359, and 0.036375.

NA	slope	intercept	$R^2$	p-value	stderr
0.0603	1.00074	23.6477	0.06603	0.33668	1.00589
0.0901	1.55716	11.1443	0.38945	0.00977	0.52108
0.1186	0.7428	9.7963	0.23539	0.05679	0.3578

Table 3.4 – Linear regression analysis for  $\mu_a = 1.35 \text{ cm}^{-1}$

Compared systems	p-value, Means	p-value, Slopes
0.0603/0.0901	0	0.6233
0.0603/0.1186	0	0.80909
0.0901/0.1186	0.00005	0.19762

Table 3.5 – Results of two-tailed test of means and slopes for  $\mu_a = 1.35 \text{ cm}^{-1}$

NA	slope	intercept	$R^2$	p-value	stderr
0.0603	-0.69007	23.8117	0.002189	0.89135	4.91117
0.0901	2.44598	11.1316	0.60359	0.001782	0.59766
0.1186	-0.43997	10.7164	0.036375	0.53253	0.68277

Table 3.6 – Linear regression analysis for  $\mu_a = 6.075 \text{ cm}^{-1}$

Compared systems	p-value, Means	p-value, Slopes
0.0603/0.0901	0	0.52616
0.0603/0.1186	0	0.95977
0.0901/0.1186	0.00006	0.00147

Table 3.7 – Results of two-tailed test of means and slopes for  $\mu_a = 6.075 \text{ cm}^{-1}$

The statistical analysis further details how effectively the trendlines fit the data, given by the p-values and the standard error reported in the tables. While the  $R^2$  value gives a measure of how well the variance in the dependent variable is predicted by the independent variable, it is inherently limited. Due to the method in which  $R^2$  is calculated, a

horizontal regression line will give a low  $R^2$  value, even if the data fit the trendline. The standard error of the regression gives the measure of how far the data points will typically fall from the trendline, and the p-value indicates the significance of the results. Notably, a p-value  $\leq 0.05$  is considered significant. The two-tailed tests are investigating the probability that the means and slopes between the data points are different, in which this probability is equal to minus the p-value.

The data reported in Table 3.4 and Table 3.6 show that, for both trials, the trendline poorly fits the data for the low NA case of 0.0603, as the standard error values are large and the p-values indicate insignificance. By contrast, the medium NA cases of 0.0901 show relatively low standard error with small p-values indicating highly significant results. The high NA case of 0.1186 shows results that are on the edge of significance for the low NA case and insignificant for the high NA case. The data reported in Table 3.5 and Table 3.7 show that the probability of the FWHM differing as a function of NA is 99.994% or higher for all tested cases. The results of the slope analysis show insignificance for all cases except when comparing the slopes between the medium NA and high NA trendlines for the high absorption trial, in which case there is a 99.853% chance the slopes are different. However, as indicated by the linear regression analysis, half of the trendlines are not significant representations of the data which does limit the efficacy of the two-tailed test of slopes.

It should be noted that moving from a low percentage of Intralipid to a high percentage has a significant impact on the number of scattering particles and the visibility of the test target. Two example images captured from the OCT have been included for reference in Figure 3.10, below. In the 1.525% Intralipid case, the noise floor had almost completely obfuscated the return from the non-chromed section of the Ronchi ruling test target. Conversely, in the 0.1525% Intralipid case, the sensitivity of the Lock-In Amplifier had to be adjusted in order to prevent the system from being overloaded by the return signal. The sensitivity for the low percent case was set to the maximum value of 1V, while the high percent case was set to 2mV, at the limit of the Lock-In Amplifier overloading. Based on the sensitivity values, the tissue phantoms being tested covered nearly the maximum testable range of reduced scattering coefficients for this experiment, as any more

scattering particles would make the glass surface of the target indistinguishable from the background and the Lock-In Amplifier would be in an overloaded state.

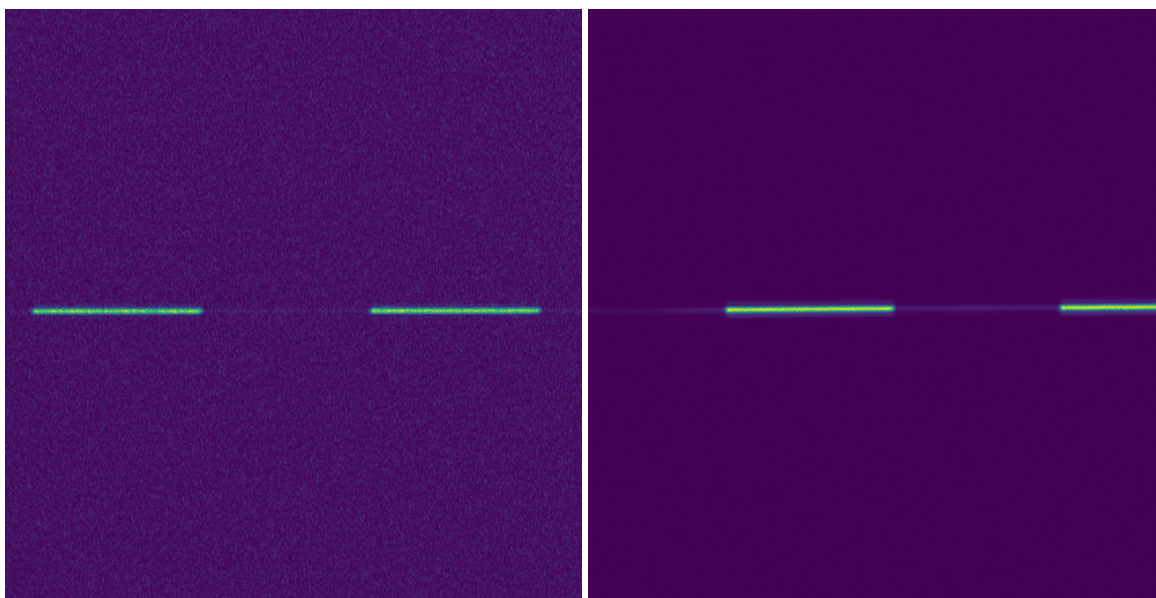


Figure 3.10 – Comparison between two OCT images for the 1.525% Intralipid case (Left) and the 0.1525% Intralipid case (Right).

These data indicate that the NA of the OCT system appears to be the dominant effect in determination of the lateral resolution. The increase in the absorption coefficient seemed to have little effect on the resolution, although it did produce confounding results when comparing the trendlines of the data. The increase in the reduced scattering coefficient possibly has an effect on the resolution, although this is not clearly shown by the reported data and the respective trendlines. The hypothesis for this part of the study was that the lateral resolution would degrade in the presence of highly scattering media, and the empirical observations and prior experiments mentioned in the Abstract that lead to this hypothesis predicted a much more significant relationship that could be observed by an OCT operator. While the trends from the data collected were not clearly identifiable, the expected result of a significant degradation in lateral resolution did not occur, at least not over the tested range of optical properties.

### 3.6 – AXIAL RESOLUTION

Similar to the lateral resolution case, the axial resolution data are reported in the following two plots, in which the low absorption case is given in Figure 3.11 and the high

absorption case is given in Figure 3.12. The y-axes represent the FWHM of the Gaussian in microns, meaning that a larger value on the y-axis corresponds to a worse resolution. As before, a “high resolution” will correspond to a smaller FWHM. Again, the x-axis is the percentage of Intralipid in the tissue phantom solution. The values on these two plots come from the average FWHM of the three runs performed with the same test parameters, with the error bars representing the standard deviation. Tables with the full sets of values from these plots have been included in the Appendix 5.11.

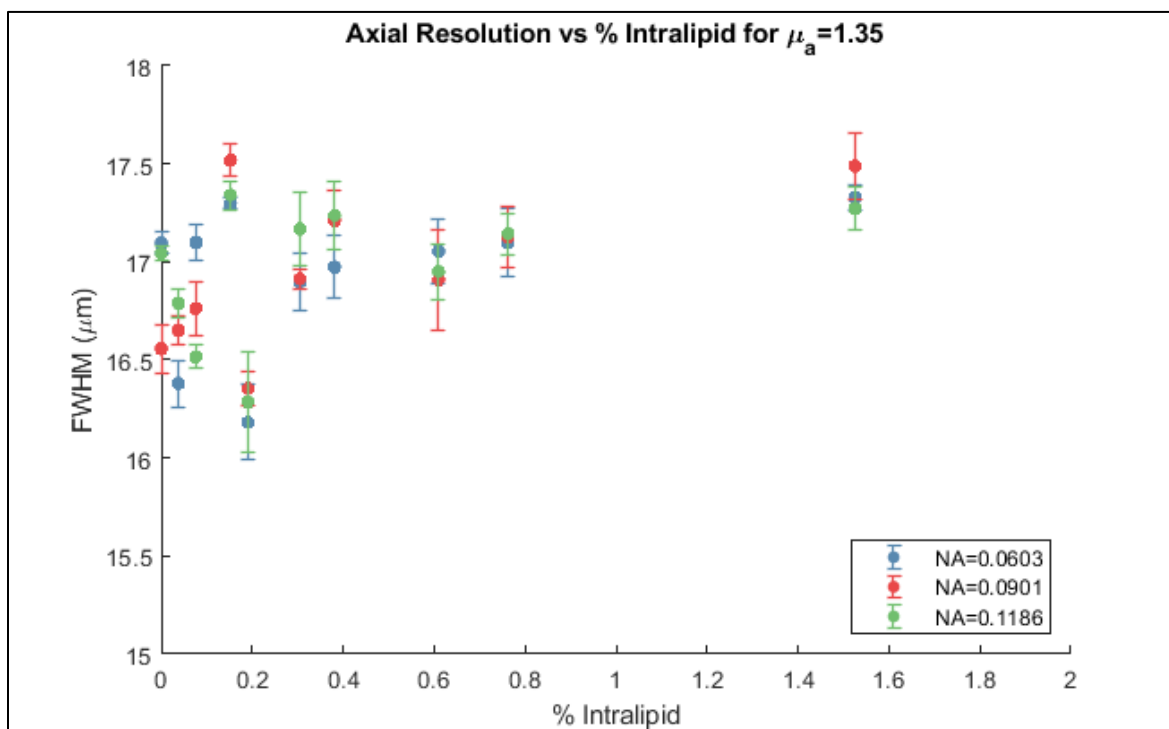


Figure 3.11 – Axial Resolution measured in FWHM as a function of Intralipid percentage for NA of 0.0603, 0.0901, and 0.1186, and  $\mu_a$  of 1.35  $\text{cm}^{-1}$ .

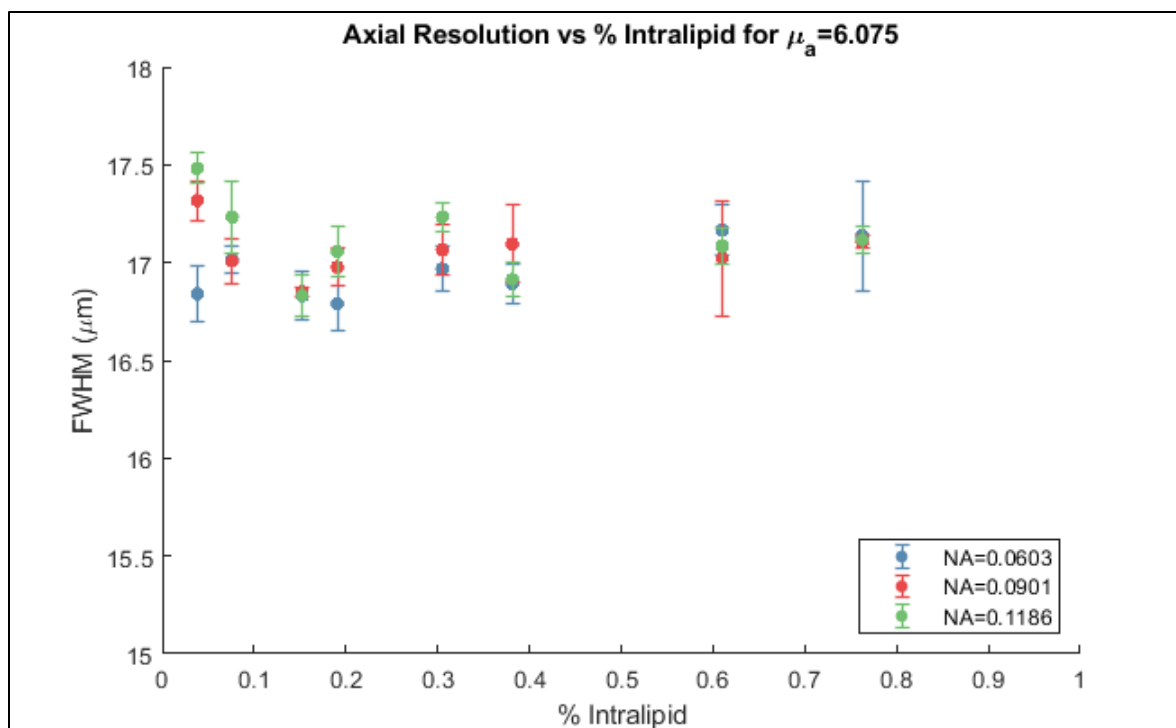


Figure 3.12 – Axial Resolution measured in FWHM as a function of Intralipid percentage for NA of 0.0603, 0.0901, and 0.1186, and  $\mu_a$  of 6.075  $\text{cm}^{-1}$ .

When analyzing the data presented in these two plots, it is important to note the scale on the y-axis in both of these cases. Unlike the lateral resolution plots, the axial resolution data was so tightly clustered that the plot was unreadable with the bottom of the y-axis set to 0  $\mu\text{m}$ . From this zoomed in view of the data, it seems that the axial resolution is unrelated to the numerical aperture of the system, the absorption coefficient, or the amount of scatterer. Perhaps the only noticeable trend for these parameters was that the higher absorption case seemed to be slightly more consistent, as the full set of data fit within a  $\Delta\text{FWHM}$  range of 1  $\mu\text{m}$  rather than 1.5  $\mu\text{m}$  for the lower absorption case.

As stated in the introduction, based on previous experimentation and empirical observation, the hypothesis for this part of the study was that the axial resolution would degrade in the presence of highly scattering media. However, as shown from the tightly clustered results given above, there does not seem to be evidence to show that this is the case. If there is some trend, the resolution may degrade by a half a micron or a micron at most. It is possible the previously perceived decrease in resolution is due to other issues that have been misidentified or misattributed. In a real world application, the target may

not be perfectly in focus, and the edge might appear to blur as a result. Alternatively, if the light returning to the system is limited and the SNR is poor, the noise floor might be high enough to confound the results and come across as a poorly resolved image instead. It may also be that in an inhomogeneous scattering medium, a degradation in axial resolution may occur more readily than in this idealized homogeneous phantom.

### 3.7 – MULTIPLY SCATTERED PHOTONS

Figure 3.13 and Figure 3.14 given below show the counts of multiply scattered photons as a function of the percentage of Intralipid in the phantom, for the low absorption case and high absorption case respectively. The y-axis is measured in counts, which were scaled from 0 to 10 and are simply the value reported from the *Mean Gray Value* function. As in the case of the lateral resolution and the axial resolution, the x-axis is the percentage of Intralipid in the tissue phantom solution. A table with the values from these plots has been included in Appendix 5.12. The reported data are only from the 4<sup>th</sup> run of image acquisition in which the sensitivity of the system was adjusted such that the reflection off the chromed section of the ruling overloaded the detector, but the reflection off the glass section did not. This change was made to assure that the signal measured, which was only under the glass section, was amplified enough to be measurable above the noise floor.

The counts of multiply scattered photons were also multiplied by the Lock-In Amplifier sensitivity values in order to account for the effect of the sensitivity on the counts reported by the LabView software, as increasing the sensitivity also increases the value of the counts. Figure 3.15 and Figure 3.16 present the counts of scaled multiply scattered photons as a function of the % Intralipid for the low absorption case and high absorption case respectively. The sensitivity values used to scale the counts range from 0.5mV to 1000mV, and are reported in full in Appendix 5.12.

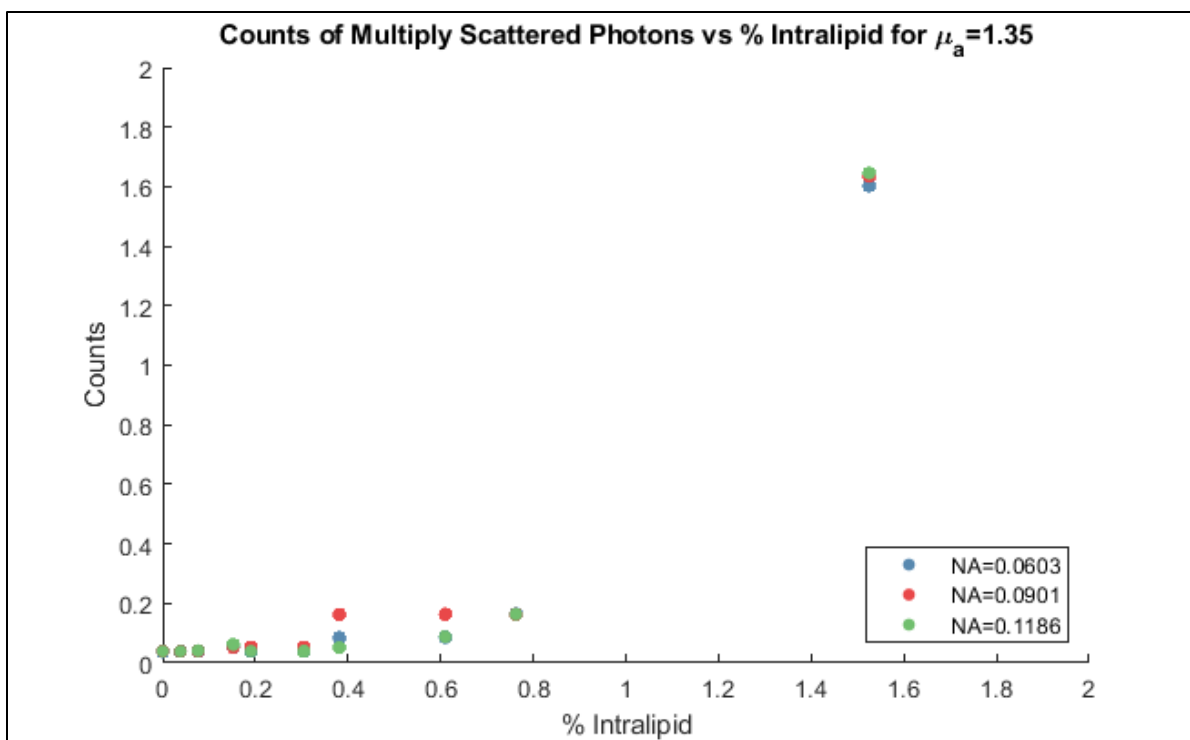


Figure 3.13 – Number of Multiply Scattered Photons measured in counts as a function of Intralipid percentage for NA of 0.0603, 0.0901, and 0.1186, and  $\mu_a$  of  $1.35 \text{ cm}^{-1}$ .

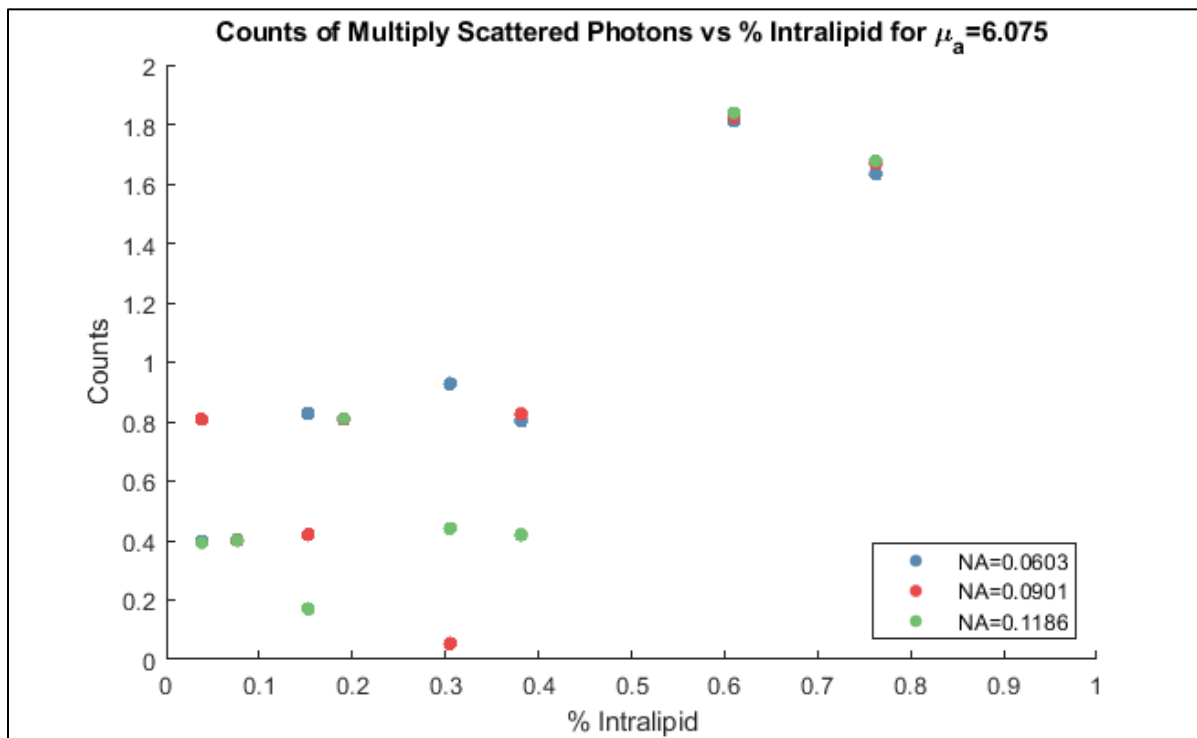


Figure 3.14 – Number of Multiply Scattered Photons measured in counts as a function of Intralipid percentage for NA of 0.0603, 0.0901, and 0.1186, and  $\mu_a$  of  $6.075 \text{ cm}^{-1}$ .

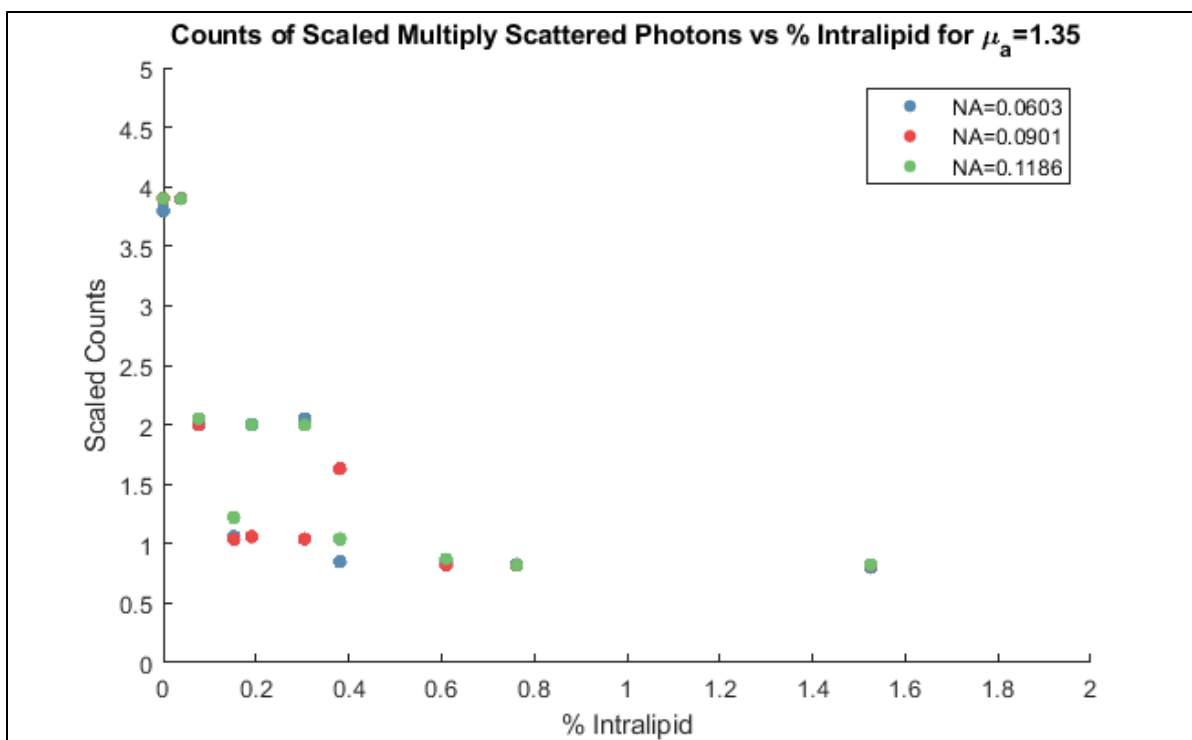


Figure 3.15 – Number of Scaled Multiply Scattered Photons measured in scaled counts as a function of Intralipid percentage for NA of 0.0603, 0.0901, and 0.1186, and  $\mu_a$  of 1.35  $\text{cm}^{-1}$ .

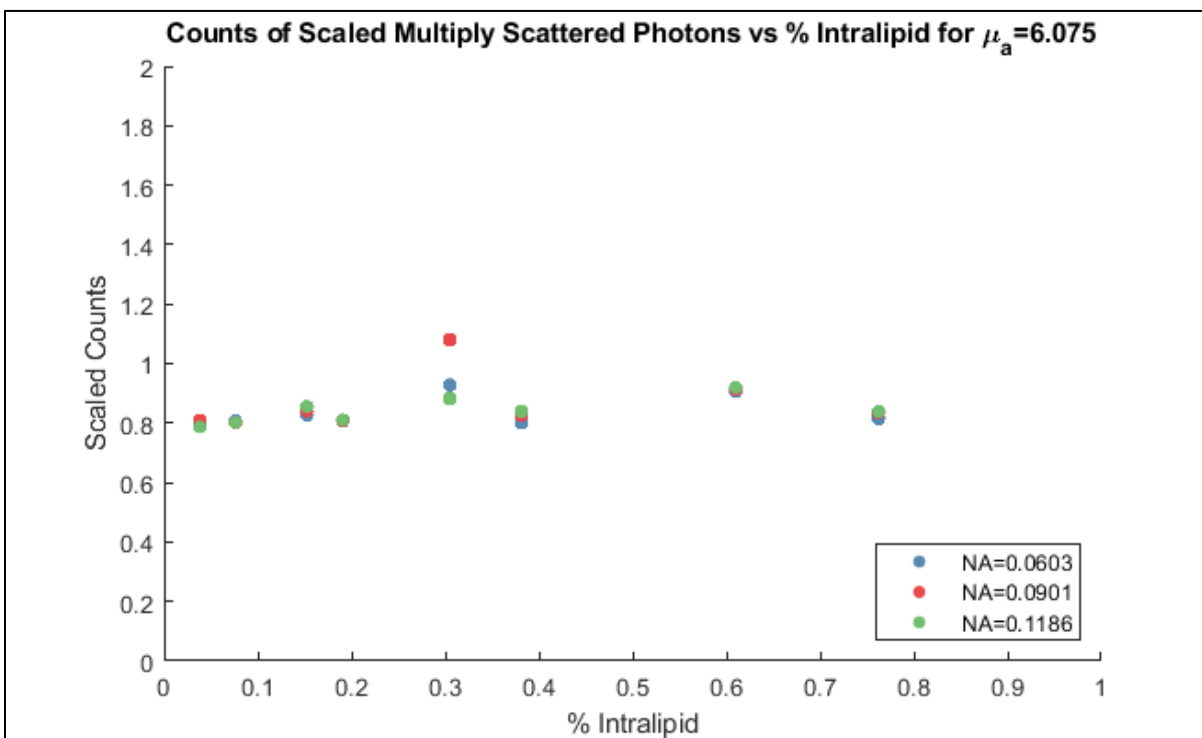


Figure 3.16 – Number of Multiply Scattered Photons measured in counts as a function of Intralipid percentage for NA of 0.0603, 0.0901, and 0.1186, and  $\mu_a$  of 6.075  $\text{cm}^{-1}$ .

The non-scaled data from the low absorption case indicates that as the scattering coefficient increases, the amount of multiply scattered photons also increases, with no correlation based on the numerical aperture. However, upon scaling the data, the opposite relationship is shown, in which the amount of multiply scattered photons decreases with the number of scattering particles present. In the high absorption case, the non-scaled data is much more randomly scattered with greater counts of multiply scattered photons than were shown in the low absorption case. Upon scaling this data, the amount of multiply scattered photons was shown to be roughly constant with no reliance on the number of scattering particles. Based on these results, scaling the counts of multiply scattered photons will show different trends than not scaling the data, and increasing the absorption coefficient will change how the multiply scattered photons relate to the amount of scatterers present in the solution.

This portion of the study seems to have been flawed in some regard, and it is likely that these results were merely a measure of background noise or incorrectly scaled based on the sensitivity. The principle behind this analysis was that no signal should be coming from below the surface of the glass, as there are no (or at least very few) scattering particles there. In theory, the only signal coming from that section should have come from the multiply scattered photons. In practice however, it is impossible to tell what signal comes from noise and what signal comes from multiply scattered photons, which is only further confounded by the changing sensitivity values. It is possible that multiplying the counts by the sensitivity of the Lock-In Amplifier was an incorrect method for analyzing this data, and that different steps could be taken to produce more meaningful data.

### 3.8 – OVERALL CONCLUSIONS AND CONSIDERATIONS

For the most part, the results from this study support the theoretical equations that show that the lateral and axial resolution are independent of the optical properties of the medium. The lateral resolution was shown to be dependent on the optics in the system and the image space numerical aperture, with an unclear link to the amount of scatterers present in the medium due to the statistical insignificance of many of the results. The axial resolution was shown to be independent of the number of scattering particles, the absorption coefficient, and the numerical aperture of the system, which supports that the

axial resolution is solely dependent on the properties of the source. The method for counting the number of multiply scattered photons seems to have been fundamentally flawed in some regard, as the Lock-In Amplifier sensitivity adjustments confounded the results, making it challenging to draw meaningful conclusions.

Overall, the results show that OCT does not seem to have systemic problems that arise when dealing with highly scattering media, and that in a number of homogeneous scattering cases, OCT lateral and axial resolution seems to behave exactly as the theory dictates for a homogeneous tissue phantom, for the range of optical properties studied, and for the design of this OCT system.

## 4 – FUTURE WORK

### 4.1 – LIMITATIONS

As it was mentioned previously in this paper, the sensitivity on the Lock-In Amplifier had to be adjusted for each trial in order to acquire images for the wide range of tested tissue phantoms. Had this not been done, the amount of collected data would have been very minimal, as the highest and lowest attenuation phantoms could not be processed with the same settings. If the highest attenuation case was visible, the low attenuation phantoms would completely overload the detector and the lock-in amplifier, potentially causing non-linearity effects and making the results unreliable at best. On the other hand, if the lowest attenuation case was visible, the returned signal from the higher attenuation phantoms would be below the noise floor. It was assumed that changing the sensitivity would not affect the FWHM of the resulting Gaussian curves, however this assumes ideal behavior of the amplifier. In the presence of any non-ideal effects of the amplifier, this fundamental assumption may be incorrect.

During this test, each of the tissue phantoms were only tested a single time. Further testing certainly would have improved the reliability of the results by introducing some repeatability in both data collection and phantom creation. In addition to this, there were a few potential issues or things to make note of with respect to the experimental setup and the procedures. First of all, this study was performed with a very strong reflecting surface, chrome, in a homogeneous medium with a substantial index mismatch between the tissue phantom and the test target. While this is not an unrealistic set of circumstances for OCT, it is relatively uncommon. This experimental setup resembles performing OCT around a metal stent or surgical implant, but many other applications of OCT have very different parameters. It is far more common to see minor index variations with targets that reflect or scatter light roughly as much as the surrounding tissue. These conditions could have been more closely imitated by the test parameters if the target had a lower maximum reflection. Additionally, it should be noted that during the data collection and analysis process, data were discarded or not taken when the signal was too low to process. If the attenuation was too strong and the glass interface disappeared in the noise, the data were considered

impossible to properly analyze. This is why some % Intralipid values are missing from the plots with the higher absorption coefficient.

## 4.2 – CONTINUED RESEARCH

When considering continued research on this topic, of greatest interest would be to perform this study again, but for light that is angularly incident on the test target. In a real world setting it is unrealistic to guarantee that the light output from the OCT will be normal with respect to the tissue. As such, the question remains: how might the axial and lateral resolution of OCT change based on angular incidence?

If this exact study were to be performed again, I would consider making a few key adjustments to the experimental setup and the procedures. As mentioned in Limitations, a test target with a weaker reflecting surface would create a test environment that is similar to more typical OCT applications. Another potential change could be to use a tissue phantom with an anisotropy value closer to that of most tissue. As mentioned before, Intralipid has a number of benefits that make it a strong candidate for use as a tissue phantom, but it also has a lower anisotropy than many types of tissue. A tissue phantom made using microspheres as the scattering particle would allow for more customized optical properties, which could allow for the creation of a phantom that simulates the scattering coefficient, reduced scattering coefficient, absorption coefficient, and anisotropy without having to choose between the scattering coefficient and the anisotropy. Microspheres are much more expensive and have their own set of challenges, such as not remaining in suspension as well as Intralipid due to having heavier particles, but it could result in a phantom that more accurately simulates tissue than the Intralipid phantoms used in this study.

It was mentioned during the axial resolution results discussion that real world OCT systems may encounter challenges that reduce image quality separate to the inherent properties of the tissue phantom or the optical system. Chief among these for future investigation is the effect of the target being out of focus on the resolution of the resulting images. The test environment used in this study was perhaps too ideal, as targets are rarely perfectly in focus when taking OCT images in a more realistic setting. To address this,

another experiment could be performed in which the test target is moved through focus across multiple trials to observe the effects on the lateral and axial resolution of the system.

A future study would do well to either maintain a constant value for the lock-in amplifier sensitivity, or calibrate the electronics with knowledge of the direct effects of changing the sensitivity value from test to test. This could be achieved by acquiring numerous images at different sensitivity values for a single test setup, and then comparing the resulting FWHM values as a function of sensitivity. I believe the results of this study were in some ways confounded by changing the sensitivity, so performing tests with a constant sensitivity or carefully monitoring the sensitivity as an independent variable would help to clarify the results from this study.

Of course, given the time and the resources, it would have been preferential to take far more data. Ideally, there would have been more trials performed with more simulated optical properties dispersed evenly over a wider range of values. The scan distance would be increased to capture more transitions that could be averaged together to provide more reliable results. However, the data presented here appear to be sufficient to support the conclusions obtained.

## 5 – APPENDIX

### 5.1 – Determination of Absorption Coefficient for India Ink SOP

#### Materials

1. 1300nm Laser Source	16. ThorLabs #VRC5 IR Viewing Card
2. SMF-28 Fiber	17. DI H <sub>2</sub> O
3. OZ Optics HPUCO-23A-1300-S-11AS Receptacle Style Fiber Collimator	18. Dr. Ph. Martin's Black Star India Ink
4. ThorLabs ND02A Reflective 25mm Diameter ND Filter, OD = 0.2	19. GeneMate 200 $\mu$ L Pipettor with associated pipette tips
5. Newport LH-100 1" Diameter Fixed Lens Mount	20. VWR Model 50D Ultrasonic Bath
6. 10mm side length Square Cuvette quantity 5	21. Fisherbrand Conical Polypropylene Centrifuge Tubes
7. Newport Model 818-IG Photodiode	22. 50mL Glass Graduated Cylinder
8. Newport Model 1835-C Multi-Function Optical Meter	23. Fisher Vortex Genie 2
9. Newport CB-2 Construction Base	24. Plastic Centrifuge Tube holder
10. Table clamps with ¼" hole quantity 2	25. Sharpie and Scotch Tape
11. ¼"-20 SHCS quantity 7	26. Nitrile Gloves
12. ¼" Washer quantity 2	27. Isopropyl Alcohol
13. #8-32 x ½" Set Screw quantity 3	28. Kimwipes
14. ½" Optical Mounting Post (with #8-32 and ¼"-20 threading) quantity 4	29. Large Rubber Band
15. ½" Optical Post Holder quantity 4	

#### Methods – Mechanical construction of experimental setup

- Using four ¼"-20 socket head cap screws, connect four ½" optical post holders to the optical bench. The four post holders should form a single line with roughly 5" of space between each post holder.
- Using the #8-32 x ½" set screws, connect the OZ Optics collimator, Newport fixed lens mount, and the Newport photodiode to three of the ½" Optical mounting posts. Using a ¼"-

20 socket head cap screw, connect the center of the Newport construction base to the last optical mounting post.

3. Insert the mounted components into the post holders in the following order: collimator, lens mount, construction base, photodiode. Roughly align them at the same height.
4. Connect the 1300nm laser source to the OZ Optics collimator using the SMF-28 Fiber. Turn on the laser and use the IR viewing card to verify that light is coming out of the collimator. Turn off the laser once verified.
5. Connect the ND Filter to the fixed lens mount. Slightly rotate the filter assembly such that the ND filter is not perpendicular to the optical axis to help prevent back reflections.
6. Connect the photodiode to the Newport optical meter. Plug in the optical meter, turn on, and set the wavelength on the optical meter to 1300nm.
7. Turn the laser back on. Move the photodiode such that it is perpendicular to the beam path and that the beam hits the center of the detector element. Verify that the laser is not overloading the detector. If overloaded, attach additional ND Filters to the one existing in the system until no longer overloaded.
8. Turn off the beam and optical meter. Using the washers and remaining  $\frac{1}{4}$ "-20 socket head cap screws, connect the table clamps to the construction base. These will be used to hold a 1cm side length square cuvette in place between them, so orient the clamps perpendicular to the beam path, but making sure they stay out of the direct path of the beam. Place a test cuvette in the center, and adjust the height of the construction base assembly such that the light passes through the middle of the cuvette. The cuvette should be perpendicular to and in the direct path of the beam.
  - a. Use nitrile gloves whenever handling the cuvette. Additionally, use isopropyl alcohol and a Kimwipe to clean the exterior of the cuvette prior to testing.
9. 15 minutes prior to testing, turn on the optical meter and take a dark reading. Zero the scale if not already at 0 Watts. Turn on the laser to let it warm up prior to data collection.

#### Methods – Creation of India Ink solutions

1. Take three cylindrical centrifuge tubes and place in the plastic centrifuge tube holder. Using the Sharpie, label the tubes with the following information:
  - a. Solution 1, 50mL Water, 50 $\mu$ L Ink

- b. Solution 2, 100mL Water, 50 $\mu$ L Ink
  - c. Solution 3, 150mL Water, 50 $\mu$ L Ink
2. Using the graduated cylinder, fill the first two centrifuge tubes with 50mL of DI H<sub>2</sub>O. Fill the third centrifuge tube with 12.5mL of DI H<sub>2</sub>O.
3. Using the 200 $\mu$ m Pipettor, measure 50 $\mu$ L of India Ink and place into the first centrifuge tube. Then, measure 25 $\mu$ L of India Ink and place into the second centrifuge tube. Mix both with vortex on power setting 7 for approximately 30 seconds each.
4. Using the graduated cylinder, remove 25mL of the mixture from the second centrifuge tube and add it to the third tube. Mix with vortex.
5. Bind the three centrifuge tubes together with a large rubber band and immerse in the ultrasonic bath. Use a clamp to hold the tubes vertically in the water. Set the timer to 30 minutes, power to 9, and ensure the heater is off. Run the ultrasonic bath.
6. Once 30 minutes have passed, remove the centrifuge tubes from the ultrasonic bath. Fill three cuvettes with roughly 3mL of liquid from each centrifuge tube. Cover the top of each cuvette with a piece of scotch tape to form a makeshift lid. Use the Sharpie to label the tape with the solution present in the cuvette. Fill a fourth cuvette with DI H<sub>2</sub>O. Clean the cuvettes with the Isopropyl alcohol as needed.

#### Methods – Running the experiment to find the absorption coefficient of India Ink

1. If the laser is not already on, perform step 9 of the “Setting up the mechanical components” methods to ensure the laser is warmed up and its performance is stable.
2. If the ink solutions were not made within the past 5 minutes, dispose of them and perform steps 5 and 6 of the “Creating the India Ink Solutions” methods again.
  - a. India Ink particles tend to clump together over time which changes their absorption/scattering behaviors. The ultrasonic bath will prevent this from occurring for 30 minutes.
3. Take a power measurement for the system with no cuvette present.
4. Place the empty cuvette onto the construction base between the two clamps. Press the cuvette against one clamp, then move and secure the second clamp such that it holds the

cuvette in place with a small amount of pressure. Take a power measurement then remove the cuvette. As before, wear nitrile gloves when handling the cuvettes.

5. Place the water cuvette onto the construction base between the two clamps. Secure the cuvette as before. Take a power measurement then remove the cuvette.
6. Place the Solution 1 cuvette onto the construction base between the two clamps. Secure the cuvette as before. Take a power measurement then remove the cuvette.
7. Place the Solution 2 cuvette onto the construction base between the two clamps. Secure the cuvette as before. Take a power measurement then remove the cuvette.
8. Place the Solution 3 cuvette onto the construction base between the two clamps. Secure the cuvette as before. Take a power measurement then remove the cuvette.
9. Repeat steps 3 through 8 of this procedure two times for a total of three trials.

## 5.2 – [Intralipid 20%, Water] Tissue Phantom Dilution SOP

### Materials

1. Eppendorf 5mL Pipettor with associated pipette tips	8. DI H <sub>2</sub> O
2. GeneMate 1mL Pipettor with associated pipette tips	9. 500mL Glass Beaker
3. GeneMate 200µL Pipettor with associated pipette tips	10. Masking Tape and Sharpie
4. Fisherbrand Conical Polypropylene Centrifuge Tubes	11. Fisher Vortex Genie 2
5. Styrofoam Centrifuge Tube holder	12. 50mL Glass Graduated Cylinder
6. Plastic Centrifuge Tube holder	13. Nitrile Gloves
7. Sigma-Aldrich 100mL Intralipid 20%	14. Kimwipes

### Methods

1. Take four conical polypropylene centrifuge tubes and set them in a plastic centrifuge tube holder. Using the masking tape and Sharpie, create temporary labels for each tube with the following text: **Master 1**, **Master 5**, **Master 9**, and **Master 13**.
  - a. Make all labels on both cap and main body of the centrifuge tubes.
2. Fill the 500mL glass beaker with DI H<sub>2</sub>O. Using the 5mL Pipettor, fill tubes **Master 5**, **Master 9**, and **Master 13** with 10mL of DI H<sub>2</sub>O. Using the 5mL Pipettor and the 1mL Pipettor, fill tube **Master 1** with 7.8mL of DI H<sub>2</sub>O.
  - a. Note that the gradation on the centrifuge tubes is approximate, use only as general guide for the amount of liquid added to the tube.
3. Using the 5mL Pipettor, 1mL Pipettor, and the 200µL Pipettor, measure 12.2mL of Intralipid 20% and place into tube **Master 1**. Cap the centrifuge tube and mix with vortex
  - a. Invert the bottle of Intralipid 20% eight times prior to removing any liquid.
  - b. Use vortex for 30 seconds on power setting 7.
  - c. When mixing the centrifuge tube with the vortex, make sure to hold both the cap and the body of the tube in order to prevent liquid spills.
  - d. Do not cross contaminate pipette tips, swap as necessary.
4. Using the 5mL Pipettor, measure 10mL of **Master 1** and add to tube **Master 5**. Cap the centrifuge tube and mix with vortex.

5. Using the 5mL Pipettor, measure 10mL of **Master 5** and add to tube **Master 9**. Cap the centrifuge tube and mix with vortex.
6. Using the 5mL Pipettor, measure 10mL of **Master 9** and add to tube **Master 13**. Cap the centrifuge tube and mix with vortex.
7. Move tubes **Master 5**, **Master 9**, and **Master 13** to the Styrofoam centrifuge tube holder. Take three fresh conical polypropylene centrifuge tubes and set them in a plastic centrifuge tube holder. Remove the temporary tube label for **Master 1**.
8. Using the Sharpie, create permanent labels for each tube. The tube formerly marked as **Master 1** shall be labeled **Test 1**. The remaining three tubes shall be labeled **Test 2**, **Test 3**, and **Test 4**. In addition to the number, the following information, detailing the Dilution Factors and % Intralipid, shall be added to each label.
  - a. For tube **Test 1** - DF1=1.64, DF2=4, %IL=3
  - b. For tube **Test 2** - DF1=1.64, DF2=8, %IL=1.5
  - c. For tube **Test 3** - DF1=1.64, DF2=20, %IL=.6
  - d. For tube **Test 4** - DF1=1.64, DF2=40, %IL=.3
9. Using the 5mL Pipettor, measure 10mL of DI H<sub>2</sub>O and add to tube **Test 2**.
10. Using the 50mL glass graduated cylinder, measure 40mL of DI H<sub>2</sub>O and add to tube **Test 3**.
11. Using the 50mL glass graduated cylinder, measure 45mL of DI H<sub>2</sub>O and add to tube **Test 4**.
12. Using the 50mL glass graduated cylinder, measure 30mL of DI H<sub>2</sub>O and add to the 10mL of mixture in tube labeled **Test 1**. Mix with vortex.
13. Using the 5mL Pipettor, measure 10mL of mixture from **Test 1** add to tube **Test 2**. Mix with vortex.
14. Using the 5mL Pipettor, measure 10mL of mixture from **Test 1** add to tube **Test 3**. Mix with vortex.
15. Using the 5mL Pipettor, measure 5mL of mixture from **Test 1** add to tube **Test 4**. Mix with vortex.
16. Move tubes **Test 1**, **Test 2**, **Test 3**, and **Test 4** to the Styrofoam centrifuge tube holder. Move three fresh conical polypropylene centrifuge tubes and the tube labeled **Master 5** to the plastic centrifuge tube holder. Remove the temporary tube label for **Master 5**.
17. Using the Sharpie, create permanent labels for each tube. The tube formerly marked as **Master 5** shall be labeled **Test 5**. The remaining three tubes shall be labeled **Test 6**, **Test 7**, and **Test 8**. In addition to the number, the following information, detailing the Dilution Factors and % Intralipid, shall be added to each label.

- a. For tube **Test 5** -  $DF1=3.28$ ,  $DF2=4$ ,  $\%IL=1.5$
  - b. For tube **Test 6** -  $DF1=3.28$ ,  $DF2=8$ ,  $\%IL=.76$
  - c. For tube **Test 7** -  $DF1=3.28$ ,  $DF2=20$ ,  $\%IL=.3$
  - d. For tube **Test 8** -  $DF1=3.28$ ,  $DF2=40$ ,  $\%IL=.15$
18. Using the 5mL Pipettor, measure 10mL of DI H<sub>2</sub>O and add to tube **Test 6**.
  19. Using the 50mL glass graduated cylinder, measure 40mL of DI H<sub>2</sub>O and add to tube **Test 7**.
  20. Using the 50mL glass graduated cylinder, measure 45mL of DI H<sub>2</sub>O and add to tube **Test 8**.
  21. Using the 50mL glass graduated cylinder, measure 30mL of DI H<sub>2</sub>O and add to the 10mL of mixture in tube labeled **Test 5**. Mix with vortex.
  22. Using the 5mL Pipettor, measure 10mL of mixture from **Test 5** add to tube **Test 6**. Mix with vortex.
  23. Using the 5mL Pipettor, measure 10mL of mixture from **Test 5** add to tube **Test 7**. Mix with vortex.
  24. Using the 5mL Pipettor, measure 5mL of mixture from **Test 5** add to tube **Test 8**. Mix with vortex.
  25. Move tubes **Test 5**, **Test 6**, **Test 7**, and **Test 8** to the Styrofoam centrifuge tube holder. Move three fresh conical polypropylene centrifuge tubes and the tube labeled **Master 9** to the plastic centrifuge tube holder. Remove the temporary tube label for **Master 9**.
  26. Using the Sharpie, create permanent labels for each tube. The tube formerly marked as **Master 9** shall be labeled **Test 9**. The remaining three tubes shall be labeled **Test 10**, **Test 11**, and **Test 12**. In addition to the number, the following information, detailing the Dilution Factors and % Intralipid, shall be added to each label.
    - a. For tube **Test 9** -  $DF1=6.56$ ,  $DF2=4$ ,  $\%IL=.76$
    - b. For tube **Test 10** -  $DF1=6.56$ ,  $DF2=8$ ,  $\%IL=.38$
    - c. For tube **Test 11** -  $DF1=6.56$ ,  $DF2=20$ ,  $\%IL=.15$
    - d. For tube **Test 12** -  $DF1=6.56$ ,  $DF2=40$ ,  $\%IL=.076$
  27. Using the 5mL Pipettor, measure 10mL of DI H<sub>2</sub>O and add to tube **Test 10**.
  28. Using the 50mL glass graduated cylinder, measure 40mL of DI H<sub>2</sub>O and add to tube **Test 11**.
  29. Using the 50mL glass graduated cylinder, measure 45mL of DI H<sub>2</sub>O and add to tube **Test 12**.
  30. Using the 50mL glass graduated cylinder, measure 30mL of DI H<sub>2</sub>O and add to the 10mL of mixture in tube labeled **Test 9**. Mix with vortex.
  31. Using the 5mL Pipettor, measure 10mL of mixture from **Test 9** add to tube **Test 10**. Mix with vortex.

32. Using the 5mL Pipettor, measure 10mL of mixture from **Test 9** add to tube **Test 11**. Mix with vortex.
33. Using the 5mL Pipettor, measure 5mL of mixture from **Test 9** add to tube **Test 12**. Mix with vortex.
34. Move tubes **Test 9**, **Test 10**, **Test 11**, and **Test 12** to the Styrofoam centrifuge tube holder. Move three fresh conical polypropylene centrifuge tubes and the tube labeled **Master 13** to the plastic centrifuge tube holder. Remove the temporary tube label for **Master 13**.
35. Using the Sharpie, create permanent labels for each tube. The tube formerly marked as **Master 13** shall be labeled **Test 13**. The remaining three tubes shall be labeled **Test 14**, **Test 15**, and **Test 16**. In addition to the number, the following information, detailing the Dilution Factors and % Intralipid, shall be added to each label.
  - a. For tube **Test 13** -  $DF1=13.11$ ,  $DF2=4$ ,  $\%IL=.38$
  - b. For tube **Test 14** -  $DF1=13.11$ ,  $DF2=8$ ,  $\%IL=.19$
  - c. For tube **Test 15** -  $DF1=13.11$ ,  $DF2=20$ ,  $\%IL=.076$
  - d. For tube **Test 16** -  $DF1=13.11$ ,  $DF2=40$ ,  $\%IL=.038$
36. Using the 5mL Pipettor, measure 10mL of DI H<sub>2</sub>O and add to tube **Test 14**.
37. Using the 50mL glass graduated cylinder, measure 40mL of DI H<sub>2</sub>O and add to tube **Test 15**.
38. Using the 50mL glass graduated cylinder, measure 45mL of DI H<sub>2</sub>O and add to tube **Test 16**.
39. Using the 5mL Pipettor, remove 10mL of mixture in tube labeled **Test 13** and throw away. Using the 50mL glass graduated cylinder, measure 30mL of DI H<sub>2</sub>O and add to the 10mL of mixture in tube labeled **Test 13**. Mix with vortex.
40. Using the 5mL Pipettor, measure 10mL of mixture from **Test 13** add to tube **Test 14**. Mix with vortex.
41. Using the 5mL Pipettor, measure 10mL of mixture from **Test 13** add to tube **Test 15**. Mix with vortex.
42. Using the 5mL Pipettor, measure 5mL of mixture from **Test 13** add to tube **Test 16**. Mix with vortex.
43. Take 16 "Test" centrifuge tubes and store them in the fridge in Styrofoam container.

### 5.3 – [India Ink, Intralipid 20%, Water] Tissue Phantom Dilution SOP

#### Materials

1. Eppendorf 5mL Pipettor with associated pipette tips	10. Dr. Ph. Martin's Black Star India Ink
2. GeneMate 1mL Pipettor with associated pipette tips	11. VWR Model 50D Ultrasonic Bath
3. GeneMate 200 $\mu$ L Pipettor with associated pipette tips	12. 50mL Glass Graduated Cylinder
4. Fisherbrand Conical Polypropylene Centrifuge Tubes	13. Masking Tape and Sharpie
5. Styrofoam Centrifuge Tube holder	14. 50mL Glass Graduated Cylinder
6. Plastic Centrifuge Tube holder	15. Nitrile Gloves
7. Sigma-Aldrich 100mL Intralipid 20%	16. Kimwipes
8. DI H <sub>2</sub> O	17. Large Rubber Band
9. 500mL Glass Beaker	

#### Methods

1. Follow the steps described in Appendix 5.2 – [Intralipid 20%, Water] Tissue Phantom Dilution SOP.
2. Place the bottle of India Ink in the Ultrasound bath, using a clamp or some other holder to keep the bottle upright. Ensure the heater is off, the power is set to 9, and run the ultrasound for 30 minutes. Once completed, remove the bottle from the ultrasound bath.
3. Using the 200 $\mu$ L Pipettor, measure 22 $\mu$ L of India Ink and add to the following tubes. When the Pipettor is removed from the ink, take a Kimwipe and wipe the outside of the pipette tip prior to ejecting the ink into the tissue phantom in order to remove the excess ink. Once the ink has been ejected, pump the tissue phantom liquid up and down with the Pipettor to mitigate the amount of ink left inside the pipette tip.
  - a. Test 1, Test 5, Test 9, and Test 13
4. Using the 200 $\mu$ L Pipettor, measure 30 $\mu$ L of India Ink and add to the following tubes for both trials. As before, remember to wipe the pipette tip and pump the Pipettor.
  - a. Test 2, Test 6, Test 10, and Test 14

5. Using the 200 $\mu$ L Pipettor, measure 74 $\mu$ L of India Ink and add to the following tubes for both trials. As before, remember to wipe the pipette tip and pump the Pipettor.
  - a. Test 3, Test 4, Test 7, Test 8, Test 11, Test 12, Test 15, and Test 16.
6. Once the ink has been added to each of the "Test" solutions, briefly mix with the vortex then place back into the refrigerator.

## 5.4 – Preparation of Tissue Phantom Holder SOP

### Materials

1. 3D Printed Tissue Phantom holder, quantity 2	10. Glass cutter or Glass scoring tool
2. 3D Printed Kinematic rod-base, quantity 1	11. Nitrile Gloves
3. 3D Printed Kinematic hole-base, quantity 2	12. Disposable Laboratory Mat
4. Newport P100-A Tip-Tilt Mount	13. Ruler
5. Hot glue gun and hot glue	14. Sharpie
6. Cyanoacrylate glue	15. Safety Glasses
7. ½” Optical Mounting Post	16. Kimwipes
8. #8-32 SHCS	17. Soft, disposable optical cleaning wipes
9. Fisherbrand Microscope Cover Glass 24mm x 60mm - 1.5mm	18. Isopropyl Alcohol

### Methods

1. Put on nitrile gloves and line a work surface with the disposable laboratory mat to help prevent against glue spills and messes.
2. Plug in the hot glue gun and set on the lab mat while it heats up.
3. Using the #8-32 socket head cap screw, connect the Newport tip-tilt mount to the ½” optical mounting post.
4. Before gluing, take the tissue phantom holder, rod-base, hole-base, and the Newport tip-tilt mount and do a “dry fit” to determine the proper alignment of the parts. The two rods on the rod-base shall be along the same diagonal to the screws on the tip-tilt stage. The hole-base will be oriented such that the rods can go into the holes. The phantom holder will be oriented such that the side with the notch will be on the same side as the mounting post attached to the tip-tilt mount. Make a mark and take a picture to verify this alignment.

5. Being sure to maintain the proper orientation, take the phantom holder and place upside-down on the lab mat. Apply a small amount of cyanoacrylate glue in the center of the tissue phantom holder's base.
6. Place the hole-base, hole-side down on the lab mat. Apply a thin line of cyanoacrylate glue along the top, making sure not to get too close to the air holes.
7. Flip the hole-base onto the tissue phantom holder and press down firmly. Press along the outer edges to keep the two pieces properly aligned. Once aligned, set aside and do not touch for approximately 5-10 minutes.
8. Once the hot glue gun has heated up, place the rod-base on top of the tip-tilt stage in the proper orientation and hold with one hand. Along one side, place three beads of hot glue at the interface between the two parts, taking care to limit the amount of strings of glue.
9. Without releasing the hold on the parts, place three similar beads along another side. Set on the lab mat, making sure to support the tip-tilt stage so the parts don't tip over.
10. After approximately 3-5 minutes have passed, check that the hot glue has cooled. Once cool, repeat the previous two steps for the remaining two sides of the interface.
11. Unplug the hot glue gun, replace nitrile gloves, put on safety glasses, and move away from the lab mat to a flat section of the lab table.
12. Take the microscope cover glass and place on the lab table next to a ruler. Use the sharpie to mark 35mm from the edge of the cover glass in the long direction. Make one mark along both edges of the glass, and then make a straight line connecting the two with a sharpie.
13. Using the glass cutter or glass scoring tool, make light scratches and cuts along the line, pressing up against the ruler to keep the line straight. After some amount of time, the cover glass will split and the cover glass for the surface of the tissue phantom will be completed.
14. Being careful of the sharp glass edge, clean the cover glass with isopropyl alcohol and Kimwipes. Once cleaned, place in the tissue phantom holder.
15. Place the completed and dried assembly in its position in the test arm of the system.

## 5.5 – Preparation of Modular Lens System and Alignment SOP

### Materials

1. KPX076AR.18 quantity 3	10. ½” Optical Mounting Posts quantity 6
2. KPX082AR.18 quantity 1	11. Newport LH-100 1inch Diameter Fixed Lens Mount quantity 6
3. KPX088AR.18 quantity 1	12. 1” OD threaded Retaining Ring quantity 6
4. KPX094AR.18 quantity 1	13. ¼”-20 SHCS quantity 16
5. Newport BKL-4 Locking 3.5 x 4” Kinematic Base	14. #8-32 x .5” set screw quantity 6
6. Newport BKL-4-T Top plate for BKL-4 quantity 2 (for a total of 3)	15. Retaining ring removal tool
7. Newport MRL-6M Miniature Optical Rail, 6inch quantity 3	16. Label Maker
8. Newport MCF Miniature Rail Flat Carrier quantity 6	17. Oscilloscope
9. ½” Optical Post Holder quantity 6	18. Tissue Phantom Holder Assembly

### Methods

1. Remove the MRL-6M miniature optical rail that is furthest from the beam collimator from the test arm of the Time-Domain OCT system. If is anything on top of the optical rail, remove prior to removing the rail from the system.
2. Take one of the BKL-4-T kinematic base top plates and attach the miniature optical rail using two ¼”-20 SHCS. The optical rail should be oriented in the center of the plate such that the “Lock” and “Open” arrows should be on the same side of the optical rail. Repeat this process for the other two sets of plates and optical rails.
3. Lock one of the kinematic plate assemblies onto the BKL-4 kinematic base by tightening the large wheel on the kinematic base.
4. Place the kinematic assembly into the test arm of the Time-Domain OCT system such that the optical rail in the assembly is parallel to the optical rail in the test arm. Using four ¼”-20 SHCS, secure the base plate to the table. Remove and set aside the top plate.
5. Attach a miniature rail carrier to the bottom of each ½” post holder using a ¼”-20 SHCS.

6. Attach a lens mount,  $\frac{1}{2}$ " post, and  $\frac{1}{2}$ " post holder together using an #8-32 set screw. Repeat this process for each of the lens mounts.
7. While wearing nitrile gloves, take one of the KPX076AR.18 lenses and carefully clean using Kimwipes and Isopropyl alcohol. Delicately place into one of the completed lens mount assemblies such that the planar side of the lens is in contact with the mounting feature in the lens mount. Attach one of the retaining rings such that the ring presses against the convex side of the lens and holds it in place. Print out a label that reads "KPX076AR.18" and attach it to the lens mount holding that lens. Slide the assembly onto an optical rail/kinematic base assembly.
8. Repeat step 7 for the KPX082AR.18 lens. Slide the assembly onto the same optical rail/kinematic base assembly as the previous lens. The lenses should be ordered such that if the assembly was placed back into the system, the KPX076AR.18 lens would be closest to the laser collimator. The planar surface of both lenses should be facing towards each other. Print a label that reads "Setup 1 NA=.0603" and attach it to the kinematic top plate.
9. Repeat steps 7 and 8 for one of the KPX076AR.18 lenses and the KPX088AR.18 lens. The label for the plate shall read "Setup 2 NA=.0901".
10. Repeat steps 7 and 8 for the last KPX076AR.18 lens and the KPX094AR.18 lens. Again, the KPX076AR.18 lens should be closest to the laser collimator, and the planar surfaces of both lenses should face each other. The label for the plate shall read "Setup 3 NA=.1186".
11. Begin the system alignment process by working without any of the lens modules added into the system. Connect the detector to an oscilloscope and set the detector to output DC only. Using a Kimwipe, block the light in the test arm. Adjust the tip and tilt of the mirror in the reference arm until the signal reaches a maximum.
12. Unblock the light in the test arm, then block the light in the reference arm with the Kimwipe. Adjust the tip and tilt of the target mirror in the test arm until the signal reaches a maximum. Remove the Kimwipe from the reference arm.
13. Look to the oscilloscope to see if there is an interference pattern. If there is not, carefully press on the translation stage attached to the galvo. Apply constant pressure and slowly increase the reference arm path length while looking at the oscilloscope screen. Eventually, small blips of interference will begin to pass by on the oscilloscope. Hold the translation stage steady and move the micrometer to the new position.

14. Once in the new position, only move the translation stage using the micrometer. Slowly move the micrometer until a stable interference pattern appears on the oscilloscope. Adjust the position of the mirror using the test arm micrometer to achieve the highest signal.
15. Move back to the lens modules. Across all three systems, set the KPX076AR.18 lenses to approximately the same position along the rail. Referencing the lens design documentation, use a ruler to approximately place the second lenses in the correct positions along the rail.
16. Take "Setup 2" and remove the KPX088AR.18 from the post holder, then set the lens aside. Place the module into the OCT system.
17. Once placed into the system, set the first lens to approximately the same height as the collimator. Using the IR viewing card, check the placement of the expanded beam footprint on the fold mirror. If deviated along the x-axis, parallel to the table and perpendicular to the optical axis, then slightly move the kinematic base plate in that direction. If deviated along the y-axis, perpendicular to the table, then slightly move the lens in the opposite direction.
  - a. Slowly iterate this process. When locking down any screws, move slowly to prevent any movement during that process. Try to keep the lens from rotating azimuthally when increasing the height.
18. Once the beam seems to point in the correct direction, check to be sure that the beam is not being vignetted. Introduce the second lens into the system and match the height of the collimator and the first lens.
19. Use the IR viewing card with a small hole punched into it to assess how the beam is returning to the original input. Place the hole over the beam output and observe where the return beam falls. If the beam is deviated in the x-axis, make small adjustments to the base plate. If the beam is deviated in the y-axis, make small adjustments to the lens heights. Move one component at a time, then check to see the position of the beam.
20. Next, use the IR viewing card with the small hole to check the beam behavior just before the focusing lens. Again, place the hole where the outgoing beam passes, then check the position of the return beam. Make slight system adjustments as before.
21. Iterate between steps 19 and 20 until the beam retroreflects along its path, which can be determined when the IR viewing card shows no beam deviation at either location. At this point, the base plate can be considered "locked in", and should not be moved again unless completely realigning the system.

22. Repeat steps 13 and 14 until the reference and test arm pathways are matched and a nice interference signal is present. Once completed, remove the lens module from the system and replace with "Setup 1".
23. Repeat Steps 16 through 21 until this lens module is properly aligned. However, the kinematic base plate should not be moved. If there is an issue with the beam deviating along the x-axis, this is most likely an issue with the lenses being rotated too much in the azimuthal direction. If azimuthal rotations will not fix the deviation, try slightly rotating the miniature optical rail.
24. Finally, perform the same alignment procedures as followed in Step 23 for "Setup 3".
25. Once fully aligned, replace the mirror at the end of the reference arm with the 3D printed assembly, and set the Ronchi ruling as the target. Adjust the test-arm micrometer and the tip and tilt of the plate in order to achieve the maximum signal on the oscilloscope.
26. Remove "Setup 3" from the system, and replace with "Setup 2". At this point, do not touch the test-arm micrometer or the position of the focusing lens. Carefully move the rear lens in the modular lens system along the miniature optical rail until the signal on the oscilloscope reaches a maximum. Using a pencil, mark the position of the rail carrier for both lenses.
27. Remove "Setup 2" from the system, and replace with "Setup 1". Do not touch the test-arm micrometer or the position of the focusing lens. Carefully move the rear lens in the modular lens system along the miniature optical rail until the signal on the oscilloscope reaches a maximum. Using a pencil, mark the position of the rail carrier for both lenses.
28. Using a pipette, add water into the tissue phantom holder. This will change the ideal focus position and the length of the reference arm, so repeat steps 13 and 14 in order to achieve interference. Once interference has been found, adjust the test arm micrometer until the signal on the oscilloscope is maximized.
29. At this point, the system has been aligned and optimized for operation with liquid present in the tissue phantom holder. Check with "Setup 2" and "Setup 3" to ensure that the focal position remains constant across all configurations. Take note of the positions of the micrometers in order to facilitate realignment in the future.
30. Unplug the oscilloscope to reduce the noise present during data collection.

## 5.6 – Software Manipulation and Troubleshooting SOP

### Methods – Turning on the OCT system and software

1. Turn on the computer and login with password - coherence1300.
2. Turn on the source by turning power switch from the “O” to “I” position. Wait for the TEC lights under "Driver 1" and "Driver 2" to turn solid green. Then press the “On/Off” buttons for "Driver 1" and "Driver 2" such that the SLD lights have both turned solid green. Using the IR viewing card, check that light is coming out of fiber into the test arm.
3. If light is not coming out of fiber into the test arm, press both “On/Off” buttons such that the SLD lights have turned off. Carefully remove the fiber connected to the source (the box labeled “2x2 Broadband SLD Combiner”), then carefully reinsert making sure the raised section on the FC side of the adapter (the fiber) is aligned with the groove on the APC side (the box). Turn on the SLD and check for beam propagation. If light is still not coming out, shut off the SLD, power down the entire source, then follow Step 2 turn the system on again. If there is still no propagation upon fully resetting the system, seek assistance.
4. Turn the switch on the detector box to the “On” position. The detector box is the small black, grey, and red box located behind the computer monitor.
5. Turn on the galvo. The galvo control box is the metal box on the small plastic bench below the computer table. The switch can be accessed from the side opposite the computer monitor and keyboard. Move the switch to the “On” position.
6. If the Lock-In Amplifier is not already on, turn it on by flipping the red switch.
7. Turn on the Motion Controller, located on top of the "control tower". Flip the red switch to the on position, at which point 4 green LEDs should light up. These LEDs are labeled “Axis 1 or 2|1”, “Axis 1 or 2|Run”, “Axis 3 or 4|3”, and “Axis 3 or 4|Run”.
8. Select "Shortcut to OCTLIFccd181024-travis" on the desktop.
9. Prior to collecting data, check that the detector has the proper settings. The upper left knob, the high pass filter, should be set to 1K. The upper right knob, the low pass filter, should always be set to the maximum. The bottom knob, the gain, should be set to 100 by moving the toggle to 2 and the magnitude to  $10^2$ .
10. Check the settings on the Lock-In Amplifier. The “Time Constant” section, the low pass filter for the lock-in amplifier, should be set to  $30\mu\text{s}$ , 24dB cutoff frequency, and No sync. The

“Signal Input” section should be set to input A, AC couple, and Float. The “Reserve” section should be set to Low noise. In the “Filters” section, all the settings should be on. The “Sensitivity” settings will vary throughout the experiment.

11. On the LabView window, check that the settings are set properly. In the “Data Format” box, make sure that “Save Phase” is off, the data type is ASCII, and the “Save log?” switch is in the down/off position. In the “B-Scan Parameters” box, set the lateral range to 2mm, the number of A-Scans to 500, and the “Sample Arm Config” to “In Air”. Under no circumstance should the settings in the “A-Scan Parameters” box be changed.
12. In order to turn off the system, follow these steps in reverse. In order to shut down the software, press the “Stop” at the upper left corner of the screen, then close out of LabView. If LabView prompts a “Save” dialogue when closing out of the software, press “Don’t Save”. The computer does not need to be shut down when turning off the system.

#### Methods – Naming, saving, and manipulating files

1. Plug a flash drive into the computer.
2. In the LabView window, type the file path for the folder “RSiposThesisTrial#” into the “Directory” box. The file path is given below. This folder should be locally saved to the desktop of the computer in the lab. The # in the file path will depend on the trial being run.
  - a. C:\Documents and Settings\Administrator\Desktop\RSiposThesisTrial#
3. Type the name of the file into the “Comment” box. The name of the file shall be based on the following format: “trial\_#\_combo\_#\_NA\_#\_run\_#\_”.
  - a. Trial # = 1 or 2 depending on which trial is currently being tested.
  - b. Combo # = 1, 2, 3, 4, 6, 8, 10, 12, 14, 16, or 17 depending on the test number of the phantom in the system. Combos 5, 7, 9, 11, 13, and 15 are redundant.
  - c. NA # = 06, 09, or 12 depending on the system setup for the test.
  - d. Run # = 1, 2, 3, or 4 depending on how many times the “Save” button has been pressed.
4. After running the experiment, press the “Save” button. Have the folder “RSiposThesisTrial#” open to make sure the run saved. Change the file name as needed for each run.

- a. Note that the file names saved to the computer will have a slightly different naming format than the name input into the “Comment” box. The computer will save the values as “YYMMDDcomment####.oca”. YYMMDD corresponds to the current data (ex. 190326 for March 26, 2019), comment corresponds to the information input into the “Comment” box during step 3, and #### corresponds to an internal count performed by the LabView code.
  - b. Upon collecting all of the data, the files will be run through a Python script that will remove the YYMMDD and #### information in the file names, leaving the file with the name “comment.oca”.
5. Upon completion of data collection, copy the folder to the flash drive, then move to a computer where it can be uploaded onto the Barton Lab Network.

#### Methods – Troubleshooting the linear translation stage

1. If the linear translation stage travels to the end of its effective range of motion, frequently the scan settings used during this experiment (lateral range of 2mm with 500 scans) will result in the stage not moving consistently during data collection. The reason for this error has not been precisely determined, but a relatively consistent set of steps can be taken to alleviate this issue.
2. The goal is to move the stage away from the end of its range of motion and not let it return if at all possible. When starting the scan from a different location, the likelihood that the stage will move and the data will be collected increases dramatically.
3. There is no way to move the translation stage’s position without running the software and acquiring an image, unless the stage and motion controller are completely disconnected from the software, which is not a realistic solution during the middle of data collection.
4. In order to move the translation stage’s starting position, attempt to take advantage of the hysteresis present in the translation stage or the occasional bug that will cause the stage to only move in one direction during a scan.
  - a. When working properly, upon pressing the “Acquire Image” button on LabView, the stage will begin moving according to the lateral range and number of scans designated. Once the scans are complete, the stage will then move back to its starting position by moving a distance equivalent to the negative lateral range.

- i. Hysteresis occurs when the stage moves a different amount of distance backward than it moved forward. This is due to the stage being more accurate in the forward direction than the backward direction.
  - ii. Occasionally, the stage will not return to its starting location at all. This happens randomly and can seemingly occur for any scan parameters.
5. Repeatedly run the “Acquire Image” script over and over until one of these two errors occurs and the stage does not return to the end of its range of motion. This is done most effectively with a fractional lateral range (such as 1.5mm) and a relatively low number of scans (such as 100 scans per mm). After enough iterations, typically one of the errors described above will occur and the stage will stop moving to the end of its range of motion.
  - a. When the stage pushes to the end of its range of motion, the motor makes a unique and identifiable sound that can be noted to determine if the troubleshooting procedure needs to be repeated. As the motor moves, a soft electronic “whirring” sound can be heard. As the motor pushes up against the end of its available motion, the sound will increase in frequency rapidly and then stop abruptly. If the motor stops in the middle of its range, the sound will decrease in frequency and fade.
6. Once the stage has moved to a better starting location, try to maintain this state for as long as possible. Watch the location at which the stage starts and stops during image acquisition. If this location starts to move too close to the end of the range, perform step 5 again to help preempt the problem.
  - a. While the hysteresis present in the stage will sometimes end up moving the stage away from the end, it will occasionally move the stage back towards the end. Rarely, even when away from the end of the rail, the stage will not move during image acquisition, and then move backwards as if it had moved. Finally, the stage may randomly move all the way back to the end of its effective range of motion with no way to stop its movement. When this occurs, return to step 5.
7. While infrequent, the stage may move so far from the end of its range that the beam actually moves beyond the edge of the tissue phantom holder. When this occurs, simply input a small negative lateral range (such as -1mm), and run the image acquisition. Repeat as necessary to return the stage to a better starting location.

## 5.7 – [Intralipid 20%, Water] Experimental Procedures SOP

### Methods

1. Set out an absorbent pad on the optical table to help protect against spills. Set an optical grade disposable cloth on top of the absorbent pad to help keep delicate optics clean and free of scratches. Wear nitrile gloves and a face mask when working with the lens modules, the Ronchi ruling, or the cover glass.
2. When proceeding through the experimental procedures, take extreme caution to avoid bumping into any part of the system accidentally, as that could require going through the alignment procedures again and potentially restarting the data collection.
3. Insert the modular lens system “Setup 1” into the kinematic base plate and tighten. Double check that the correct system has been inserted by confirming with the label on the kinematic top plate, the labels on the lenses, and the printed lens prescriptions.
4. Clean the Ronchi ruling and the cover glass with Isopropyl alcohol and the soft optical cleaning wipes, then place the ruling into the tissue phantom holder. Note that the chromed surface of the ruling should be facing up. Do not use Kimwipes to clean the ruling, as the surface could be easily scratched or damaged by a rough wipe.
5. Run through the “Naming, saving, and manipulating files” and “Turning on the OCT system and software” methods in Appendix 5.6.
6. Take the Trial 1 tissue phantoms and set aside for use throughout the experiment. Slowly add 4.125 mL of water from the centrifuge tube labeled “Test 17” to the phantom holder onto the ruling. Lightly press down on the ruling to confirm it is not floating in the liquid. Place the cover glass over the water to form a smooth interface.
7. Carefully place the holder onto the 3D printed part such that the notch is closest to the micrometer stage. Move the test arm micrometer slightly up and down in order to find the position in which the A-scan peak is at its highest. This is the position in which the beam is focused on the surface of the ruling. Adjust the sensitivity on the Lock-In Amplifier as necessary to maximize the signal return from the chrome without overloading.

8. Check the “A-Scan” box in the LabView window to ensure the system is properly aligned. If correct, the sharp peak should be centered at 250 on the x-axis. If the sharp peak is centered on a different value, move the reference arm micrometer until the correct value is reached.
9. Type the appropriate file name into the “Comment” box in the LabView window based on the naming procedures defined in Appendix 5.6. The first file name should be “trial\_1\_combo\_17\_NA\_06\_run\_1\_”. Ensure the proper file pathway is selected.
10. Check the settings on LabView. The correct values are as follows:
  - a. In “B-Scan Parameters”, Lateral Range = 2mm, Number of A-Scans = 500, and In-Air
11. Press “Acquire Image”. Step away from the computer and the table while the system completes the scans. Once the scans are finished, press “Save”. For this and all future scans, check that the files saved properly before continuing onto the next step.
  - a. If the motorized linear translation stage is not moving, consult the troubleshooting procedures in Appendix 5.6.
12. Rename the comment to “trial\_1\_combo\_17\_NA\_06\_run\_2\_”. Check the settings on LabView, then press “Acquire Image”. Step away from the computer and the table while the system completes the scans. Once the scans are finished, press “Save”.
13. Rename the comment to “trial\_1\_combo\_17\_NA\_06\_run\_3\_”. Check the settings on LabView, then press “Acquire Image”. Step away from the computer and the table while the system completes the scans. Once the scans are finished, press “Save”.
14. Rename the comment to “trial\_1\_combo\_17\_NA\_06\_run\_4\_”. Decrease the sensitivity such that the peak from the glass reflection is maximized without being overloaded. Note that the reflection off the chrome will be overloaded. Check the settings on LabView, then press “Acquire Image”. Step away from the computer and the table while the system completes the scans. Once the scans are finished, press “Save”.
15. Swap the modular lens setup to “Setup 2”. Lock the kinematic base plate, then move the test arm micrometer slightly up and down in order to find the position in which the oscilloscope peak is at its highest. Then, check the “A-Scan” box in the LabView window to ensure the system is properly aligned. If correct, the sharp peak should be centered at 250 on the x-axis. If the sharp peak is centered on a different value, move the reference arm micrometer

until the correct value is reached. Adjust the sensitivity on the Lock-In Amplifier to maximize the signal return from the chrome without overloading.

16. Rename the comment to "trial\_1\_combo\_17\_NA\_09\_run\_1\_".
17. Check the settings on LabView.
18. Press "Acquire Image". Step away from the computer and the table while the system completes the scans. Once the scans are finished, press "Save".
19. Rename the comment to "trial\_1\_combo\_17\_NA\_09\_run\_2\_". Check the settings on LabView, then press "Acquire Image". Step away from the computer and the table while the system completes the scans. Once the scans are finished, press "Save".
20. Rename the comment to "trial\_1\_combo\_17\_NA\_09\_run\_3\_". Check the settings on LabView, then press "Acquire Image". Step away from the computer and the table while the system completes the scans. Once the scans are finished, press "Save".
21. Rename the comment to "trial\_1\_combo\_17\_NA\_09\_run\_4\_". Decrease the sensitivity such that the peak from the glass reflection is maximized without being overloaded. Check the settings on LabView, then press "Acquire Image". Step away from the computer and the table while the system completes the scans. Once the scans are finished, press "Save".
22. Swap the modular lens setup to "Setup 3". Lock the kinematic base plate, then move the test arm micrometer slightly up and down in order to find the position in which the oscilloscope peak is at its highest. Then, check the "A-Scan" box in the LabView window to ensure the system is properly aligned. If correct, the sharp peak should be centered at 250 on the x-axis. If the sharp peak is centered on a different value, move the reference arm micrometer until the correct value is reached. Adjust the sensitivity on the Lock-In Amplifier to maximize the signal return from the chrome without overloading.
23. Rename the comment to "trial\_1\_combo\_17\_NA\_12\_run\_1\_".
24. Check the settings on LabView.
25. Press "Acquire Image". Step away from the computer and the table while the system completes the scans. Once the scans are finished, press "Save".

26. Rename the comment to "trial\_1\_combo\_17\_NA\_12\_run\_2\_". Check the settings on LabView, then press "Acquire Image". Step away from the computer and the table while the system completes the scans. Once the scans are finished, press "Save".
27. Rename the comment to "trial\_1\_combo\_17\_NA\_12\_run\_3\_". Check the settings on LabView, then press "Acquire Image". Step away from the computer and the table while the system completes the scans. Once the scans are finished, press "Save".
28. Rename the comment to "trial\_1\_combo\_17\_NA\_12\_run\_4\_". Decrease the sensitivity such that the peak from the glass reflection is maximized without being overloaded. Check the settings on LabView, then press "Acquire Image". Step away from the computer and the table while the system completes the scans. Once the scans are finished, press "Save".
29. Remove the phantom holder from the system. Being careful to not drop the cover glass or the Ronchi ruling, remove the phantom from the holder and rinse with DI Water. Dry the interior of the phantom holder with a Kimwipe and clean the cover glass and Ronchi ruling with isopropyl alcohol and soft optical cleaning wipes.
30. Once clean and dry, put the Ronchi ruling back into its original position. Fill with 4.125 mL of phantom from the tube labeled "Test 16". Cover the phantom with the cover glass.
31. Swap the modular lens setup to "Setup 1". Lock the kinematic base plate, then move the test arm micrometer slightly up and down in order to find the position in which the oscilloscope peak is at its highest. Then, check the "A-Scan" box in the LabView window to ensure the system is properly aligned. Move the reference arm micrometer until the sharp peak is centered on 250 on the x-axis. Adjust the sensitivity on the Lock-In Amplifier to maximize the signal return from the chrome without overloading.
32. Rename the comment to "trial\_1\_combo\_16\_NA\_06\_run\_1\_".
33. Check the settings on LabView.
34. Press "Acquire Image". Step away from the computer and the table while the system completes the scans. Once the scans are finished, press "Save".
35. Rename the comment to "trial\_1\_combo\_16\_NA\_06\_run\_2\_". Check the settings on LabView, then press "Acquire Image". Step away from the computer and the table while the system completes the scans. Once the scans are finished, press "Save".

36. Rename the comment to "trial\_1\_combo\_16\_NA\_06\_run\_3\_". Check the settings on LabView, then press "Acquire Image". Step away from the computer and the table while the system completes the scans. Once the scans are finished, press "Save".
37. Rename the comment to "trial\_1\_combo\_16\_NA\_06\_run\_4\_". Decrease the sensitivity such that the peak from the glass reflection is maximized without being overloaded. Check the settings on LabView, then press "Acquire Image". Step away from the computer and the table while the system completes the scans. Once the scans are finished, press "Save".
38. Swap the modular lens setup to "Setup 2". Lock the kinematic base plate, then move the test arm micrometer slightly up and down in order to find the position in which the oscilloscope peak is at its highest. Then, check the "A-Scan" box in the LabView window to ensure the system is properly aligned. Move the reference arm micrometer until the sharp peak is centered on 250 on the x-axis. Adjust the sensitivity on the Lock-In Amplifier to maximize the signal return from the chrome without overloading.
39. Rename the comment to "trial\_1\_combo\_16\_NA\_09\_run\_1\_".
40. Check the settings on LabView.
41. Press "Acquire Image". Step away from the computer and the table while the system completes the scans. Once the scans are finished, press "Save".
42. Rename the comment to "trial\_1\_combo\_16\_NA\_09\_run\_2\_". Check the settings on LabView, then press "Acquire Image". Step away from the computer and the table while the system completes the scans. Once the scans are finished, press "Save".
43. Rename the comment to "trial\_1\_combo\_16\_NA\_09\_run\_3\_". Check the settings on LabView, then press "Acquire Image". Step away from the computer and the table while the system completes the scans. Once the scans are finished, press "Save".
44. Rename the comment to "trial\_1\_combo\_16\_NA\_09\_run\_4\_". Decrease the sensitivity such that the peak from the glass reflection is maximized without being overloaded. Check the settings on LabView, then press "Acquire Image". Step away from the computer and the table while the system completes the scans. Once the scans are finished, press "Save".
45. Swap the modular lens setup to "Setup 3". Lock the kinematic base plate, then move the test arm micrometer slightly up and down in order to find the position in which the oscilloscope

peak is at its highest. Then, check the “A-Scan” box in the LabView window to ensure the system is properly aligned. Move the reference arm micrometer until the sharp peak is centered on 250 on the x-axis. Adjust the sensitivity on the Lock-In Amplifier to maximize the signal return from the chrome without overloading.

46. Rename the comment to “trial\_1\_combo\_16\_NA\_12\_run\_1\_”.
47. Check the settings on LabView.
48. Press “Acquire Image”. Step away from the computer and the table while the system completes the scans. Once the scans are finished, press “Save”.
49. Rename the comment to “trial\_1\_combo\_16\_NA\_12\_run\_2\_”. Check the settings on LabView, then press “Acquire Image”. Step away from the computer and the table while the system completes the scans. Once the scans are finished, press “Save”.
50. Rename the comment to “trial\_1\_combo\_16\_NA\_12\_run\_3\_”. Check the settings on LabView, then press “Acquire Image”. Step away from the computer and the table while the system completes the scans. Once the scans are finished, press “Save”.
51. Rename the comment to “trial\_1\_combo\_16\_NA\_12\_run\_4\_”. Decrease the sensitivity such that the peak from the glass reflection is maximized without being overloaded. Check the settings on LabView, then press “Acquire Image”. Step away from the computer and the table while the system completes the scans. Once the scans are finished, press “Save”.
52. Remove the phantom holder from the system. Being careful to not drop the cover glass or the Ronchi ruling, remove the phantom from the holder and rinse with DI Water. Dry the interior of the phantom holder with a Kimwipe and clean the cover glass and Ronchi ruling with isopropyl alcohol and soft optical cleaning wipes.
53. Once clean and dry, put the Ronchi ruling back into its original position. Fill with 4.125 mL of phantom from the tube labeled “Test 14”. Cover the phantom with the cover glass.
54. Repeat steps 31 through 51 for the “Test 14” phantom, making sure to set the comment to the proper naming scheme of “trial\_1\_combo\_14\_NA\_#\_run\_#\_”.
55. Remove the phantom holder from the system. Being careful to not drop the cover glass or the Ronchi ruling, remove the phantom from the holder and rinse with DI Water. Dry the

interior of the phantom holder with a Kimwipe and clean the cover glass and Ronchi ruling with isopropyl alcohol and soft optical cleaning wipes.

56. Once clean and dry, put the Ronchi ruling back into its original position. Fill with 4.125 mL of phantom from the tube labeled "Test 12". Cover the phantom with the cover glass.
57. Repeat steps 31 through 51 for the "Test 12" phantom, making sure to set the comment to the proper naming scheme of "trial\_1\_combo\_12\_NA\_#\_run\_#\_".
  
58. Remove the phantom holder from the system. Being careful to not drop the cover glass or the Ronchi ruling, remove the phantom from the holder and rinse with DI Water. Dry the interior of the phantom holder with a Kimwipe and clean the cover glass and Ronchi ruling with isopropyl alcohol and soft optical cleaning wipes.
59. Once clean and dry, put the Ronchi ruling back into its original position. Fill with 4.125 mL of phantom from the tube labeled "Test 10". Cover the phantom with the cover glass.
60. Repeat steps 31 through 51 for the "Test 10" phantom, making sure to set the comment to the proper naming scheme of "trial\_1\_combo\_10\_NA\_#\_run\_#\_".
  
61. Remove the phantom holder from the system. Being careful to not drop the cover glass or the Ronchi ruling, remove the phantom from the holder and rinse with DI Water. Dry the interior of the phantom holder with a Kimwipe and clean the cover glass and Ronchi ruling with isopropyl alcohol and soft optical cleaning wipes.
62. Once clean and dry, put the Ronchi ruling back into its original position. Fill with 4.125 mL of phantom from the tube labeled "Test 8". Cover the phantom with the cover glass.
63. Repeat steps 31 through 51 for the "Test 8" phantom, making sure to set the comment to the proper naming scheme of "trial\_1\_combo\_8\_NA\_#\_run\_#\_".
  
64. Remove the phantom holder from the system. Being careful to not drop the cover glass or the Ronchi ruling, remove the phantom from the holder and rinse with DI Water. Dry the interior of the phantom holder with a Kimwipe and clean the cover glass and Ronchi ruling with isopropyl alcohol and soft optical cleaning wipes.

65. Once clean and dry, put the Ronchi ruling back into its original position. Fill with 4.125 mL of phantom from the tube labeled "Test 6". Cover the phantom with the cover glass.
66. Repeat steps 31 through 51 for the "Test 6" phantom, making sure to set the comment to the proper naming scheme of "trial\_1\_combo\_6\_NA\_#\_run\_#\_".
67. Remove the phantom holder from the system. Being careful to not drop the cover glass or the Ronchi ruling, remove the phantom from the holder and rinse with DI Water. Dry the interior of the phantom holder with a Kimwipe and clean the cover glass and Ronchi ruling with isopropyl alcohol and soft optical cleaning wipes.
68. Once clean and dry, put the Ronchi ruling back into its original position. Fill with 4.125 mL of phantom from the tube labeled "Test 4". Cover the phantom with the cover glass.
69. Repeat steps 31 through 51 for the "Test 4" phantom, making sure to set the comment to the proper naming scheme of "trial\_1\_combo\_4\_NA\_#\_run\_#\_".
70. Remove the phantom holder from the system. Being careful to not drop the cover glass or the Ronchi ruling, remove the phantom from the holder and rinse with DI Water. Dry the interior of the phantom holder with a Kimwipe and clean the cover glass and Ronchi ruling with isopropyl alcohol and soft optical cleaning wipes.
71. Once clean and dry, put the Ronchi ruling back into its original position. Fill with 4.125 mL of phantom from the tube labeled "Test 3". Cover the phantom with the cover glass.
72. Repeat steps 31 through 51 for the "Test 3" phantom, making sure to set the comment to the proper naming scheme of "trial\_1\_combo\_3\_NA\_#\_run\_#\_".
73. Remove the phantom holder from the system. Being careful to not drop the cover glass or the Ronchi ruling, remove the phantom from the holder and rinse with DI Water. Dry the interior of the phantom holder with a Kimwipe and clean the cover glass and Ronchi ruling with isopropyl alcohol and soft optical cleaning wipes.
74. Once clean and dry, put the Ronchi ruling back into its original position. Fill with 4.125 mL of phantom from the tube labeled "Test 2". Cover the phantom with the cover glass.

75. Repeat steps 31 through 51 for the "Test 2" phantom, making sure to set the comment to the proper naming scheme of "trial\_1\_combo\_2\_NA\_#\_run\_#\_".
76. Remove the phantom holder from the system. Being careful to not drop the cover glass or the Ronchi ruling, remove the phantom from the holder and rinse with DI Water. Dry the interior of the phantom holder with a Kimwipe and clean the cover glass and Ronchi ruling with isopropyl alcohol and soft optical cleaning wipes.
77. Once clean and dry, put the Ronchi ruling back into its original position. Fill with 4.125 mL of phantom from the tube labeled "Test 1". Cover the phantom with the cover glass.
78. Repeat steps 31 through 51 for the "Test 1" phantom, making sure to set the comment to the proper naming scheme of "trial\_1\_combo\_1\_NA\_#\_run\_#\_".

## 5.8 – [India Ink, Intralipid 20%, Water] Experimental Procedures SOP

### Methods

1. Set out an absorbent pad on the optical table to help protect against spills. Set an optical grade disposable cloth on top of the absorbent pad to help keep delicate optics clean and free of scratches. Wear nitrile gloves and a face mask when working with the lens modules, the Ronchi ruling, or the cover glass.
2. Take the Trial 2 tissue phantoms and set aside for use throughout the experiment. Set the “Test 16” centrifuge tube and place in the Ultrasonic bath for at least 30 minutes on power 9 with no heat. Continue with the next steps during the ultrasonic application.
3. When proceeding through the experimental procedures, take extreme caution to avoid bumping into any part of the system accidentally, as that could require going through the alignment procedures again and potentially restarting the data collection.
4. Insert the modular lens system “Setup 1” into the kinematic base plate and tighten. Double check that the correct system has been inserted by confirming with the label on the kinematic top plate, the labels on the lenses, and the printed lens prescriptions.
5. Clean the Ronchi ruling and the cover glass with Isopropyl alcohol and the soft optical cleaning wipes, then place the ruling into the tissue phantom holder. Note that the chromed surface of the ruling should be facing up. Do not use Kimwipes to clean the ruling, as the surface could be easily scratched or damaged by a rough wipe.
6. Run through the “Naming, saving, and manipulating files” and “Turning on the OCT system and software” methods in Appendix 5.6.
7. Upon completion of the ultrasonic application, remove the “Test 16” tube from the bath. Get rid of the hot water in the Ultrasound bath and fill to the line with room temperature DI water. Start the “Test 14” tube in the ultrasound bath at the same settings.
8. Slowly add 4.125 mL of phantom from “Test 16” to the phantom holder onto the ruling. Lightly press down on the ruling to confirm it is not floating in the liquid. Place the cover glass over the water to form a smooth interface.
9. Carefully place the holder onto the 3D printed part such that the notch is closest to the micrometer stage. Move the test arm micrometer slightly up and down in order to find the

position in which the A-scan peak is at its highest. This is the position in which the beam is focused on the surface of the ruling. Adjust the sensitivity on the Lock-In Amplifier as necessary to maximize the signal return from the chrome without overloading.

10. Check the “A-Scan” box in the LabView window to ensure the system is properly aligned. If correct, the sharp peak should be centered at 250 on the x-axis. If the sharp peak is centered on a different value, move the reference arm micrometer until the correct value is reached.
11. Type the appropriate file name into the “Comment” box in the LabView window based on the naming procedures defined in Appendix 5.6. The first file name should be “trial\_2\_combo\_16\_NA\_06\_run\_1\_”. Ensure the proper file pathway is selected.
12. Check the settings on LabView. The correct values are as follows:
  - a. In “B-Scan Parameters”, Lateral Range = 2mm, Number of A-Scans = 500, and In-Air
13. Press “Acquire Image”. Step away from the computer and the table while the system completes the scans. Once the scans are finished, press “Save”. For this and all future scans, check that the files saved properly before continuing onto the next step.
  - a. If the motorized linear translation stage is not moving, consult the troubleshooting procedures in Appendix 5.6.
14. Rename the comment to “trial\_2\_combo\_16\_NA\_06\_run\_2\_”. Check the settings on LabView, then press “Acquire Image”. Step away from the computer and the table while the system completes the scans. Once the scans are finished, press “Save”.
15. Rename the comment to “trial\_2\_combo\_16\_NA\_06\_run\_3\_”. Check the settings on LabView, then press “Acquire Image”. Step away from the computer and the table while the system completes the scans. Once the scans are finished, press “Save”.
16. Rename the comment to “trial\_2\_combo\_16\_NA\_06\_run\_4\_”. Decrease the sensitivity such that the peak from the glass reflection is maximized without being overloaded. Note that the reflection off the chrome will be overloaded. Check the settings on LabView, then press “Acquire Image”. Step away from the computer and the table while the system completes the scans. Once the scans are finished, press “Save”.
17. Swap the modular lens setup to “Setup 2”. Lock the kinematic base plate, then move the test arm micrometer slightly up and down in order to find the position in which the oscilloscope

peak is at its highest. Then, check the “A-Scan” box in the LabView window to ensure the system is properly aligned. If correct, the sharp peak should be centered at 250 on the x-axis. If the sharp peak is centered on a different value, move the reference arm micrometer until the correct value is reached. Adjust the sensitivity on the Lock-In Amplifier to maximize the signal return from the chrome without overloading.

18. Rename the comment to “trial\_2\_combo\_16\_NA\_09\_run\_1\_”.
19. Check the settings on LabView.
20. Press “Acquire Image”. Step away from the computer and the table while the system completes the scans. Once the scans are finished, press “Save”.
21. Rename the comment to “trial\_2\_combo\_16\_NA\_09\_run\_2\_”. Check the settings on LabView, then press “Acquire Image”. Step away from the computer and the table while the system completes the scans. Once the scans are finished, press “Save”.
22. Rename the comment to “trial\_2\_combo\_16\_NA\_09\_run\_3\_”. Check the settings on LabView, then press “Acquire Image”. Step away from the computer and the table while the system completes the scans. Once the scans are finished, press “Save”.
23. Rename the comment to “trial\_2\_combo\_16\_NA\_09\_run\_4\_”. Decrease the sensitivity such that the peak from the glass reflection is maximized without being overloaded. Check the settings on LabView, then press “Acquire Image”. Step away from the computer and the table while the system completes the scans. Once the scans are finished, press “Save”.
24. Swap the modular lens setup to “Setup 3”. Lock the kinematic base plate, then move the test arm micrometer slightly up and down in order to find the position in which the oscilloscope peak is at its highest. Then, check the “A-Scan” box in the LabView window to ensure the system is properly aligned. If correct, the sharp peak should be centered at 250 on the x-axis. If the sharp peak is centered on a different value, move the reference arm micrometer until the correct value is reached. Adjust the sensitivity on the Lock-In Amplifier to maximize the signal return from the chrome without overloading.
25. Rename the comment to “trial\_2\_combo\_16\_NA\_12\_run\_1\_”.
26. Check the settings on LabView.

27. Press "Acquire Image". Step away from the computer and the table while the system completes the scans. Once the scans are finished, press "Save".
28. Rename the comment to "trial\_2\_combo\_16\_NA\_12\_run\_2\_". Check the settings on LabView, then press "Acquire Image". Step away from the computer and the table while the system completes the scans. Once the scans are finished, press "Save".
29. Rename the comment to "trial\_2\_combo\_16\_NA\_12\_run\_3\_". Check the settings on LabView, then press "Acquire Image". Step away from the computer and the table while the system completes the scans. Once the scans are finished, press "Save".
30. Rename the comment to "trial\_2\_combo\_16\_NA\_12\_run\_4\_". Decrease the sensitivity such that the peak from the glass reflection is maximized without being overloaded. Check the settings on LabView, then press "Acquire Image". Step away from the computer and the table while the system completes the scans. Once the scans are finished, press "Save".
31. Remove the phantom holder from the system. Being careful to not drop the cover glass or the Ronchi ruling, remove the phantom from the holder and rinse with DI Water. Dry the interior of the phantom holder with a Kimwipe and clean the cover glass and Ronchi ruling with isopropyl alcohol and soft optical cleaning wipes.
32. Upon completion of the "Test 14" ultrasound, remove the centrifuge tube and set aside. Replace the heated water in the ultrasonic bath with room temperature DI Water as before, and start the ultrasound process for "Test 12".
33. Once clean and dry, put the Ronchi ruling back into its original position. Fill with 4.125 mL of phantom from the tube labeled "Test 14". Cover the phantom with the cover glass.
34. Swap the modular lens setup to "Setup 1". Lock the kinematic base plate, then move the test arm micrometer slightly up and down in order to find the position in which the oscilloscope peak is at its highest. Then, check the "A-Scan" box in the LabView window to ensure the system is properly aligned. Move the reference arm micrometer until the sharp peak is centered on 250 on the x-axis. Adjust the sensitivity on the Lock-In Amplifier to maximize the signal return from the chrome without overloading.
35. Rename the comment to "trial\_2\_combo\_14\_NA\_06\_run\_1\_".
36. Check the settings on LabView.

37. Press "Acquire Image". Step away from the computer and the table while the system completes the scans. Once the scans are finished, press "Save".
38. Rename the comment to "trial\_2\_combo\_14\_NA\_06\_run\_2\_". Check the settings on LabView, then press "Acquire Image". Step away from the computer and the table while the system completes the scans. Once the scans are finished, press "Save".
39. Rename the comment to "trial\_2\_combo\_14\_NA\_06\_run\_3\_". Check the settings on LabView, then press "Acquire Image". Step away from the computer and the table while the system completes the scans. Once the scans are finished, press "Save".
40. Rename the comment to "trial\_2\_combo\_14\_NA\_06\_run\_4\_". Decrease the sensitivity such that the peak from the glass reflection is maximized without being overloaded. Check the settings on LabView, then press "Acquire Image". Step away from the computer and the table while the system completes the scans. Once the scans are finished, press "Save".
41. Swap the modular lens setup to "Setup 2". Lock the kinematic base plate, then move the test arm micrometer slightly up and down in order to find the position in which the oscilloscope peak is at its highest. Then, check the "A-Scan" box in the LabView window to ensure the system is properly aligned. Move the reference arm micrometer until the sharp peak is centered on 250 on the x-axis. Adjust the sensitivity on the Lock-In Amplifier to maximize the signal return from the chrome without overloading.
42. Rename the comment to "trial\_2\_combo\_14\_NA\_09\_run\_1\_".
43. Check the settings on LabView.
44. Press "Acquire Image". Step away from the computer and the table while the system completes the scans. Once the scans are finished, press "Save".
45. Rename the comment to "trial\_2\_combo\_14\_NA\_09\_run\_2\_". Check the settings on LabView, then press "Acquire Image". Step away from the computer and the table while the system completes the scans. Once the scans are finished, press "Save".
46. Rename the comment to "trial\_2\_combo\_14\_NA\_09\_run\_3\_". Check the settings on LabView, then press "Acquire Image". Step away from the computer and the table while the system completes the scans. Once the scans are finished, press "Save".

47. Rename the comment to "trial\_2\_combo\_14\_NA\_09\_run\_4\_". Decrease the sensitivity such that the peak from the glass reflection is maximized without being overloaded. Check the settings on LabView, then press "Acquire Image". Step away from the computer and the table while the system completes the scans. Once the scans are finished, press "Save".
48. Swap the modular lens setup to "Setup 3". Lock the kinematic base plate, then move the test arm micrometer slightly up and down in order to find the position in which the oscilloscope peak is at its highest. Then, check the "A-Scan" box in the LabView window to ensure the system is properly aligned. Move the reference arm micrometer until the sharp peak is centered on 250 on the x-axis. Adjust the sensitivity on the Lock-In Amplifier to maximize the signal return from the chrome without overloading.
49. Rename the comment to "trial\_2\_combo\_14\_NA\_12\_run\_1\_".
50. Check the settings on LabView.
51. Press "Acquire Image". Step away from the computer and the table while the system completes the scans. Once the scans are finished, press "Save".
52. Rename the comment to "trial\_2\_combo\_14\_NA\_12\_run\_2\_". Check the settings on LabView, then press "Acquire Image". Step away from the computer and the table while the system completes the scans. Once the scans are finished, press "Save".
53. Rename the comment to "trial\_2\_combo\_14\_NA\_12\_run\_3\_". Check the settings on LabView, then press "Acquire Image". Step away from the computer and the table while the system completes the scans. Once the scans are finished, press "Save".
54. Rename the comment to "trial\_2\_combo\_14\_NA\_12\_run\_4\_". Decrease the sensitivity such that the peak from the glass reflection is maximized without being overloaded. Check the settings on LabView, then press "Acquire Image". Step away from the computer and the table while the system completes the scans. Once the scans are finished, press "Save".
55. Remove the phantom holder from the system. Being careful to not drop the cover glass or the Ronchi ruling, remove the phantom from the holder and rinse with DI Water. Dry the interior of the phantom holder with a Kimwipe and clean the cover glass and Ronchi ruling with isopropyl alcohol and soft optical cleaning wipes.

56. Upon completion of the "Test 12" ultrasound, remove the centrifuge tube and set aside.  
Replace the heated water in the ultrasonic bath with room temperature DI Water as before, and start the ultrasound process for "Test 10".
57. Once clean and dry, put the Ronchi ruling back into its original position. Fill with 4.125 mL of phantom from the tube labeled "Test 12". Cover the phantom with the cover glass.
58. Repeat steps 34 through 54 for the "Test 12" phantom, making sure to set the comment to the proper naming scheme of "trial\_2\_combo\_12\_NA\_#\_run\_#\_".
59. Remove the phantom holder from the system. Being careful to not drop the cover glass or the Ronchi ruling, remove the phantom from the holder and rinse with DI Water. Dry the interior of the phantom holder with a Kimwipe and clean the cover glass and Ronchi ruling with isopropyl alcohol and soft optical cleaning wipes.
60. Upon completion of the "Test 10" ultrasound, remove the centrifuge tube and set aside.  
Replace the heated water in the ultrasonic bath with room temperature DI Water as before, and start the ultrasound process for "Test 8".
61. Once clean and dry, put the Ronchi ruling back into its original position. Fill with 4.125 mL of phantom from the tube labeled "Test 10". Cover the phantom with the cover glass.
62. Repeat steps 34 through 54 for the "Test 10" phantom, making sure to set the comment to the proper naming scheme of "trial\_2\_combo\_10\_NA\_#\_run\_#\_".
63. Remove the phantom holder from the system. Being careful to not drop the cover glass or the Ronchi ruling, remove the phantom from the holder and rinse with DI Water. Dry the interior of the phantom holder with a Kimwipe and clean the cover glass and Ronchi ruling with isopropyl alcohol and soft optical cleaning wipes.
64. Upon completion of the "Test 8" ultrasound, remove the centrifuge tube and set aside.  
Replace the heated water in the ultrasonic bath with room temperature DI Water as before, and start the ultrasound process for "Test 6".
65. Once clean and dry, put the Ronchi ruling back into its original position. Fill with 4.125 mL of phantom from the tube labeled "Test 8". Cover the phantom with the cover glass.

66. Repeat steps 34 through 54 for the "Test 8" phantom, making sure to set the comment to the proper naming scheme of "trial\_2\_combo\_8\_NA\_#\_run\_#\_".
67. Remove the phantom holder from the system. Being careful to not drop the cover glass or the Ronchi ruling, remove the phantom from the holder and rinse with DI Water. Dry the interior of the phantom holder with a Kimwipe and clean the cover glass and Ronchi ruling with isopropyl alcohol and soft optical cleaning wipes.
68. Upon completion of the "Test 6" ultrasound, remove the centrifuge tube and set aside. Replace the heated water in the ultrasonic bath with room temperature DI Water as before, and start the ultrasound process for "Test 4".
69. Once clean and dry, put the Ronchi ruling back into its original position. Fill with 4.125 mL of phantom from the tube labeled "Test 6". Cover the phantom with the cover glass.
70. Repeat steps 34 through 54 for the "Test 6" phantom, making sure to set the comment to the proper naming scheme of "trial\_2\_combo\_6\_NA\_#\_run\_#\_".
71. Remove the phantom holder from the system. Being careful to not drop the cover glass or the Ronchi ruling, remove the phantom from the holder and rinse with DI Water. Dry the interior of the phantom holder with a Kimwipe and clean the cover glass and Ronchi ruling with isopropyl alcohol and soft optical cleaning wipes.
72. Upon completion of the "Test 4" ultrasound, remove the centrifuge tube and set aside. Replace the heated water in the ultrasonic bath with room temperature DI Water as before, and start the ultrasound process for "Test 3".
73. Once clean and dry, put the Ronchi ruling back into its original position. Fill with 4.125 mL of phantom from the tube labeled "Test 4". Cover the phantom with the cover glass.
74. Repeat steps 34 through 54 for the "Test 4" phantom, making sure to set the comment to the proper naming scheme of "trial\_2\_combo\_4\_NA\_#\_run\_#\_".
75. Remove the phantom holder from the system. Being careful to not drop the cover glass or the Ronchi ruling, remove the phantom from the holder and rinse with DI Water. Dry the interior of the phantom holder with a Kimwipe and clean the cover glass and Ronchi ruling with isopropyl alcohol and soft optical cleaning wipes.

76. Upon completion of the "Test 3" ultrasound, remove the centrifuge tube and set aside.  
Replace the heated water in the ultrasonic bath with room temperature DI Water as before, and start the ultrasound process for "Test 2".
77. Once clean and dry, put the Ronchi ruling back into its original position. Fill with 4.125 mL of phantom from the tube labeled "Test 3". Cover the phantom with the cover glass.
78. Repeat steps 34 through 54 for the "Test 3" phantom, making sure to set the comment to the proper naming scheme of "trial\_2\_combo\_3\_NA\_#\_run\_#\_".
79. Remove the phantom holder from the system. Being careful to not drop the cover glass or the Ronchi ruling, remove the phantom from the holder and rinse with DI Water. Dry the interior of the phantom holder with a Kimwipe and clean the cover glass and Ronchi ruling with isopropyl alcohol and soft optical cleaning wipes.
80. Upon completion of the "Test 2" ultrasound, remove the centrifuge tube and set aside.  
Replace the heated water in the ultrasonic bath with room temperature DI Water as before, and start the ultrasound process for "Test 1".
81. Once clean and dry, put the Ronchi ruling back into its original position. Fill with 4.125 mL of phantom from the tube labeled "Test 2". Cover the phantom with the cover glass.
82. Repeat steps 34 through 54 for the "Test 2" phantom, making sure to set the comment to the proper naming scheme of "trial\_2\_combo\_2\_NA\_#\_run\_#\_".
83. Remove the phantom holder from the system. Being careful to not drop the cover glass or the Ronchi ruling, remove the phantom from the holder and rinse with DI Water. Dry the interior of the phantom holder with a Kimwipe and clean the cover glass and Ronchi ruling with isopropyl alcohol and soft optical cleaning wipes.
84. Upon completion of the "Test 1" ultrasound, remove the centrifuge tube and set aside.  
Replace the heated water in the ultrasonic bath with room temperature DI Water as before.
85. Once clean and dry, put the Ronchi ruling back into its original position. Fill with 4.125 mL of phantom from the tube labeled "Test 1". Cover the phantom with the cover glass.
86. Repeat steps 34 through 54 for the "Test 1" phantom, making sure to set the comment to the proper naming scheme of "trial\_2\_combo\_1\_NA\_#\_run\_#\_".

5.9 – Engineering Drawings of 3D Printed Components

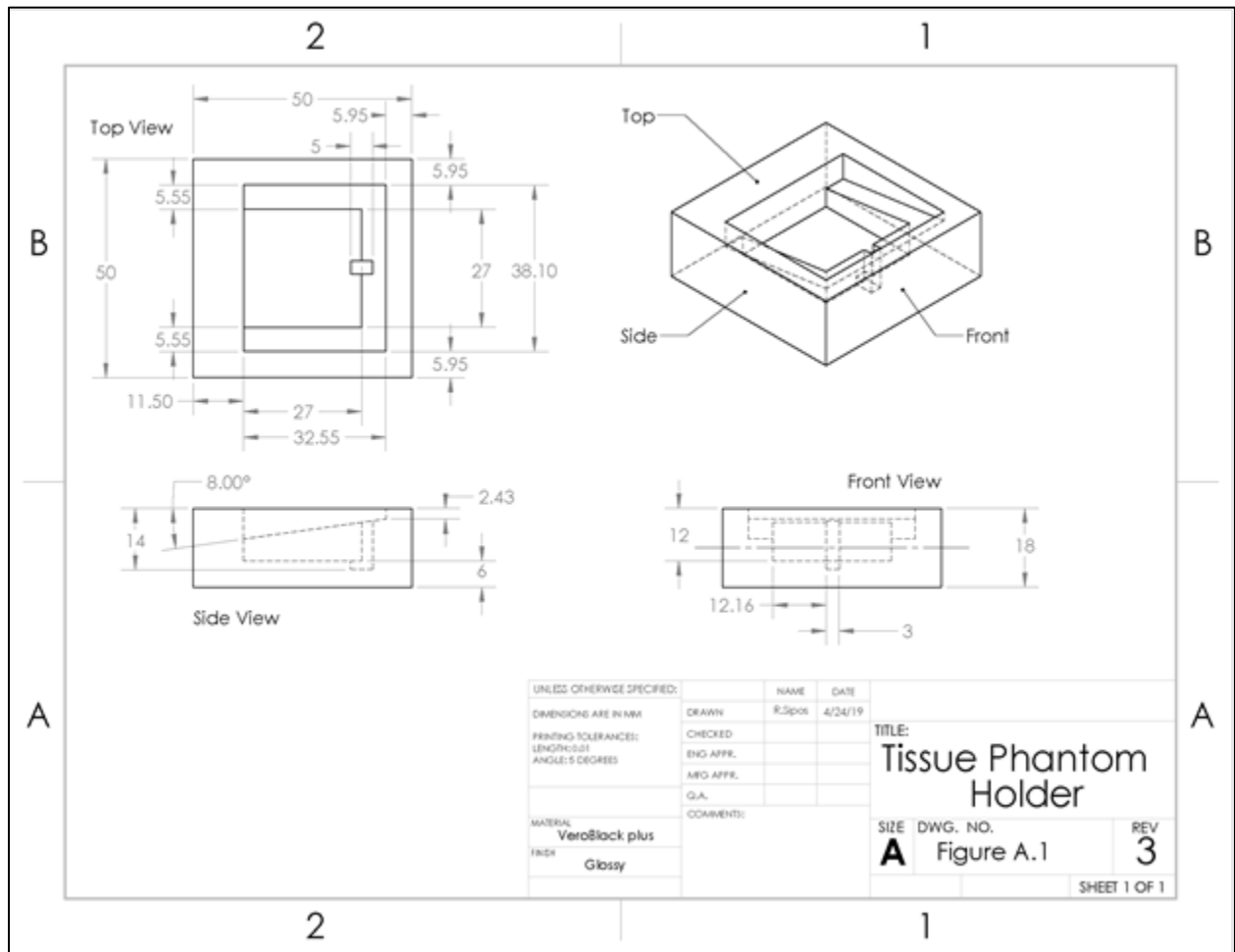


Figure A.1 – Tissue Phantom Holder design drawing

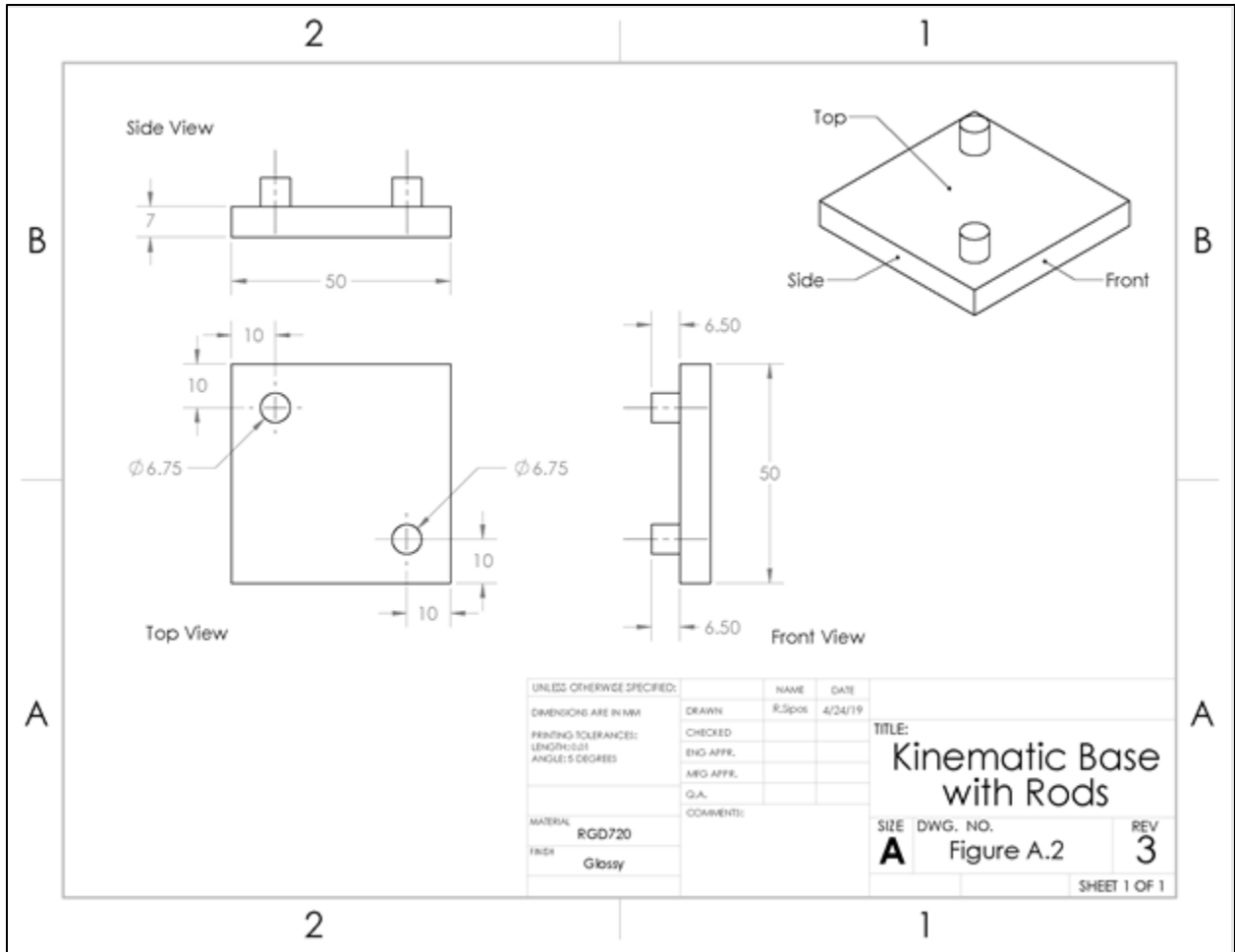


Figure A.2 – Kinematic Base with Rods design drawing

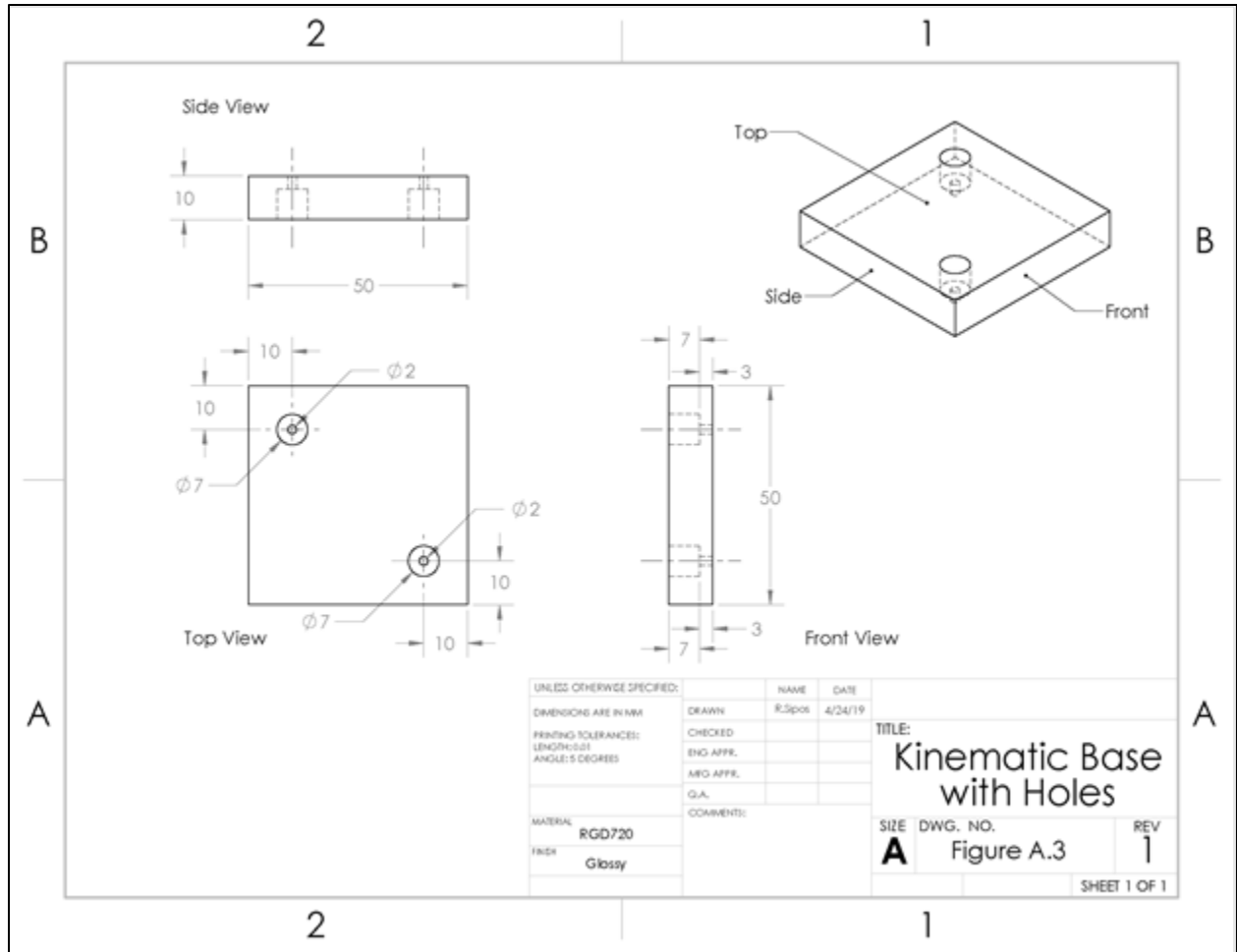


Figure A.3 – Kinematic Base with Holes design drawing

### 5.10 – Table of Results for Lateral Resolution

Combo #	NA	cm <sup>-1</sup> mu_a(desired)	Dilution Factor 1	Dilution Factor 2	IL Concentration	Lateral Resolution		
						pixels FWHM	μm FWHM	μm STDEV FWHM
2	0.0603	1.35	1.639344262	8	1.525	6.253333	25.01333	0.78
3	0.0603	1.35	1.639344262	20	0.61	6.248333	24.99333	1.06
4	0.0603	1.35	1.639344262	40	0.305	6.264667	25.05867	0.54
5	0.0603	1.35	3.278688525	4	1.525	6.253333	25.01333	0.78
6	0.0603	1.35	3.278688525	8	0.7625	6.138333	24.55333	0.61
7	0.0603	1.35	3.278688525	20	0.305	6.264667	25.05867	0.54
8	0.0603	1.35	3.278688525	40	0.1525	4.901826	19.60731	0.26
9	0.0603	1.35	6.557377049	4	0.7625	6.138333	24.55333	0.61
10	0.0603	1.35	6.557377049	8	0.38125	6.005	24.02	0.20
11	0.0603	1.35	6.557377049	20	0.1525	4.901826	19.60731	0.26
12	0.0603	1.35	6.557377049	40	0.07625	5.944	23.776	0.21
13	0.0603	1.35	13.1147541	4	0.38125	6.005	24.02	0.20
14	0.0603	1.35	13.1147541	8	0.190625	6.476333	25.90533	0.93
15	0.0603	1.35	13.1147541	20	0.07625	5.944	23.776	0.21
16	0.0603	1.35	13.1147541	40	0.038125	6.1395	24.558	0.11
17	0.0603	1.35	0	0	0	6.524667	26.09867	0.13
3	0.0603	6.075	1.639344262	20	0.61	6.405232	25.62093	0.64
4	0.0603	6.075	1.639344262	40	0.305	5.534667	22.13867	0.15
6	0.0603	6.075	3.278688525	8	0.7625	4.03576	16.14304	0.88
7	0.0603	6.075	3.278688525	20	0.305	5.534667	22.13867	0.15
8	0.0603	6.075	3.278688525	40	0.1525	5.015333	20.06133	0.15
9	0.0603	6.075	6.557377049	4	0.7625	4.03576	16.14304	0.88
10	0.0603	6.075	6.557377049	8	0.38125	5.803	23.212	0.30
11	0.0603	6.075	6.557377049	20	0.1525	5.015333	20.06133	0.15
12	0.0603	6.075	6.557377049	40	0.07625	6.094	24.376	0.24
13	0.0603	6.075	13.1147541	4	0.38125	5.803	23.212	0.30
14	0.0603	6.075	13.1147541	8	0.190625	6.777667	27.11067	0.33
15	0.0603	6.075	13.1147541	20	0.07625	6.094	24.376	0.24
16	0.0603	6.075	13.1147541	40	0.038125	6.945	27.78	0.66

Table A.1 – Results for Lateral Resolution, NA = 0.0603

Combo #	NA	cm <sup>-1</sup> mu_a(desired)	Dilution Factor 1	Dilution Factor 2	IL Concentration	Lateral Resolution		
						pixels FWHM	μm FWHM	μm STDEV FWHM
2	0.0901	1.35	1.639344262	8	1.525	3.313	13.252	0.30
3	0.0901	1.35	1.639344262	20	0.61	2.980667	11.92267	0.43
4	0.0901	1.35	1.639344262	40	0.305	2.527667	10.11067	0.21
5	0.0901	1.35	3.278688525	4	1.525	3.313	13.252	0.30
6	0.0901	1.35	3.278688525	8	0.7625	3.267333	13.06933	0.35
7	0.0901	1.35	3.278688525	20	0.305	2.527667	10.11067	0.21
8	0.0901	1.35	3.278688525	40	0.1525	3.150667	12.60267	0.05
9	0.0901	1.35	6.557377049	4	0.7625	3.267333	13.06933	0.35
10	0.0901	1.35	6.557377049	8	0.38125	3.045667	12.18267	0.56
11	0.0901	1.35	6.557377049	20	0.1525	3.150667	12.60267	0.05
12	0.0901	1.35	6.557377049	40	0.07625	2.514	10.056	0.52
13	0.0901	1.35	13.1147541	4	0.38125	3.045667	12.18267	0.56
14	0.0901	1.35	13.1147541	8	0.190625	3.075	12.3	0.43
15	0.0901	1.35	13.1147541	20	0.07625	2.514	10.056	0.52
16	0.0901	1.35	13.1147541	40	0.038125	2.9525	11.81	0.11
17	0.0901	1.35	0	0	0	2.752343	11.00937	0.10
3	0.0901	6.075	1.639344262	20	0.61	3.310333	13.24133	0.23
4	0.0901	6.075	1.639344262	40	0.305	2.834	11.336	0.93
6	0.0901	6.075	3.278688525	8	0.7625	3.270667	13.08267	0.38
7	0.0901	6.075	3.278688525	20	0.305	2.834	11.336	0.93
8	0.0901	6.075	3.278688525	40	0.1525	2.807667	11.23067	0.28
9	0.0901	6.075	6.557377049	4	0.7625	3.270667	13.08267	0.38
10	0.0901	6.075	6.557377049	8	0.38125	2.96	11.84	0.53
11	0.0901	6.075	6.557377049	20	0.1525	2.807667	11.23067	0.28
12	0.0901	6.075	6.557377049	40	0.07625	2.800278	11.20111	0.37
13	0.0901	6.075	13.1147541	4	0.38125	2.96	11.84	0.53
14	0.0901	6.075	13.1147541	8	0.190625	2.959667	11.83867	0.68
15	0.0901	6.075	13.1147541	20	0.07625	2.800278	11.20111	0.37
16	0.0901	6.075	13.1147541	40	0.038125	3.127	12.508	0.12

Table A.2 – Results for Lateral Resolution, NA = 0.0901

Combo #	NA	cm <sup>-1</sup>				Lateral Resolution			
		mu_a(desired)	Dilution Factor 1	Dilution Factor 2	IL Concentration	pixels FWHM	μm FWHM	μm STDEV FWHM	
2	0.1186	1.35	1.639344262	8	1.525	2.7095	10.838	0.57	
3	0.1186	1.35	1.639344262	20	0.61	2.460667	9.842667	0.21	
4	0.1186	1.35	1.639344262	40	0.305	2.482333	9.929333	0.09	
5	0.1186	1.35	3.278688525	4	1.525	2.7095	10.838	0.57	
6	0.1186	1.35	3.278688525	8	0.7625	2.623	10.492	0.13	
7	0.1186	1.35	3.278688525	20	0.305	2.482333	9.929333	0.09	
8	0.1186	1.35	3.278688525	40	0.1525	2.567667	10.27067	0.13	
9	0.1186	1.35	6.557377049	4	0.7625	2.623	10.492	0.13	
10	0.1186	1.35	6.557377049	8	0.38125	2.586667	10.34667	0.20	
11	0.1186	1.35	6.557377049	20	0.1525	2.567667	10.27067	0.13	
12	0.1186	1.35	6.557377049	40	0.07625	2.150333	8.601333	0.09	
13	0.1186	1.35	13.1147541	4	0.38125	2.586667	10.34667	0.20	
14	0.1186	1.35	13.1147541	8	0.190625	2.842	11.368	0.09	
15	0.1186	1.35	13.1147541	20	0.07625	2.150333	8.601333	0.09	
16	0.1186	1.35	13.1147541	40	0.038125	2.391	9.564	0.15	
17	0.1186	1.35	0	0	0	2.597667	10.39067	0.12	
3	0.1186	6.075	1.639344262	20	0.61	2.699333	10.79733	0.40	
4	0.1186	6.075	1.639344262	40	0.305	2.488333	9.953333	0.33	
6	0.1186	6.075	3.278688525	8	0.7625	2.638667	10.55467	0.13	
7	0.1186	6.075	3.278688525	20	0.305	2.488333	9.953333	0.33	
8	0.1186	6.075	3.278688525	40	0.1525	2.553667	10.21467	0.49	
9	0.1186	6.075	6.557377049	4	0.7625	2.638667	10.55467	0.13	
10	0.1186	6.075	6.557377049	8	0.38125	2.588667	10.35467	0.30	
11	0.1186	6.075	6.557377049	20	0.1525	2.553667	10.21467	0.49	
12	0.1186	6.075	6.557377049	40	0.07625	2.929	11.716	0.11	
13	0.1186	6.075	13.1147541	4	0.38125	2.588667	10.35467	0.30	
14	0.1186	6.075	13.1147541	8	0.190625	2.720333	10.88133	0.41	
15	0.1186	6.075	13.1147541	20	0.07625	2.929	11.716	0.11	
16	0.1186	6.075	13.1147541	40	0.038125	2.550667	10.20267	0.88	

Table A.3 – Results for Lateral Resolution, NA = 0.1186

### 5.11 – Table of Results for Axial Resolution

Combo #	NA	cm <sup>-1</sup>		Dilution Factor 1	Dilution Factor 2	IL Concentration	Axial Resolution		
		mu_a(desired)					pixels	μm	μm
							FWHM	FWHM	STDEV FWHM
2	0.0603	1.35	1.639344262	8	1.525	4.436099	17.328513	0.06	
3	0.0603	1.35	1.639344262	20	0.61	4.366104	17.0550951	0.16	
4	0.0603	1.35	1.639344262	40	0.305	4.326341	16.8997682	0.15	
5	0.0603	1.35	3.278688525	4	1.525	4.436099	17.328513	0.06	
6	0.0603	1.35	3.278688525	8	0.7625	4.376845	17.0970495	0.17	
7	0.0603	1.35	3.278688525	20	0.305	4.326341	16.8997682	0.15	
8	0.0603	1.35	3.278688525	40	0.1525	4.428104	17.2972813	0.03	
9	0.0603	1.35	6.557377049	4	0.7625	4.376845	17.0970495	0.17	
10	0.0603	1.35	6.557377049	8	0.38125	4.34528	16.9737513	0.16	
11	0.0603	1.35	6.557377049	20	0.1525	4.428104	17.2972813	0.03	
12	0.0603	1.35	6.557377049	40	0.07625	4.377525	17.0997083	0.09	
13	0.0603	1.35	13.1147541	4	0.38125	4.34528	16.9737513	0.16	
14	0.0603	1.35	13.1147541	8	0.190625	4.142508	16.1816719	0.19	
15	0.0603	1.35	13.1147541	20	0.07625	4.377525	17.0997083	0.09	
16	0.0603	1.35	13.1147541	40	0.038125	4.193379	16.3803867	0.12	
17	0.0603	1.35	0	0	0	4.376453	17.0955208	0.05	
3	0.0603	6.075	1.639344262	20	0.61	4.394345	17.1654115	0.13	
4	0.0603	6.075	1.639344262	40	0.305	4.343907	16.9683867	0.12	
6	0.0603	6.075	3.278688525	8	0.7625	4.387533	17.1387995	0.28	
7	0.0603	6.075	3.278688525	20	0.305	4.343907	16.9683867	0.12	
8	0.0603	6.075	3.278688525	40	0.1525	4.308516	16.8301393	0.13	
9	0.0603	6.075	6.557377049	4	0.7625	4.387533	17.1387995	0.28	
10	0.0603	6.075	6.557377049	8	0.38125	4.32478	16.8936719	0.10	
11	0.0603	6.075	6.557377049	20	0.1525	4.308516	16.8301393	0.13	
12	0.0603	6.075	6.557377049	40	0.07625	4.355519	17.0137474	0.07	
13	0.0603	6.075	13.1147541	4	0.38125	4.32478	16.8936719	0.10	
14	0.0603	6.075	13.1147541	8	0.190625	4.298175	16.7897461	0.14	
15	0.0603	6.075	13.1147541	20	0.07625	4.355519	17.0137474	0.07	
16	0.0603	6.075	13.1147541	40	0.038125	4.311052	16.8400482	0.14	

Table A.4 – Results for Axial Resolution, NA = 0.0603

Combo #	NA	cm <sup>-1</sup> mu_a(desired)	Dilution Factor 1	Dilution Factor 2	IL Concentration	Axial Resolution		
						pixels FWHM	µm FWHM	µm STDEV FWHM
2	0.0901	1.35	1.639344262	8	1.525	4.477056	17.4884987	0.17
3	0.0901	1.35	1.639344262	20	0.61	4.328902	16.9097747	0.26
4	0.0901	1.35	1.639344262	40	0.305	4.329691	16.9128542	0.05
5	0.0901	1.35	3.278688525	4	1.525	4.477056	17.4884987	0.17
6	0.0901	1.35	3.278688525	8	0.7625	4.383734	17.1239622	0.16
7	0.0901	1.35	3.278688525	20	0.305	4.329691	16.9128542	0.05
8	0.0901	1.35	3.278688525	40	0.1525	4.484522	17.5176654	0.08
9	0.0901	1.35	6.557377049	4	0.7625	4.383734	17.1239622	0.16
10	0.0901	1.35	6.557377049	8	0.38125	4.405792	17.210125	0.15
11	0.0901	1.35	6.557377049	20	0.1525	4.484522	17.5176654	0.08
12	0.0901	1.35	6.557377049	40	0.07625	4.291374	16.763181	0.14
13	0.0901	1.35	13.1147541	4	0.38125	4.405792	17.210125	0.15
14	0.0901	1.35	13.1147541	8	0.190625	4.18685	16.3548815	0.09
15	0.0901	1.35	13.1147541	20	0.07625	4.291374	16.763181	0.14
16	0.0901	1.35	13.1147541	40	0.038125	4.262685	16.651112	0.08
17	0.0901	1.35	0	0	0	4.238429	16.5563633	0.13
3	0.0901	6.075	1.639344262	20	0.61	4.35791	17.0230846	0.29
4	0.0901	6.075	1.639344262	40	0.305	4.368768	17.0655013	0.13
6	0.0901	6.075	3.278688525	8	0.7625	4.379181	17.1061771	0.03
7	0.0901	6.075	3.278688525	20	0.305	4.368768	17.0655013	0.13
8	0.0901	6.075	3.278688525	40	0.1525	4.313818	16.8508516	0.02
9	0.0901	6.075	6.557377049	4	0.7625	4.379181	17.1061771	0.03
10	0.0901	6.075	6.557377049	8	0.38125	4.376532	17.0958281	0.20
11	0.0901	6.075	6.557377049	20	0.1525	4.313818	16.8508516	0.02
12	0.0901	6.075	6.557377049	40	0.07625	4.354197	17.0085807	0.11
13	0.0901	6.075	13.1147541	4	0.38125	4.376532	17.0958281	0.20
14	0.0901	6.075	13.1147541	8	0.190625	4.346284	16.9776706	0.10
15	0.0901	6.075	13.1147541	20	0.07625	4.354197	17.0085807	0.11
16	0.0901	6.075	13.1147541	40	0.038125	4.32944	17.31776	0.10

Table A.5 – Results for Axial Resolution, NA = 0.0901

Combo #	NA	cm <sup>-1</sup> mu_a(desired)	Dilution Factor 1	Dilution Factor 2	IL Concentration	Axial Resolution		
						pixels FWHM	μm FWHM	μm STDEV FWHM
2	0.1186	1.35	1.639344262	8	1.525	4.421689	17.272224	0.11
3	0.1186	1.35	1.639344262	20	0.61	4.33891	16.9488685	0.14
4	0.1186	1.35	1.639344262	40	0.305	4.394973	17.167862	0.19
5	0.1186	1.35	3.278688525	4	1.525	4.421689	17.272224	0.11
6	0.1186	1.35	3.278688525	8	0.7625	4.388327	17.1419036	0.11
7	0.1186	1.35	3.278688525	20	0.305	4.394973	17.167862	0.19
8	0.1186	1.35	3.278688525	40	0.1525	4.43916	17.3404701	0.07
9	0.1186	1.35	6.557377049	4	0.7625	4.388327	17.1419036	0.11
10	0.1186	1.35	6.557377049	8	0.38125	4.412465	17.2361901	0.17
11	0.1186	1.35	6.557377049	20	0.1525	4.43916	17.3404701	0.07
12	0.1186	1.35	6.557377049	40	0.07625	4.228128	16.5161237	0.06
13	0.1186	1.35	13.1147541	4	0.38125	4.412465	17.2361901	0.17
14	0.1186	1.35	13.1147541	8	0.190625	4.168637	16.283737	0.26
15	0.1186	1.35	13.1147541	20	0.07625	4.228128	16.5161237	0.06
16	0.1186	1.35	13.1147541	40	0.038125	4.297932	16.7887982	0.07
17	0.1186	1.35	0	0	0	4.363507	17.0449479	0.04
3	0.1186	6.075	1.639344262	20	0.61	4.373563	17.0842292	0.09
4	0.1186	6.075	1.639344262	40	0.305	4.411899	17.2339792	0.08
6	0.1186	6.075	3.278688525	8	0.7625	4.381839	17.1165573	0.07
7	0.1186	6.075	3.278688525	20	0.305	4.411899	17.2339792	0.08
8	0.1186	6.075	3.278688525	40	0.1525	4.309166	16.832681	0.11
9	0.1186	6.075	6.557377049	4	0.7625	4.381839	17.1165573	0.07
10	0.1186	6.075	6.557377049	8	0.38125	4.329926	16.9137721	0.09
11	0.1186	6.075	6.557377049	20	0.1525	4.309166	16.832681	0.11
12	0.1186	6.075	6.557377049	40	0.07625	4.411609	17.2328477	0.18
13	0.1186	6.075	13.1147541	4	0.38125	4.329926	16.9137721	0.09
14	0.1186	6.075	13.1147541	8	0.190625	4.366732	17.0575482	0.13
15	0.1186	6.075	13.1147541	20	0.07625	4.411609	17.2328477	0.18
16	0.1186	6.075	13.1147541	40	0.038125	4.370467	17.4818667	0.08

Table A.6 – Results for Axial Resolution, NA = 0.1186

### 5.12 – Table of Results for Multiply Scattered Photons

Combo #	NA	cm <sup>-1</sup>		Dilution Factor 1	Dilution Factor 2	IL Concentration	Multiply Scattered Photons		
		mu_a(desired)					counts MSP	counts Scaled MSP	mV Sensitivity
2	0.0603	1.35	1.639344262	8	1.525	1.603	0.8015	0.5	
3	0.0603	1.35	1.639344262	20	0.61	0.086	0.86	10	
4	0.0603	1.35	1.639344262	40	0.305	0.041	2.05	50	
5	0.0603	1.35	3.278688525	4	1.525	1.603	0.8015	0.5	
6	0.0603	1.35	3.278688525	8	0.7625	0.165	0.825	5	
7	0.0603	1.35	3.278688525	20	0.305	0.041	2.05	50	
8	0.0603	1.35	3.278688525	40	0.1525	0.053	1.06	20	
9	0.0603	1.35	6.557377049	4	0.7625	0.165	0.825	5	
10	0.0603	1.35	6.557377049	8	0.38125	0.085	0.85	10	
11	0.0603	1.35	6.557377049	20	0.1525	0.053	1.06	20	
12	0.0603	1.35	6.557377049	40	0.07625	0.04	2	50	
13	0.0603	1.35	13.1147541	4	0.38125	0.085	0.85	10	
14	0.0603	1.35	13.1147541	8	0.190625	0.04	2	50	
15	0.0603	1.35	13.1147541	20	0.07625	0.04	2	50	
16	0.0603	1.35	13.1147541	40	0.038125	0.039	3.9	100	
17	0.0603	1.35	0	0	0	0.038	3.8	100	
3	0.0603	6.075	1.639344262	20	0.61	1.813	0.9065	0.5	
4	0.0603	6.075	1.639344262	40	0.305	0.928	0.928	1	
6	0.0603	6.075	3.278688525	8	0.7625	1.633	0.8165	0.5	
7	0.0603	6.075	3.278688525	20	0.305	0.928	0.928	1	
8	0.0603	6.075	3.278688525	40	0.1525	0.827	0.827	1	
9	0.0603	6.075	6.557377049	4	0.7625	1.633	0.8165	0.5	
10	0.0603	6.075	6.557377049	8	0.38125	0.802	0.802	1	
11	0.0603	6.075	6.557377049	20	0.1525	0.827	0.827	1	
12	0.0603	6.075	6.557377049	40	0.07625	0.403	0.806	2	
13	0.0603	6.075	13.1147541	4	0.38125	0.802	0.802	1	
14	0.0603	6.075	13.1147541	8	0.190625	0.808	0.808	1	
15	0.0603	6.075	13.1147541	20	0.07625	0.403	0.806	2	
16	0.0603	6.075	13.1147541	40	0.038125	0.398	0.796	2	

Table A.7 – Results for Multiply Scattered Photons (Scaled and Unscaled), NA = 0.0603

Combo #	NA	cm <sup>-1</sup> mu_a(desired)	Dilution Factor 1	Dilution Factor 2	IL Concentration	Multiply Scattered Photons		
						counts MSP	counts Scaled MSP	mV Sensitivity
2	0.0901	1.35	1.639344262	8	1.525	1.634	0.817	0.5
3	0.0901	1.35	1.639344262	20	0.61	0.164	0.82	5
4	0.0901	1.35	1.639344262	40	0.305	0.052	1.04	20
5	0.0901	1.35	3.278688525	4	1.525	1.634	0.817	0.5
6	0.0901	1.35	3.278688525	8	0.7625	0.164	0.82	5
7	0.0901	1.35	3.278688525	20	0.305	0.052	1.04	20
8	0.0901	1.35	3.278688525	40	0.1525	0.052	1.04	20
9	0.0901	1.35	6.557377049	4	0.7625	0.164	0.82	5
10	0.0901	1.35	6.557377049	8	0.38125	0.163	1.63	10
11	0.0901	1.35	6.557377049	20	0.1525	0.052	1.04	20
12	0.0901	1.35	6.557377049	40	0.07625	0.04	2	50
13	0.0901	1.35	13.1147541	4	0.38125	0.163	1.63	10
14	0.0901	1.35	13.1147541	8	0.190625	0.053	1.06	20
15	0.0901	1.35	13.1147541	20	0.07625	0.04	2	50
16	0.0901	1.35	13.1147541	40	0.038125	0.039	3.9	100
17	0.0901	1.35	0	0	0	0.039	3.9	100
3	0.0901	6.075	1.639344262	20	0.61	1.822	0.911	0.5
6	0.0901	6.075	3.278688525	8	0.7625	1.669	0.8345	0.5
8	0.0901	6.075	3.278688525	40	0.1525	0.42	0.84	2
9	0.0901	6.075	6.557377049	4	0.7625	1.669	0.8345	0.5
10	0.0901	6.075	6.557377049	8	0.38125	0.825	0.825	1
11	0.0901	6.075	6.557377049	20	0.1525	0.42	0.84	2
12	0.0901	6.075	6.557377049	40	0.07625	0.401	0.802	2
13	0.0901	6.075	13.1147541	4	0.38125	0.825	0.825	1
14	0.0901	6.075	13.1147541	8	0.190625	0.808	0.808	1
15	0.0901	6.075	13.1147541	20	0.07625	0.401	0.802	2
16	0.0901	6.075	13.1147541	40	0.038125	0.808	0.808	1

Table A.8 – Results for Multiply Scattered Photons (Scaled and Unscaled), NA = 0.0901

Combo #	NA	cm <sup>-1</sup> mu_a(desired)	Dilution Factor 1	Dilution Factor 2	IL Concentration	Multiply Scattered Photons		
						counts MSP	counts Scaled MSP	mV Sensitivity
2	0.1186	1.35	1.639344262	8	1.525	1.645	0.8225	0.5
3	0.1186	1.35	1.639344262	20	0.61	0.087	0.87	10
4	0.1186	1.35	1.639344262	40	0.305	0.04	2	50
5	0.1186	1.35	3.278688525	4	1.525	1.645	0.8225	0.5
6	0.1186	1.35	3.278688525	8	0.7625	0.164	0.82	5
7	0.1186	1.35	3.278688525	20	0.305	0.04	2	50
8	0.1186	1.35	3.278688525	40	0.1525	0.061	1.22	20
9	0.1186	1.35	6.557377049	4	0.7625	0.164	0.82	5
10	0.1186	1.35	6.557377049	8	0.38125	0.052	1.04	20
11	0.1186	1.35	6.557377049	20	0.1525	0.061	1.22	20
12	0.1186	1.35	6.557377049	40	0.07625	0.041	2.05	50
13	0.1186	1.35	13.1147541	4	0.38125	0.052	1.04	20
14	0.1186	1.35	13.1147541	8	0.190625	0.04	2	50
15	0.1186	1.35	13.1147541	20	0.07625	0.041	2.05	50
16	0.1186	1.35	13.1147541	40	0.038125	0.039	3.9	100
17	0.1186	1.35	0	0	0	0.039	3.9	100
3	0.1186	6.075	1.639344262	20	0.61	1.837	0.9185	0.5
4	0.1186	6.075	1.639344262	40	0.305	0.441	0.882	2
6	0.1186	6.075	3.278688525	8	0.7625	1.677	0.8385	0.5
7	0.1186	6.075	3.278688525	20	0.305	0.441	0.882	2
8	0.1186	6.075	3.278688525	40	0.1525	0.171	0.855	5
9	0.1186	6.075	6.557377049	4	0.7625	1.677	0.8385	0.5
10	0.1186	6.075	6.557377049	8	0.38125	0.419	0.838	2
11	0.1186	6.075	6.557377049	20	0.1525	0.171	0.855	5
12	0.1186	6.075	6.557377049	40	0.07625	0.401	0.802	2
13	0.1186	6.075	13.1147541	4	0.38125	0.419	0.838	2
14	0.1186	6.075	13.1147541	8	0.190625	0.81	0.81	1
15	0.1186	6.075	13.1147541	20	0.07625	0.401	0.802	2
16	0.1186	6.075	13.1147541	40	0.038125	0.394	0.788	2

Table A.9 – Results for Multiply Scattered Photons (Scaled and Unscaled), NA = 0.1186

## 6 – REFERENCES

- [1] A. J. Welch and M. J. C. van Gemert, "Optical Thermal Response of Laser-Irradiated Tissue," 2<sup>nd</sup> ed. Springer, (2011)
- [2] A. N. Bashkatov, E. A. Genina, V. I. Kochubey and V. V. Tuchin, "Optical properties of human skin, subcutaneous and mucous tissues in the wavelength range from 400 to 2000 nm," (2005)
- [3] B. Aernouts, E. Zamora-Rojas, R. Van Beers, R. Watté, L. Wang, M. Tsuta, J. Lammertyn, and W. Saeys, "Supercontinuum laser based optical characterization of Intralipid® phantoms in the 500-2250 nm range," *Opt. Express* 21, 32450-32467, (2013)
- [4] B. Aernouts, R. Van Beers, R. Watté, J. Lammertyn, and W. Saeys, "Dependent scattering in Intralipid® phantoms in the 600-1850 nm range," *Opt. Express* 22, 6086-6098 (2014)
- [5] B. Pogue and M. S. Patterson, "Review of tissue simulating phantoms for optical spectroscopy, imaging and dosimetry," *Journal of biomedical optics*, 11, (2006), 041102. 10.1117/1.2335429
- [6] C. Boudoux, "Fundamentals of Biomedical Optics," 1<sup>st</sup> ed. Pollux Editions, (2017)
- [7] D. Gopalakrishnan, C. Akhildev, P. V. Sreenivasan, K. K. Leelamma, L. Joseph, and E. Anila, "Determination of Absorption Coefficient of a Solution by a Simple Experimental Setup," 1391, (2011), 10.1063/1.3643553
- [8] D. J. Segelstein, "The complex refractive index of water," *MS Thesis* Department of Physics, University of Missouri-Kansas City, (1981)
- [9] D. M. Vu, A. S. Thomas, A. P. Finn, and D. Grewal, "CHORIOCAPILLARIS FLOW VOIDS IN CRYPTOCOCCAL CHOROIDITIS USING OPTICAL COHERENCE TOMOGRAPHY ANGIOGRAPHY," *Retinal Cases & Brief Reports*, 1, (2018), 10.1097/ICB.0000000000000703
- [10] D. Wangpraseurt, S. Jacques, N. Lyndby, J. B. Holm, C. F. Pages, and M. Kühl, "Microscale light management and inherent optical properties of intact corals studied with optical coherence tomography," *J. R. Soc. Interface*, 16: 20180567, (2019), <http://dx.doi.org/10.1098/rsif.2018.0567>
- [11] G. Montesano, C. M. Way, G. Ometto, H. Ibrahim, P. Jones, R. Carmichael, X. Liu, T. Aslam, P. Keane, D. Crabb, and A. Denniston, "Optimizing OCT acquisition parameters for assessments of vitreous haze for application in uveitis," *Scientific Reports*, 8, (2018), 10.1038/s41598-018-20092-y

- [12] H. J. van Staveren, C. J. M. Moes, J. van Marie, S. A. Prahl, and M. J. C. van Gemert, "Light scattering in Intralipid-10% in the wavelength range of 400–1100 nm," *Appl. Opt.* 30, 4507-4514, (1991)
- [13] J. A. Izatt, M. D. Kulkarni, S. Yazdanfar, J. K. Barton, and A. J. Welch, "In vivo bidirectional color Doppler flow imaging of picoliter blood volumes using optical coherence tomography," *Opt. Lett.* 22, 1439-1441, (1997)
- [14] J. Liu, N. Ding, Y. Yu, X. Yuan, S. Luo, J. Luan, Y. Zhao, Y. Wang, and Z. Ma, "Optimized depth-resolved estimation to measure optical attenuation coefficients from optical coherence tomography and its application in cerebral damage determination," *J. Biomed. Opt.* 24(3), 035002, (2019), doi:10.1117/1.JBO.24.3.035002
- [15] J. M. Schmitt, A. R. Knüttel, A. H. Gandjbakhche, and R. F. Bonner, "Optical characterization of dense tissues using low-coherence interferometry," *Proc. SPIE 1889, Holography, Interferometry, and Optical Pattern Recognition in Biomedicine III*, (3 September 1993), doi:10.1117/12.155715
- [16] J. M. Schmitt, A. R. Knüttel, and M. J. Yadlowsky, "Interferometric versus confocal techniques for imaging microstructures in turbid biological media," *Proc. SPIE 2135, Advances in Laser and Light Spectroscopy to Diagnose Cancer and Other Diseases*, (19 May 1994), doi:10.1117/12.175999
- [17] J. M. Schmitt, A. R. Knüttel, M. J. Yadlowsky, and M. A. Eckhaus, "Optical-coherence tomography of a dense tissue: Statistics of attenuation and backscattering," *Physics in medicine and biology*, 39, 1705-20, (1994), 10.1088/0031-9155/39/10/013
- [18] J. M. Schmitt, A. R. Knüttel, and R. F. Bonner, "Measurement of optical properties of biological tissues by low-coherence reflectometry," *Appl. Opt.* 32, 6032-6042, (1993)
- [19] J. M. van Golde, F. Tetschke, J. Walther, T. Rosenauer, F. Hempel, C. Hannig, E. Koch and L. R. Kirsten, "Detection of carious lesions utilizing depolarization imaging by polarization sensitive optical coherence tomography," *Journal of biomedical optics* 23 7, (2018), 1-8
- [20] J. Walther, M. Gaertner, P. Cimalla, A. Burkhardt, L. Kirsten, S. Meissner, and E. Koch, "Optical coherence tomography in biomedical research," *Analytical and Bioanalytical Chemistry*, 400, 2721–2743, (2011), <https://doi.org/10.1007/s00216-011-5052-x>
- [21] K. F. Palmer and D. Williams, "Optical properties of water in the near infrared\*," *J. Opt. Soc. Am.* 64, 1107-1110, (1974)
- [22] L. Kou, D. Labrie, and P. Chylek, "Refractive indices of water and ice in the 0.65- to 2.5- $\mu\text{m}$  spectral range," *Appl. Opt.* 32, 3531-3540, (1993)

- [23] M. Gu, X. Gan, and X. Deng, "Microscopic Imaging Through Turbid Media," Berlin, Germany: Springer-Verlag, (2015)
- [24] M. J. Yadlowsky, J. M. Schmitt, and R. F. Bonner, "Multiple scattering in optical coherence microscopy," *Appl. Opt.* 34, 5699-5707, (1995)
- [25] P. Di Ninni, F. Martelli, and G. Zaccanti, "The use of India ink in tissue-simulating phantoms," *Opt. Express* 18, 26854-26865, (2010)
- [26] R. A. Leitgeb, R. M. Werkmeister, C. Blatter, and L. Schmetterer, "Doppler optical coherence tomography," *Progress in retinal and eye research*, 41(100), 26-43, (2014), doi:10.1016/j.preteyeres.2014.03.00
- [27] R. Michels, F. Foschum, and A. Kienle, "Optical properties of fat emulsions," *Opt. Express* 16, 5907-5925, (2008)
- [28] S. Flock, B. C. Wilson, and M. S. Patterson, "Total attenuation coefficients and scattering phase functions of tissues and phantom materials at 633 nm," *Medical physics*, (1987), 14. 835-41. 10.1118/1.596010
- [29] S. Flock, S. Jacques, B. C. Wilson, W. M. Star, and M. J. C. van Gemert "Optical properties of Intralipid: A phantom medium for light propagation studies," *Lasers in Surgery and Medicine*, 12, 510 – 519, (1992), 10.1002/lsm.1900120510
- [30] S. L. Jacques, "Optical properties of biological tissues: a review," *Physics in medicine and biology*, 58, R37-14, 10.1088/0031-9155/58/14/R37
- [31] T. Troy and S. Thennadil. "Optical properties of human skin in the near infrared wavelength range of 1000 to 2200 nm," *Journal of biomedical optics*, 6, (2001), 167-76, 10.1117/1.1344191
- [32] W. Drexler and J. G. Fujimoto "State-of-the-art retinal optical coherence tomography," *Progress in retinal and eye research*, 27, 45-88, (2008), 10.1016/j.preteyeres.2007.07.005
- [33] X. J. Wang, T. E. Milner, and J. S. Nelson, "Characterization of fluid flow velocity by optical Doppler tomography," *Opt. Lett.* 20, 1337-1339, (1995)
- [34] Y. Hoshi and Y. Yamada, "Overview of diffuse optical tomography and its clinical applications," *J. Biomed. Opt.* 21(9), 091312, (2016), doi:10.1117/1.JBO.21.9.091312
- [35] Z. Chen, T. E. Milner, S. Srinivas, X. Wang, A. Malekafzali, M. J. C. van Gemert, and J. S. Nelson, "Noninvasive imaging of in vivo blood flow velocity using optical Doppler tomography," *Opt. Lett.* 22, 1119-1121, (1997)